

FUNDAMENTALS OF LUBRICATED FRICTION IN  
DEEP DRAWING OF ZINC COATED SHEET METAL  
CONSIDERING CONTACTING SURFACE  
MORPHOLOGY AND CHEMISTRY

Zur Erlangung des akademischen Grades eines  
DOKTORS DER INGENIEURWISSENSCHAFT (Dr.-Ing.)

von der KIT-Fakultät für Maschinenbau des  
Karlsruher Instituts für Technologie (KIT)

genehmigte  
DISSERTATION

von  
M.Sc. Manitra Rakotomahefa  
aus Antananarivo - Madagaskar

Tag der mündlicher Prüfung: 30. Januar 2020  
Hauptreferenz: Prof. Dr.-Ing. habil. M. Scherge  
Koreferent: Prof. Dr.-Ing. habil. V. Schulze



---

## ERKLÄRUNG

Hiermit versichere ich, dass ich die vorliegende Arbeit selbstständig verfasst und keine anderen als die angegebenen Quellen und Hilfsmittel benutzt habe, dass alle Stellen der Arbeit, die wörtlich oder sinngemäß aus anderen Quellen übernommen wurden, als solche kenntlich gemacht sind und dass die Arbeit in gleicher oder ähnlicher Form noch keiner Prüfungsbehörde vorgelegt wurde.

Pforzheim, den 29.08.2019



# Acknowledgement

Many people provided me their help and assistance as well as they offered me their support without which I would not have been able to complete this work. This is the right place to thank you all for what you have done for me. I may never be able to repay you, so please accept at least my profound gratitude and my sincere acknowledgement.

Before everything I thank God and my Lord and Savior Jesus Christ for loving me and blessing me every day of my life, for putting so many caring people on my path.

In the first instance, my thoughts go to thyssenkrupp Steel Europe AG for giving me the opportunity to write this thesis. My sincere appreciation is to all my former colleagues from the team of metal forming with a special mention to the former team leader Dr. Keßler for accepting me to the team, to the present team leader Mr. Sikora for the good advise and help of any kind, to Mr. Schulze-Kraasch for the discussion and the thousand measurements, to Mr. Birkenstock for providing all necessary materials and access to the labs, to all the colleagues in the Lab in Duisburg and Dortmund who I had to bother many times. My deep and most special thankfulness go to Dr. Vogt for always providing all the assistance one can ever ask especially in time of greatest need.

In the second instance, I would like to express my deep acknowledgement to Professor Scherge for accepting me at his chair without any reserve, for his time, for providing reasonable hints and advise, for the discussion upon completion of this work. I would like to thank Professor Schulze as well for accepting to be the second assessor of the work and for his consideration. My thanks also go to Dr. Linsler for the good collaboration.

At this point, I would like to thank all my good friends and acquaintances without exception for their support and for being there for me. A special mention goes to Ricardo, Leonardo and Alejandra, Ildar and Zamira, Mahenina, Natacha, Sarat, Ousman, Sonja, Rita and Szilard, Yichuan, Svetlana, Andrei, Misa.

At last, I recall my family in Madagascar, my Father Bonaventure, my Mother Lygie, my sisters Miora, Mihaja and Diamondra, my niece Kanto and my nephew Tandriky. Thank you for your love and caring, for your encouragement and for enduring my absence for many years. A thought also goes to my second family Dadazaka, Mme Clo and Ranjara. I do not forget all my cousins and close relatives from my father and mother's sides who I have only the opportunity to meet on very rare occasions, unfortunately. A special mention goes to my family in law as well and very last but not least, my big thanks go to my beloved Fisandratana Ezaka for her unconditional love.



# Abstract

The work is dedicated to tribological system in deep drawing, more precisely to zinc coated sheet metal steel and tool steel with liquid lubricant at room temperature. In particular, the main focus is the connection between frictional and wear behaviors of the tribosystem and the composition and topology of the contacting surfaces. This is based on the general hypothesis that is friction and wear are the results of adhesion and ploughing. The investigation follows a modular experimental framework combining tribological experiments, surface analyses and mechanical testing. As an onset, the first part consists of a large overview of the main approaches for the characterization of friction and wear, the theory of friction mechanics as well as the existing friction modeling approaches, and characterization of wear including concept of third body. This is followed by the description of the applied methodology and materials for the investigation. The next parts present the results of the experiments which constitutes the main part of the work. In the first instance, the influence of surface topology on friction is considered. While topography of the surface of the used tool depends mostly on the type and quality of the finishing process, that of sheet metal surface depends considerably on skin-pass rolling. The outcome of the investigation allowed to identify important characteristics of the surfaces that play an important role in the frictional behavior of the corresponding tribosystem. To do so, sheet metal from coil that was subject to different skin-pass levels as well as tools with different surface finish were tested in strip drawing and pin-on-disk tests. In the second instance, the role of sheet metal surface structure in friction and wear constitutes another major part of the work. Related to that, comparison of two different types of zinc coating enabled to see that a small change in the chemical composition of the zinc coating can bring about substantial difference of friction and wear behavior of the corresponding tribosystem. This also allows to understand more the main mechanics that govern friction in deep drawing. For the study, pure zinc coating and zinc-magnesium coating are employed. Strip drawing and pin-on-disk tests are extensively performed along with surface analysis, topography measurement and mechanical testing.



# Kurzfassung

Die vorliegende Dissertation beschäftigt sich mit dem tribologischen System beim Tiefziehen, das sich aus verzinktem Stahlblech, Werkzeugstahl und flüssigem Schmierstoff bei Raumtemperatur zusammensetzt. Der Schwerpunkt der Arbeit liegt insbesondere auf dem Zusammenhang zwischen dem Reib- und Verschleißverhalten des Tribosystems und der Zusammensetzung und der Topologie der Kontaktflächen. Die Beschreibung des Tribosystems basiert auf der Annahme, dass die Reibung und der Verschleiß durch Adhäsion und Furchung entstehen. Die Untersuchungen folgen einem modularen experimentellen Rahmen, der tribologische Versuche, Oberflächenanalysen und mechanisches Testen verbindet. Die Arbeit beginnt mit einer umfangreichen Übersicht des Stands der Technik, in der die wichtigsten Ansätze bezüglich der Charakterisierung von Reibung und Verschleiß, der Theorie des Reibmechanismus, die bestehenden Reibungsmodellierungsverfahren und das Konzept des dritten Körpers betrachtet werden. Es folgt die Beschreibung der angewendeten Vorgehensweise und der für die Untersuchung genutzten Materialien. Im Hauptteil der Dissertation werden die Ergebnisse der Versuche vorgestellt. Zunächst wird der Einfluss der Oberflächentopologie auf die Reibung betrachtet. Hierbei hängt die Topographie der Werkzeugoberfläche im Wesentlichen von der Art und der Genauigkeit des Endbearbeitungsprozesses ab. Die Ausgestaltung der Blechoberfläche wird durch das dem Walzprozess folgende Dressieren bestimmt. Anhand der Untersuchungen konnten die wesentlichen Eigenschaften der Kontaktoberflächen, die das Reibverhalten des Tribosystems beeinflussen, ermittelt werden. Es wurden Bleche von einem Coil mit stufenweise unterschiedlichen Dressiergraden in Streifenzieh- und Stiftscheiberversuchen untersucht, wobei Werkzeuge mit unterschiedlichen Oberflächenbeschaffenheiten eingesetzt wurden. Ein wichtiger Teil der Arbeit stellt die anschließende Ermittlung des Anteils der Oberflächenstruktur am Reib- und Verschleißverhalten des Tribosystems dar. Bei einem Vergleich zweier unterschiedlicher Arten von Zinkbeschichtung, nämlich der reinen Zinkbeschichtung und der Zink-Magnesium-Beschichtung konnte beobachtet werden, dass eine Änderung der chemischen Zusammensetzung der Beschichtung einen erheblichen Unterschied im Verhalten des jeweiligen Tribosystems zur Folge hat. Diese Erkenntnis ermöglicht weitere Einsichten hinsichtlich des Hauptmechanismus der Reibung beim Tiefziehen.



# List of Publications



# Contents

<b>Acknowledgement</b>	<b>iii</b>
<b>Abstract</b>	<b>v</b>
<b>Kurzfassung</b>	<b>vii</b>
<b>List of Publications</b>	<b>ix</b>
<b>List of figures</b>	<b>xiv</b>
<b>List of tables</b>	<b>xviii</b>
<b>1 Introduction</b>	<b>1</b>
1.1 Background . . . . .	1
1.2 Motivation . . . . .	2
1.3 Objective and methodology . . . . .	3
<b>2 Literature Background</b>	<b>5</b>
2.1 Contact conditions in deep drawing . . . . .	5
2.1.1 Contact pressure . . . . .	5
2.1.2 Velocity . . . . .	5
2.1.3 Lubrication . . . . .	6
2.2 Approaches in tribological characterization . . . . .	6
2.2.1 Coefficient of friction . . . . .	6
2.2.2 Wear rate . . . . .	6
2.2.3 $p v$ or pressure $p \times$ velocity $v$ factor . . . . .	7
2.2.4 Stribeck curve and velocity/pressure factor . . . . .	8
2.3 Lubricated friction . . . . .	8
2.3.1 Characterization . . . . .	8
2.3.2 Lubrication regimes . . . . .	9

2.3.2.1	Hydrodynamic lubrication . . . . .	9
2.3.2.2	Mixed lubrication . . . . .	9
2.3.2.3	Boundary lubrication . . . . .	9
2.3.2.4	Hydrostatic lubrication . . . . .	10
2.4	Friction mechanics . . . . .	11
2.4.1	Adhesion . . . . .	12
2.4.1.1	Description and classification . . . . .	12
2.4.1.2	Mechanism of adhesion . . . . .	12
2.4.1.3	Quantitative evaluation of adhesion . . . . .	13
2.4.1.4	Influencing factors . . . . .	13
2.4.2	Plastic interaction of asperities . . . . .	16
2.4.2.1	Description . . . . .	16
2.4.2.2	Quantitative estimation . . . . .	16
2.4.2.3	Influencing factors . . . . .	17
2.5	Friction modeling . . . . .	17
2.5.1	Empirical friction models . . . . .	17
2.5.2	Physics-based friction models . . . . .	18
2.5.3	Estimation of the real contact area . . . . .	20
2.5.3.1	Modeling of the rough surface . . . . .	20
2.5.3.2	Approaches in the estimation of the real area of contact	21
2.6	Wear . . . . .	22
2.6.1	Adhesive wear as severe wear . . . . .	22
2.6.2	Abrasive wear and severe-mild wear transition . . . . .	23
2.6.3	Third body concept . . . . .	24
2.7	Relationship between third-body and friction . . . . .	26
<b>3</b>	<b>Methods and Materials</b>	<b>27</b>
3.1	Description of the tribological tests . . . . .	27
3.1.1	Strip drawing . . . . .	27
3.1.2	Pin-on-disk with radionuclide-technique . . . . .	30
3.2	Chemical analysis of surface . . . . .	32
3.2.1	X-ray fluorescence measurement . . . . .	32
3.2.2	X-ray Photoelectron Spectroscopy (XPS) . . . . .	32
3.2.3	XPS-depth profiling . . . . .	32
3.2.4	Scanning Electron Microscopy (SEM) . . . . .	33

3.2.5	Focused Ion Beam system . . . . .	33
3.3	Nanoindentation . . . . .	34
3.4	Surface topography measurement . . . . .	35
3.4.1	Topography characterization . . . . .	35
3.4.2	Measurement equipment . . . . .	37
3.5	Plan of experiments . . . . .	37
3.5.1	Characterization of wear . . . . .	37
3.5.2	Characterization of friction and lubrication . . . . .	38
3.5.3	Summary of parameter setup for tribological tests . . . . .	39
3.6	Materials . . . . .	41
3.6.1	Tool . . . . .	41
3.6.1.1	Tool material . . . . .	41
3.6.1.2	Tool surface . . . . .	42
3.6.2	Sheet metals substrate . . . . .	42
3.6.3	Sheet Metal Coating . . . . .	43
3.6.3.1	Chemical composition . . . . .	47
3.6.3.2	Microstructure . . . . .	48
3.6.4	Lubricants . . . . .	48
<b>4</b>	<b>Influence of topology of contacting surfaces on friction</b>	<b>49</b>
4.1	Parameter variation in strip drawing test . . . . .	49
4.1.1	Experimental results . . . . .	49
4.1.2	Observation . . . . .	51
4.2	Parameter variation in pin-on-disk test . . . . .	51
4.2.1	Experimental results . . . . .	51
4.2.2	Observation . . . . .	51
4.3	Lubricant amount variation in strip drawing . . . . .	54
4.3.1	Experimental results . . . . .	54
4.3.2	Observation . . . . .	55
4.4	Influence of surface topography on friction . . . . .	57
4.4.1	Experimental results with consideration of blank surface morphology	57
4.4.2	Observation . . . . .	58
4.4.3	Experimental results with consideration of tool surface morphology	59
4.4.4	Observation . . . . .	59
4.5	Discussion . . . . .	60

4.5.1	Characterization of lubrication regimes . . . . .	60
4.5.2	Importance of tool surface finishing . . . . .	61
4.5.3	Role of sheet metal surface topography . . . . .	62
<b>5</b>	<b>Influence of surface coating type on friction and wear</b>	<b>65</b>
5.1	Running-in test by pin-on-disk with radionuclide-technique . . . . .	65
5.2	Running-in test by strip drawing . . . . .	67
5.3	Analysis of the surface of strip drawing tool . . . . .	68
5.3.1	Topography analysis . . . . .	68
5.3.2	Analysis of the microstructure of near-surface zone . . . . .	70
5.3.3	Analysis of the chemical composition of the surface . . . . .	71
5.3.3.1	XPS-Analysis - Depth profiling of the tool surface . . . . .	71
5.3.3.2	Glow-discharged optical emission spectrometry of tool surfaces . . . . .	75
5.4	Analysis of the sheet metal coating surface . . . . .	76
5.4.1	Topography analysis . . . . .	76
5.4.2	Analysis of microstructure of near-surface zone . . . . .	78
5.4.2.1	Before drawing . . . . .	78
5.4.2.2	After drawing . . . . .	79
5.4.3	Analysis of chemical composition . . . . .	80
5.4.4	Nanohardness measurement . . . . .	83
<b>6</b>	<b>Inference</b>	<b>89</b>
6.1	Summary . . . . .	89
6.1.1	Influence of type of surface coating . . . . .	89
6.1.2	Influence of surface topography . . . . .	90
6.1.3	Source of error in tribological tests . . . . .	90
6.2	Conclusion . . . . .	91
6.2.1	Friction mechanics . . . . .	91
6.2.2	Friction modelling . . . . .	91
6.2.3	Wear behavior . . . . .	92
6.3	Future research possibilities . . . . .	92

# List of Figures

1.1	Schematic of system approach in metal forming (using deep drawing of a tophat profile as an example) [according to [Kar12]]. . . . .	2
2.1	Schematic representation of a Stribeck curve. . . . .	11
2.2	Schematic representation of superficial layer of various samples [Fay92]. . . . .	25
3.1	(a) - Strip drawing test equipment; (b) - Schematic representation of the strip drawing test with flat dies. . . . .	28
3.2	Strip drawing tools with different sizes: (a) tool 1 –660 mm <sup>2</sup> ; (b) tool 2 –1200 mm <sup>2</sup> ; (c) tool 3 –2680 mm <sup>2</sup> . . . . .	29
3.3	Comparison of the frictional behavior of tribosystems with different tool sizes at $v = 15$ mm/s. . . . .	29
3.4	Comparison of the frictional behavior of tribosystems with different tool sizes at $v = 30$ mm/s. . . . .	29
3.5	Comparison of the frictional behavior of tribosystems with different tool sizes at $v = 60$ mm/s. . . . .	30
3.6	Schematic representation of the setup for the pin-on-disk wear testing machine (source: [Ant10]). . . . .	31
3.7	Pin-on-disk tribometer. Left: contact principle; right: structure of the tribometer and measurement principle (Source: [Sch14a; Lin16]). . . . .	32
3.8	Geometry of a three-sided Berkovich indenter [Fen10]. . . . .	34
3.9	Geometric deviations from intended shape [Whi03]. . . . .	36
3.10	Strip drawing tools with different surface finishing: (a) –grinded tool; (b) –plasma nitride treated tool; (c) –polished tool. . . . .	38
3.11	Micrographs of: (a) - unworn DP500+Z; (b) - unworn DP500+ZM. . . . .	44
3.12	Surface topography of the dual-phase steels: (a) - with zinc coating DP500+Z (outer-skin); (b) - with zinc-magnesium coating DP500+ZM (outer-skin); (c) - with zinc coating DP500+Z (multipurpose). . . . .	45
3.13	Topography parameters of DX57D+Z with various skin-pass levels. . . . .	46
3.14	Graphical representation of the topography parameters of DX57D+Z with various skin-pass levels. . . . .	47

4.1	General Stribeck curve from strip drawing test with DP500+Z (multipurpose, $R_a = 0.78$ , $RP_c = 4.17$ ). . . . .	50
4.2	General Stribeck curve from strip drawing test with DP500+Z (multipurpose, $R_a = 0.78$ , $RP_c = 4.17$ ). Each curve represents the average curve of three experiments with the same parameters . . . . .	50
4.3	Friction power density curve from strip drawing test with DP500+Z (multipurpose, $R_a = 0.78$ , $RP_c = 4.17$ ). . . . .	50
4.4	Stribeck-curve with DP500+Z(outerskin, $R_a = 0.86$ , $RP_c = 9.2$ )and lubricant amount = $0.5 \text{ g/m}^2$ . . . . .	52
4.5	Stribeck-curve with DP500+Z(outerskin, $R_a = 0.86$ , $RP_c = 9.2$ )and lubricant amount = $1.5 \text{ g/m}^2$ . . . . .	52
4.6	Stribeck-curve with DP500+ZM ( $R_a = 0.84$ , $RP_c = 11.7$ ) and lubricant amount = $0.5 \text{ g/m}^2$ . . . . .	52
4.7	Stribeck-curve with DP500+ZM ( $R_a = 0.84$ , $RP_c = 11.7$ ) and lubricant amount = $1.5 \text{ g/m}^2$ . . . . .	53
4.8	Simplified Stribeck curves for pin-on-disk with DP500+Z (car outer skin, $R_a = 0.86$ , $RP_c = 9.2$ ): (a) – first revolution; (b) – third revolution. . . .	53
4.9	Simplified Stribeck curves for pin-on-disk with DP500+ZM ( $R_a = 0.84$ , $RP_c = 11.7$ ): (a) – first rotation; (b) – third rotation. . . . .	53
4.10	Simplified Stribeck curve with DP500+Z (multipurpose, $R_a = 0.78$ , $RP_c = 4.17$ ) and lubricant amount variation. . . . .	54
4.11	Simplified Stribeck curve with DP500+Z (outerskin, $R_a = 0.86$ , $RP_c = 9.2$ ) and lubricant amount variation. . . . .	55
4.12	Stribeck curve: left – lubrication regime area in strip drawing; right – the different zones of boundary lubrication in strip drawing. . . . .	56
4.13	Stribeck curve with the different zones of mixed and boundary lubrications: (left) – multi-purpose zinc coated DP500 ( $R_a = 0.78$ , $RP_c = 4.17$ ); (right) – car outer skin zinc coated DP500 ( $R_a = 0.86$ , $RP_c = 9.2$ ). . . . .	56
4.14	Simplified Stribeck curve of the DX57D+Z with different skin-pass levels. . . . .	57
4.15	Simplified Stribeck curve with lubricant amount variation on DX57D+Z: (a) – skin-pass level 8; (b) – skin-pass level 1 vs level 8. . . . .	57
4.16	Comparison of the frictional behavior of tribosystems with grinded and polished tool surfaces. . . . .	59
4.17	Lubricant squeezed out of the contact interface (lubricant amount $4.5 \text{ g/m}^2$ ): (a) – on the side; (b) – at the entrance into the contact. . . . .	61
5.1	Result of pin-on-disk for the investigation of running-in behavior of tool with DP500+Z (one test consists of three revolutions). . . . .	66
5.2	Result of pin-on-disk for the investigation of running-in behavior of tool with DP500+ZM (one test consists of three revolutions). . . . .	66

5.3	Result of radionuclide-technique for running-in test of the tool steel with DP500+Z. . . . .	67
5.4	Result of radionuclide-technique for running-in test of the tool steel with DP500+ZM. . . . .	67
5.5	Result of strip drawing test for the investigation of the difference of frictional and running-in behaviors between DP500+Z and DP500+ZM. . .	68
5.6	Topography of the tool before (a) and after drawing with DP500+Z (b) and DP500+ZM (c) with the corresponding height distribution (not at the same location). . . . .	69
5.7	SEM picture of the strip drawing tool surface: (a) - before drawing; (b) - after drawing with DP500+Z and (c) - after drawing with DP500+ZM. .	70
5.8	SEM picture of FIB profiles of the tool from secondary electrons: (a) - before drawing; (b) - after drawing with DP500+Z and (c) - after drawing with DP500+ZM. . . . .	71
5.9	XPS depth profile of tool surface drawn with DP500+Z (in original format): (a) - before drawing; (b) - after drawing with DP500+Z. . . . .	72
5.10	XPS depth profile for the tool drawn with DP500+ZM (in original format): (a) - before drawing; (b) - after drawing with DP500+ZM. . . . .	72
5.11	XPS depth profiles of O1s.Oxide for the tools: (a) - drawn with DP500+Z; (b) - drawn with DP500+ZM. . . . .	73
5.12	XPS depth profiles of Fe-metal/oxide for the tools: (a) - drawn with DP500+Z; (b) - drawn with DP500+ZM. . . . .	73
5.13	XPS depth profiles of C/CHx for the tools: (a) - drawn with DP500+Z; (b) - drawn with DP500+ZM. . . . .	74
5.14	Comparison of XPS depth profiles of Zn2p3-oxide on tools. . . . .	74
5.15	Tools (cut) from the running-in test analyzed with GDOES with the measurement spots: left - drawn with DP500+Z; right - drawn with DP500+ZM (N.B: the tools are not in their full size anymore). . . . .	75
5.16	Surface topography of DP500+Z with the corresponding volume parameters ( $V_{vc}$ : core void volume, $V_{mc}$ : core material volume). . . . .	76
5.17	Surface topography of DP500+ZM with the corresponding volume parameters ( $V_{vc}$ : core void volume, $V_{mc}$ : core material volume). . . . .	77
5.18	Surface topography of the strips with the corresponding volume parameters: (a) - DP500+Z; (b) - DP500+ZM. . . . .	77
5.19	Surface topography of the strips with the corresponding volume parameters: (a) - DP500+Z; (b) - DP500+ZM. . . . .	78
5.20	FIB-SEM images of the section of the coating of DP500+Z: (a) - untouched region; (b) - deformed region by skin pass rolling. . . . .	79
5.21	FIB-SEM images of the section of the coating of DP500+ZM before drawing. . . . .	79

5.22	FIB-SEM images of the profile of the surface coatings after drawing: (a) – DP500+Z at the contact zone; (b) – DP500+Z at the untouched zone; (c) – DP500+ZM at the contact zone; (d) – DP500+ZM at the untouched zone. . . . .	80
5.23	XPS-depth profile of the strip surfaces before and after drawing. . . . .	81
5.24	Specimens from the strips for xps measurements. . . . .	82
5.25	Specimen for nanoindentation from DP500+Z (left) and DP500+ZM (right). 84	
5.26	AFM measurements of four showcase measurement locations (Korn: grain; Eut: eutectic phase; x: impression where a quantitative evaluation was impossible). . . . .	85
5.27	Diagrams of the measured hardness $H$ and reduced elastic modulus $E_r$ of the pure zinc coating with respect to the indentation depth $h_c$ . The average values are represented by the horizontal lines. . . . .	86
5.28	Diagrams of the measured hardness $H$ and reduced elastic modulus $E_r$ of zinc-magnesium coating with respect to the indentation depth $h_c$ . The average values are represented by the horizontal lines. The values of the indentation on the eutectic phase between the zinc grains are marked in red. 86	

# List of Tables

2.1	Ranges of the coefficient of friction for various types of friction and lubrication regimes (1 – metall/metall, 2 – ceramic/ceramic) [Som14]. . . . .	10
3.1	Parameters defined in ISO 4287:1997 [De 00]. . . . .	36
3.2	Setup of strip drawing tests for the establishment of Stribeck curve. . . . .	39
3.3	Setup of strip drawing tests with lubricant amount variation. . . . .	39
3.4	Setup of pin-on-disk tests for the investigation of lubrication regime. . . . .	39
3.5	Setup of strip drawing test with various skin-pass levels. . . . .	40
3.6	Setup of strip drawing test with grinded and polished tools. . . . .	40
3.7	Setup of the first series of strip drawing for running-in investigation. . . . .	40
3.8	Setup of pin-on-disk test for the investigation of tool running-in. . . . .	41
3.9	Typical chemical composition of tool steel 1.2379 (mass percentage in % according to DIN EN ISO 4957). . . . .	41
3.10	Tool surface hardness. . . . .	42
3.11	Topography parameters of the used tools. . . . .	42
3.12	Roughness parameters of the dual-phase steel with zinc coating DP500+Z and the dual-phase steel with zinc-magnesium coating DP500+ZM according to ISO 4287. . . . .	44
5.1	Topography parameters of the tool before and after drawing with DP500+Z and DP500+ZM. . . . .	69
5.2	Surface coverage of the transfer material on the tool. . . . .	75
5.3	Chemical composition of the surface and the corresponding oxide layer thickness. . . . .	82
5.4	Ratio of Mg, Al and Zn within the oxide layer. . . . .	82
5.5	Hardness and reduced elasticity modulus of the specimen coatings. . . . .	84



# Chapter 1

## Introduction

### 1.1 Background

Sheet Metal Forming (SMF) is a manufacturing process which is applied for the production of goods in almost all sectors from home appliance and food industry to automotive and aerospace. It comprises a myriad of processes which consist in bringing a sheet metal into a desired shape. It is described according to DIN 8582. This work focuses exclusively on deep drawing which is one of the SMF processes. Deep drawing is defined as a tensile-compression forming of a sheet metal blank, a film or a plate depending on the material, a cut-out or a section into a hollow body without an intended alteration of thickness [DIN 8584-1].

Figure 1.1 gives a schematic representation of the process as an illustration. Generally, a sheet metal or blank (1) is brought into a desired shape by submitting it to specific plastic deformations between tools such as die, punch and blank holder (2). More precisely, the central portion of the blank is pushed into the die opening with the punch while the forming wrinkles at the flange are compressed by the blankholder. The core of deep drawing processes is the transfer of the applied forces from the tools of a press shop (5) to the sheet metal [Sem06]. It is carried out through the tool/sheet metal interface (3) in terms of distributed pressure [Kar12]. One major part of the force  $F_{St}$  from the punch force is allotted to the deforming of the material itself and designated as the deforming force. This concerns the necessary force  $F_U$  for the forming of the flange and the bending/reverse-bending at the die radius. Another part serves to overcome the friction occurring at the tool/sheet interface and is designated as the friction force  $F_R$  [Sie56]. The involved forces can then be described by the formula:

$$F_{St} = F_U + F_R \quad (1.1)$$

Friction as one of the main components of tribology is defined as the resistance to relative motion between two contacting surfaces [Det02] which are the tool and blank surfaces in the case of deep drawing. It represents a control parameter over the variation of material flow and the sheet thickness during the drawing process [Boc93]. Friction takes its origin from the surface roughness [Mat08]. In deep drawing, the surface of the sheet metal and the tools are, indeed, not perfectly smooth. While tool surfaces are usually smoothed through grinding or polishing, sheet metal surface exhibits higher roughness parameters according to DIN EN ISO 4287 in order to ensure optimal qualities including paint

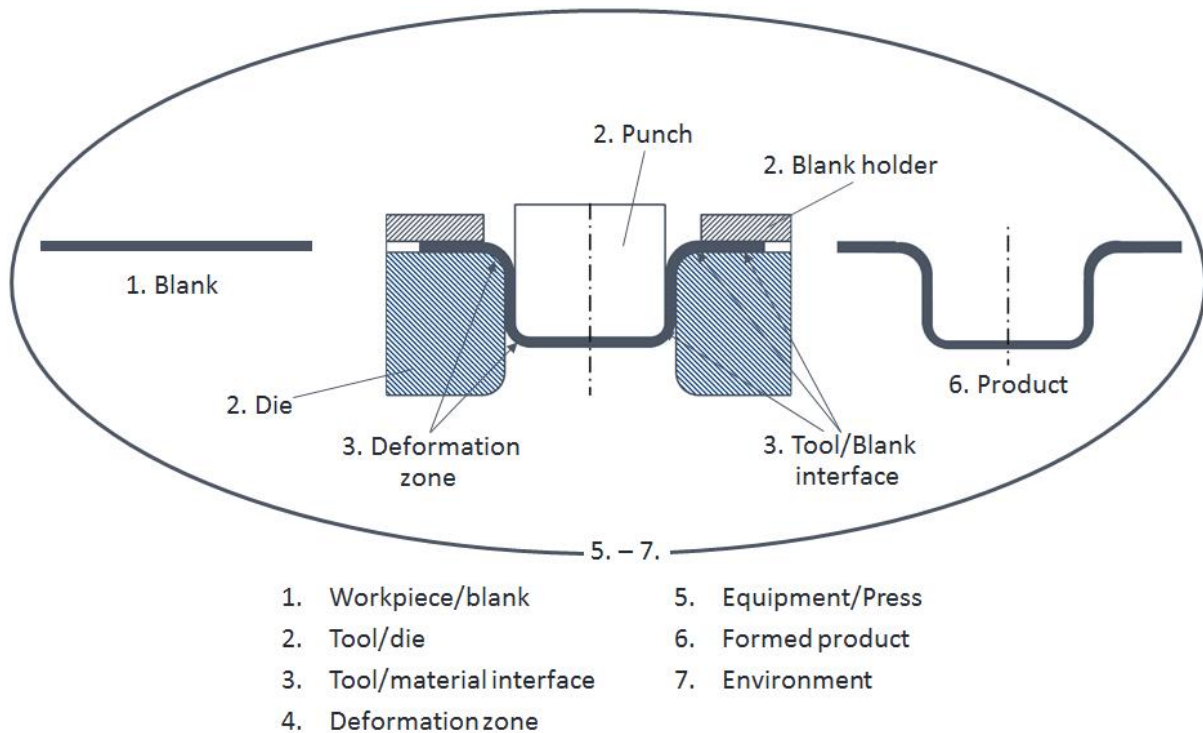


Figure 1.1: Schematic of system approach in metal forming (using deep drawing of a tophat profile as an example) [according to [Kar12]].

adhesion and optical characteristics of painting [Blu16; Fro14] as well as good transport of lubricant.

Tribology also involves wear. Effectively, friction is primarily an entropy-producing or "dissipative" phenomenon and the critical issue is to understand its dissipative nature [Tab92; Bre00]. The involved friction energy is dissipated over a certain real volume which cannot unfortunately be measured [Die15]. The dissipation process is carried out mainly through heat generation. It may also be accompanied by particle generation as well as change of the material structure in the aforementioned volume [Sha04]. Particle generation equals material loss. And according to [DIN 50320], "wear is the continuing loss of material from surfaces of a solid body due to mechanical action, i.e. contact and relative movement of a solid, fluid or gaseous counter body". Scherge stated that wear and friction are strongly coupled dynamics processes [Sch03b]. Although no clear correlation between friction and wear [Gar95] is available, the assessment of the frictional behavior of the tribosystem cannot be entirely dissociated from wear.

## 1.2 Motivation

Equation 1.1 shows that friction is an important influencing factor on deep drawing along with material properties [Doe76]. This reflects on the process performance and on the final product properties [ter96]. It is neither a physical nor a mechanical property but rather a system property that is sensitive to any variation within the entire so-called "tribological system" or usually shortened as "tribosystem" [Mat15]. In deep drawing, the tribological system is composed of the sheet metal and the tool surfaces, the applied lubricant in

between and the ambient medium. Since many decades sheet metal surfaces have been subjected to development and optimization in terms of coating type and morphology for painting and corrosion protection purposes, inter alia. Any outcome brings a change into the tribosystem with a subsequent influence on the friction behavior. Thereby, relating the fundamentals of lubricated friction in deep drawing to the coating type and morphology is founded. In this work, the subject of investigation is mainly sheet metal steel with zinc coating. On the one hand, new types of zinc coatings have emerged as the results of the increase in zinc coating research [Mar00]. This includes the addition and dosing of other elements into the composition of the pure zinc coating such as aluminium and magnesium. Thereby, zinc coatings such as Galfan and Galvalume were developed. On the other hand, desired characteristics can be set on the coating surface during the skin-pass rolling operation from the working rolls in a skin pass mill stand. The working rolls are usually treated by conventional texturing methods which consist of deforming the roll surface plastically by shot blast (Shot Blast Texturing or SBT) or by partially melting (Electric Discharge Texturing or EDT, Electron Beam Texturing or EBT, Laser Texturing or LT) [Deu95]. It can be seen that the research in either of the fields i.e. zinc coating development and surface texturing has already borne its fruits. Nevertheless, a full understanding of the influence of the coating on the frictional response of the tribosystem is still to be achieved for further more purposeful development of the zinc coating and its surface.

### **1.3 Objective and methodology**

The main objective of this thesis is to characterize the tribological behavior of the deep drawing tribosystem in terms of its microstructure and morphology. More precisely, the role of the characteristics and properties of the tribosystem in its response to the imposed contact conditions is the main focus of the work. Chemical compositions and mechanical properties of the surfaces, microstructure and topology of the near-surface are inter alia the regarded features of the tribosystem under varied contact conditions namely contact pressure, sliding velocity and lubricant amount. In order to do so, an experimental framework is chosen which enables a modular combination of chemical analyses and mechanical testing as well as tribological experiments. Destructive and non-destructive tests are considered. This will be explained in detail in chapter 3 along with the used materials after the necessary background information as well as the state-of-the-art of the regarded topic is provided in chapter 2. An important point is that the properties at the near surface materials can be very different from the bulk materials and the traditional methods are not very appropriate anymore. In addition, preliminary experiments are performed which treat the consistency of the results in strip drawing with respect to tool size.

Chapter 4 constitutes the first main part of the work. It treats the influence of the surface topography on the frictional behavior of the corresponding tribosystem as well as the occurring lubrication regime. In the first instance, first strip drawing and pin-on-disk tests are performed considering the presence of the liquid lubricant in different amount. The obtained Stribeck curves are discussed for the characterization of the occurring lubrication regime specific. It also allows to narrow down the area of investigation especially with respect to the possible outcome of tribological loading. In the second instance, sheet

metals taken from a coil with different skin pass level as well as tools with different surface finish were drawn. This allows to underline certain characteristics of the surface topography that count the most in the frictional behavior of the tribosystem.

Chapter 5 is the second main part of the work and it focuses on the role of the surface coating type with an emphasis on its chemical composition, microstructure and mechanical properties. The results are interpreted according to the theory of friction mechanics. All analyses will be performed on worn and unworn surfaces to enable comparison between the initial and final states.

The work is concluded by chapter 6 which highlights the main lines of the done work along with the conclusion. Future research possibilities will also be mentioned.

# Chapter 2

## Literature Background

### 2.1 Contact conditions in deep drawing

#### 2.1.1 Contact pressure

Gao *et al.* [Gao10] measured the contact pressure between punch and blank. They determined the variation of the pressure value. The highest pressure lays near the punch corner with a pressure value about 2.5 MPa. The overall contact pressure is, therefore, relatively low at the punch blank interface.

Contact pressure is also low in the flange at the beginning of the process since the contact area is large. As the deep drawing process progresses, the area reduces due to the flow of the material into the die. Thereby, the contact pressure increases under constant blankholder force. It should be noticed, however, that blank thickening [Kar12] and wrinkling during the process can cause high local pressure at some zones while it releases it at others.

Pereira *et al.* [Per08] investigated the contact conditions at the die radius in deep drawing process. They identified three different stages namely initial, intermediate and final stage during which different contact conditions occur. At the initial and intermediate stage, transient but severe and localized contact conditions take place with contact pressures significantly greater than the blank material yield strength. Moreover, Pereira *et al.* [Per09] found out that the bending ratio implying the die corner radius and the material ultimate tensile strength had the most influence on those high contact pressures while friction and the blankholder force had minor influence.

#### 2.1.2 Velocity

Deep drawing belongs to low speed processes. Drawing velocity can be constant or varied depending in the first place on the used press-shop and in some cases the drawing requirements. For mechanical press used in automotive industries, the diverse servopress shops that are discussed by Schuler [Sch14b] develop oscillating drawing speed within the range of 1 to 200 mm/s. This is not as high as the 10000 mm/s that are usually encountered in bearing application conditions.

### 2.1.3 Lubrication

Liquid lubricant is very often applied on the blank surface in deep drawing. It aims to reduce friction and wear of the contacting surfaces by impeding their direct interaction. The principle consists of separating the contacting surfaces with a lubricant film. In deep drawing, liquid lubricants are applied in limited amount. The contact interface is not continuously supplied with lubricant, neither is a superabundance of lubricant desirable in opposite to popular investigated systems such as bearings. Typical liquid lubricant amount lies in the range between 0.5 and 3 g/m<sup>2</sup> [Mei05] so that the lubricant thickness can be theoretically at most 3.75 μm. At the input state, depending on the roughness of the blank as well as the actual distribution of the lubricant oils overall the surface; lubricant may or may not cover all the irregularities of the surface. In general, sheet metals for car body parts have a mean surface roughness Ra about 1 μm and they are drawn with a lubricant amount of 1 g/m<sup>2</sup>.

## 2.2 Approaches in tribological characterization

### 2.2.1 Coefficient of friction

Friction is characterized by the coefficient of friction which is defined as the ratio of the friction force to the normal one. It is designated by the Greek letter ( $\mu$ ) which was first introduced by Leonhard Euler (1750)[Eul50]. It is a dimensionless quantity. As mentioned earlier, friction is primarily an entropy-producing or dissipative phenomenon. The dissipated energy throughout friction can be characterized by the friction power  $P_F$  initially defined as:

$$P_F = \frac{d}{dt} \int F_F \cdot ds = \mu \cdot F_N \cdot v \quad (2.1)$$

with  $F_F$  - the friction force,  $\mu$  - the coefficient of friction,  $F_N$  - the normal force and  $v$  the sliding speed.

While the normal force and the sliding speed are input factors, the coefficient of friction depends entirely on the regarded tribosystem. It results from the response of the tribosystem to the inputs. The power dissipated by friction was earlier established as an important variable to identify the critical wear characteristics of friction materials [Dan09].

### 2.2.2 Wear rate

Wear is characterized by its rate which is defined as the removed material mass (rarely used) or volume (used more often) per unit sliding distance or time. As volume is more frequently used than mass, units are then referred to it as [mm<sup>3</sup>/m] or [mm<sup>3</sup>/h]. Wear coefficient is also widely used as the ratio of the volume loss to the applied normal force and the sliding distance is also used when wear behavior of the tribosystem is linear following the Archard model [Arc53]. It has the unit [mm<sup>3</sup>/(Nm)]. Wear rate is also expressed by means of loss of material thickness per unit time [nm/h] [Lin16].

In their study of unlubricated friction, Archard and Hirst [Arc56] were the first to introduce the notion of "mild wear" and "severe wear". The value of wear coefficient at the boundary between mild and severe wear is assumed to be  $10^{-6} \text{ mm}^3/(\text{N}\cdot\text{m})$  [Czi00]. It is important to mention that the difference in wear coefficient between these two types of wear is the consequences of the different loadings of the tribosystem at the first place as Archard *et al.* described in their work. Effectively, mild and severe wear are caused by low and high loads respectively. Depending on the loading, the mechanism of wear occurs on different scale of size. Furthermore, mild wear and severe wear processes are different not only in scale but also in kind. The main characteristics of severe and mild wear are as follow [Arc56]:

- Severe wear
  - Heavily distorted crystal structure of the surface layers.
  - Probable extension of deformation to a considerable depth.
  - Occurrence of damage by welding and plucking of the surfaces.
  - Occurrence of fragment transfer between the rubbing partners.
  - Occurrence of plastic deformation far below the surface due to the involved forces.
  - Low contact resistance.
  - Occurrence of extensive intermetallic contact.
  - Retention of the metallic appearance of the contacting surface.
  - Large wear particles (typical dimensions being of order of  $10\mu\text{m} - 2\text{mm}$ ).
- Mild wear
  - Little indication of subsurface damage.
  - Slow removal of the tips of the higher asperities by a process on a scale too small to be reached by for instance Talysurf instrument.
  - Confinement of plastic deformation to regions very close to the rubbing interface.
  - Occurrence of surface change in kind (high oxidation).
  - Generally no intermetallic junctions between the substrates of the contacting pairs.
  - More frequent intermetallic junctions between metallic inclusions within the surface skin, or contacts between one of the underlying metals and the surface skin.

### 2.2.3 pv or pressure $p \times$ velocity $v$ factor

Based on the definition of friction power, the term pv factor or pv condition referring to the product of contact pressure ( $p$ ) and sliding velocity ( $v$ ) is introduced where the dissipated energy in mechanical wear process (friction heat) is proportional to  $pv$  [Lar07]. This proportionality is represented by the coefficient of friction. It is a measure of the energy

input rate to the sliding interface and usually expressed in MPa.m/s or in psi.ft/min. Generally, there is a threshold or maximum permissible value of the pv factor also known as the "pv limit" for a given tribosystem beyond which wear can increase exponentially due to the generated heat [Ebn05]. This limit pv factor corresponds to the wear inflection point which can be determined by varying load and speed in an experimental test [Tholl; Ebn05]. The pv limit for a given tribosystem or in a given application depends on several factors including the presence of lubricant.

#### 2.2.4 Stribeck curve and velocity/pressure factor

Stribeck curve represents the general characteristic of lubricated moving surfaces as a function of lubricant kinematic viscosity  $\eta$ , the sliding velocity  $v$  and the contact pressure  $p$  or more precisely  $(\eta.v/p)$  which is a non-dimensional quantity known as the "Hersey number". Considering the units of the involved quantities, kinematic viscosity is in [Pa.s], the pressure in [MPa] and the sliding velocity is represented by the rotational speed [rpm] owing to the original investigation on journal bearing. The primary requirement for generating a Stribeck curve is a fluid that can be drawn into a converging gap, thus creating a pressure increase to support the load [Czi00; Sha14]. By keeping viscosity as constant, the characteristic variables reduce to pressure and velocity. Therefore, the velocity/pressure ( $v/p$ ) factor is used for lubrication characterization conserving the concept of Stribeck curve and Hersey number and keeping in mind that viscosity is still involved within the general equation. The Stribeck curve originates from the work of Stribeck (1902) [Str02] and Hersey (1914) [Her14]. Thurston (1879) [Thu79] and Martens (1888)[Mar88] have also performed fundamental investigations on lubricants using axle-bearings. A historical review of the origin of the Stribeck curve is given in [Woy10].

## 2.3 Lubricated friction

### 2.3.1 Characterization

The presence of liquid lubricant in the tribosystem urges to study friction and lubrication together. Effectively, lubricated friction is very often described by means of the Stribeck curve where the friction coefficient is plotted with respect to the Hersey number. The same Stribeck curve describes a plot showing the frictional characteristics of a liquid lubricant over conditions usually spanning the boundary, mixed and hydrodynamic regimes. By means of the Stribeck curve, the effect of changes to the viscosity and additive package of the lubricant is evaluated as well as the effect of surface roughness.

Microcontact mechanisms in the presence of lubricant can be categorized in different modes called "lubrication regimes" namely hydrodynamic lubrication, boundary lubrication and mixed lubrication regimes. Each regime is defined by the ratio of the film thickness to the surface roughness known as the  $\lambda$  - ratio [Azu12]. In turn, the lubricant film thickness ( $h$ ) depends upon the constituent chemistry (viscosity of the formulated base oil), the operating conditions, in particular the applied load and sliding velocity, the geometrical configuration and arrangement of the contacting surfaces along with their roughness [Bar13; Czi15]. The change of the lubricant properties during deep drawing

process is rarely considered. The initial properties such as viscosity has been rather emphasized [Kim07; Lia15; Kar16].

Although the  $p_v$  factor is more applied to wear characterization, the friction coefficient can also be related to the  $p_v$  factor based on the definition of the friction power in equation 2.1. Some examples of this relationship is given in Blau [Bla08] with sliding bearing systems. A graphical representation the coefficient of friction with respect to the  $p_v$  factor is also given in [Wan12]. Wang *et al.* [Wan12] investigated for instance the effect of  $p_v$  factor on the tribological behavior of a copper-impregnated metallized carbon with and without electrical current. Fouvry *et al.* [Fou14] formalized the friction behavior of a tribosystem subject to fretting wear in terms of  $p_v$  factor using the friction energy density concept.

The possibility to set a large spectrum of combination of  $p$  and  $v$  enables to investigate various aspects of the frictional behavior of the desired tribosystem. The approaches  $p_v$  and the  $v/p$  factors represent a relevant physical interpretation of friction and lubrication. Moreover, the lubricant viscosity is not considered. Thereofere, a plot of the coefficient of friction with respect to the  $v/p$  and  $p_v$  factors can be an informative representation of friction for lubricated contact in deep drawing.

## 2.3.2 Lubrication regimes

### 2.3.2.1 Hydrodynamic lubrication

It is characterized by a thick lubricant film so that the opposing solid surfaces are prevented from coming into contact. It was first investigated by Osbourne Reynolds (1842-1912) on a shaft and a bearing. The applied normal load is fully carried by pressure generated within the fluid, and frictional resistance to motion arises entirely from the shearing of the viscous fluid [Ham04]. One of the general requirements is a high relative sliding velocity in order to generate the hydrodynamic forces [Lan94]. Deep drawing process is, however, relatively slow and the required velocity is generally not reached for the hydrodynamic lubrication to take place.

### 2.3.2.2 Mixed lubrication

Mixed lubrication regime occurs when the film thickness is such that a significant fraction of the load between the surfaces is borne by contact between the asperities. The remaining part of the load is carried by the pressure in the lubricant film separating the surfaces in the rough valleys [Wil78]. Mixed lubrication regime combines shearing of the lubricant layers and hydrodynamic flow between surfaces during sliding [Kar13].

### 2.3.2.3 Boundary lubrication

Boundary lubrication occurs when the film thickness is very small, typically less than the composite surface roughness [Ham04]. This implies there is considerable asperity contact and the normal load is entirely carried by the contacting asperities. In this case, the external pressure is sustained only by elastic-plastic deformation of the surface asperities of

the less resistant body. Experiments have indicated that in boundary lubrication at most a few monolayers of lubrication molecules are present between the sliding surfaces, but these have a profound effect on the sliding process [Per98]. Those layers are usually called boundary layers and they prevent dry metal-metal contact from occurring. According to their structures, the boundary layers can be divided into adsorption film, chemical reaction film and thicker viscosity film. According to lubrication mechanisms, boundary films are divided into polished film or softening film [Wen11]. Boundary lubrication regime is the most common lubrication regime in sheet metal forming including in deep drawing.

### 2.3.2.4 Hydrostatic lubrication

In some cases, hydrostatic lubrication occurs at some restricted parts of the contact zones. It is characterized by the repartition of the contact forces between the asperities and the trapped lubricant in the closed volumes of the raw surface [Vol02]. Another example can also serve the observed lubricant macro-pockets which are formed between the thickened border of the flange and the die corner during the drawing of a rotation symmetric part [Lan94].

Figure 2.1 gives a schematic representation of the Stribeck curve which includes the different lubrication regimes. Table 2.1 also provides possible values of the coefficient of friction with respect to the lubrication regime. It is to notice that in deep drawing, velocity is expressed in mm/s which gives the Hersey parameter the unit [mm]. This parameter can, hence, be related to the thickness of the lubricant film as well as to  $\lambda$ -ratio.

Type of friction	friction state		Interface element	$\mu$
Sliding friction	I	dry friction	vacuum	$> 1^{(1,2)}$
	II	unlubricated friction	gaz, vapours	0.1 – 2
	III	boundary lubrication	lowest lubricant amount	0.1 – 0.3
	IV	mixed lubrication	partially lubricated	0.01 – 0.1
	V	hydrodynamic lubrication	oil	$\leq 0.01$
		aerodynamic lubrication	gaz	0.0001
Rolling friction	elastohydrodynamic or mixed lubrication		oil, grease	0.001 – 0.005

Table 2.1: Ranges of the coefficient of friction for various types of friction and lubrication regimes (1 – metall/metall, 2 – ceramic/ceramic) [Som14].

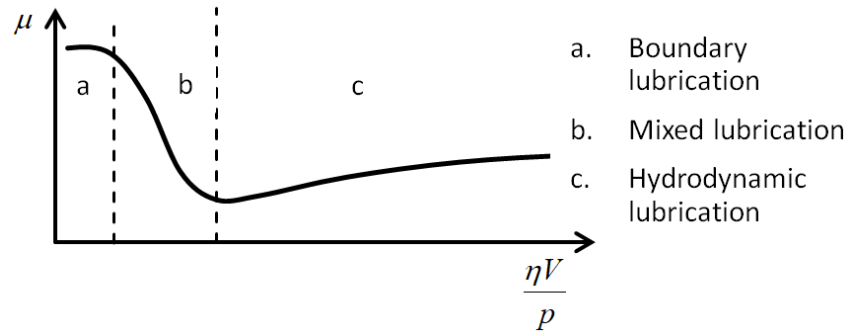


Figure 2.1: Schematic representation of a Stribeck curve.

## 2.4 Friction mechanics

Contact between rough surfaces happens only on a very small fraction of the apparent area at the tips of the contacting asperities. This was first put in evidence experimentally by Bowden and Tabor [Bow39] and Schnurmann [Sch42]. The generated contact pressures at these contacting asperities are sufficient to cause local adhesion and welding. Hence, the tangential force that is required to shear those junctions is a major component of friction force between the sliding metal surfaces [Bow43]. Moreover, the junctions are assumed to be related to the hardness and the shear flow stress of the contacting materials. For certain conditions namely when a hard surface slides over a soft one, the so-called "ploughing" can also contribute to the resulting friction [Bow50]. This is the case in deep drawing where tool surface is usually harder than the zinc coating of the blank. Thereby, the asperities of the tool surface penetrate the soft ones of the zinc coating and plough them via plastic deformation. If shear strength is exceeded, it results either in grooves or in fracture, tearing or fragmentation. Teer and Arnell [Tee78] well summarized the above explanations in their work. They stated that material interaction during sliding friction manifests itself in the form of adhesion and material displacement. These cause, in turn, energy losses due to the resulting elastic and plastic deformations as well as fracture. Therefore, one can distinguish adhesion and ploughing forces as the main components of the overall friction force.

Beside the introduction of  $\mu$  to designate the coefficient of friction, Euler also promoted the distinction between static and kinetic friction and that the coefficient of static friction must be greater than that of the kinetic friction [Eul50; Bla08]. Later on, Lecornu (1905) formulated the hypothesis that before macrosliding occurs, there exists a microsliding which is proportional to the applied compression force [Lec05]. However the most trustable experimental proof was published only later by Verkhovski [Kra77] and Rankin [Ran26]. Verkhovski introduced the term "pre-sliding" which precedes the steady sliding [Kra77]. During pre-sliding, microslip occurs at some points while unbroken contact still remains at some others as long as the applied load does not cross a certain threshold called "static friction force". Beyond the threshold, all contact will break whence the observed macro-sliding. This phase is called "gross sliding" or "kinetic friction" [Par04]. The transition from stiction to motion or kinetic friction is called "break-away". In the first phase of deep drawing process, the material flow is taken only from the blank thickness since the transmitted punch force does not excel yet the friction force in the flange which is equivalent to the break-away force. In the following phase when the transmitted

punch force is high enough, the actual deep drawing process begins corresponding to the gross sliding. Here, the punch force is transmitted to the flange zone through the sidewall [Fri08; Doe10]. In this work, the focus will remain only on the gross sliding and the pre-sliding will not be discussed further.

### 2.4.1 Adhesion

#### 2.4.1.1 Description and classification

Before the model of Bowden and Tabor saw light, Newton (1643-1727) put already two basics questions during his observation of the adhesion phenomenon. The first question invokes the required force to separate the bonded components. It is defined as the practical adhesion. The second one refers to the mechanism that holds the component together. It is called fundamental adhesion. An extensive review of the history of the latter is given by Packham [Pac18]. The real steps in the investigation of adhesion were undertaken only few centuries after Newton by McBain and Hopkins (1925). They considered that there were two kinds of adhesion namely specific adhesion and mechanical adhesion [McB25].

The main idea behind mechanical adhesion is that adhesion occurs in the form of penetration and the following solidification of liquid adhesives into pores, cavities and other irregularities of the surface of the substrate or adherent. It is discussed in detail by Packham [Pac92]. In turn, specific adhesion refers to the adsorption theory of adhesion. It implies that interaction between the surface and the adhesive takes place in the form of physical adsorption, chemical adsorption or simple wetting. The adhesive can be one of the contacting surface and the adherent the counterpart.

Other theories such as the electrostatic theory and the diffusion theory also exist. The former is characterized by the transfer of electric charges between the adhesive and the substrate. It is more relevant for the adhesion of small particles. In turn, the diffusion theory is more appropriate to contact between polymers than between metals.

#### 2.4.1.2 Mechanism of adhesion

In the model proposed by Bowden, the adhesion term  $\mu_a$  in the coefficient of friction refers to the adsorption theory where physical or chemical adsorption occurs depending on the type of bonding [Pac18]. Chemical adsorption includes mainly the covalent bonds where electrons are shared between the atoms of the two surfaces. In turn, physical adsorption comprises diverse types of bonding including hydrogen bonding, ionic bonding, ion-dipole interactions and bonding from weak secondary forces resulting from dipoles best known as the van der Waals forces.

When the bonds are weak and can be easily broken, the adhesion force which is equivalent to the adhesive strength is small. On the other side, when adhesion results in strong junctions, the formed bond is in general stronger than the cohesive bond of the weakest of the two materials [Buc71]. The adhesive strength is then greater than the shear strength of the softest material of the contacting primary surfaces. In order to separate the joint asperities, the weakest asperity has to be shorn which results either in material

transfer to the surface of the stronger material or generation of wear particles. The progressive accumulation of transferred material from the sheet metal on the tool surface alters the latter by creating localized macroscopic roughness. Later on, this will cause pronounced scratching on the sheet metal surface. The whole material transfer process with the subsequent scratching is called "galling". Many literatures cover the galling effect in metal forming. The conditions of its initiations are thoroughly elaborated in Kim [Kim08] and Wang [Wan15]. The mechanism of its formation is extensively explained by Schedin [Sch93; Sch94].

#### 2.4.1.3 Quantitative evaluation of adhesion

The identification of surface film and material transfer formed during tribological contact can be achieved by surface analyses. The utility of a particular analysis depends on the importance of one or more of the properties of the applied analytical techniques namely lateral resolution, specimen damage, depth resolution and the availability of chemical information. Auger Electron Spectroscopy (AES) and X-ray photoelectron spectroscopy (XPS) are, by a wide margin, the most used surface analytic techniques in tribology [Whe84]. By means of chemical techniques for instance, it is possible to reveal the existence of the localized adhesion and its distribution over the contacting surfaces.

The amount of transferred material can also be characterized by optical measurements. Thereby, the size, the thickness and the form of the flakes of transferred material can be determined with good accuracy using electronic microscope [Puj12].

Adhesion can be quantified through assessment of galling in deep drawing. Effectively, depending on the size and amount of transferred material on the tool surface, the resulting scratches on the workpiece surface can be analyzed. The size of those scratches is evaluated by means of surface topography measurement and the surface can be categorized into scratched, lightly galled and medium galled [And98].

#### 2.4.1.4 Influencing factors

The occurrence of a particular type of adsorption depends mostly on the nature of the contacting surfaces and the type of lubricant. The force necessary to separate the interfacial bonds is the adhesive strength. The presence of surface films such as oxide and lubricant can reduce the adhesive strength. The degree of reduction also depends on the chemical properties of the metal and lubricant, the lubricant viscosity, the lubricant pressure and the lubrication regime either mixed or boundary [Kli94].

##### Cleanliness of the contacting surface

The cleanliness of the contacting surfaces i.e. the degree of absence of a covering oxide or other layer is an important factor on the enhancement of adhesion. Effectively, a study of Bowden and Moore [Bow45] on copper – steel sliding contact has shown that when the contacting surfaces are clean, many particles of copper were left adhering to the steel. A simple low resolution micrograph was enough to measure the size of an adhered copper particle. Similarly, Buckley performed extended experimental investigation [Buc71] with various nonferrous metals (copper, gold, silver, nickel, platinum, lead, tantalum, aluminum and cobalt) contacting an iron surface. He states that strong adhesion always

occurs when both nonferrous and iron have clean surfaces resulting in material transfer. In turn, So [So,04] pointed out that oxide layers have profound effects on friction and wear of the parent metals. The frictional force caused by rubbing between metals can be reduced in the presence of oxide films. Due to frictional heating, considerably thick oxide films can also be formed on the rubbing surfaces of metals, when the normal load and sliding speed are high enough. Khan *et al.* [Kha16] observed change of adhesive shear stress with respect to the heat treatment temperatures of the surfaces. Hereupon they state that oxides developed on the alloy surfaces adversely affect the adhesive shear strength and therefore affect adhesion. It is, however, not evident to tell whether friction is governed by metal-metal, metal-oxide or oxide-oxide contact based on simple observation only. Each individual case must be examined carefully as explained by Dorinson [Dor85]. In general, there are few cases that can be distinguished with respect to the hardness of the substrate and the strength of the oxide layer.

In the first case, if the parent metal it is soft and the superficial oxide layer is weak, then the oxide layer can extensively disintegrate even at the lightest load leading easily to a predominant metal-to-metal contact. Welding of the contacting asperities takes place as a result of covalent bonding. If the oxide is still softer than the underlying metal, such as  $\text{Fe}_3\text{O}_4$ ,  $\text{Cu}_2\text{O}$ , or  $\text{ZnO}$ , it will function as lubricant on the rubbing surfaces and will reduce the frictional force as well as wear of the parent metals [So,04].

In the second case, if the parent underlying metal is hard with robust oxide layer, then the contact is oxide against oxide. Although there is no welding, adhesion in terms of physical adsorption still occurs by means of weak van der Waals forces.

There are cases when the underlying metal is soft such as copper, but the oxide layer holds for light loads, sustaining therefore an oxide-to-oxide contact. The asperities, however, deform already plastically leading to a constant coefficient of friction. The load gradually increases and the oxide layer starts to break down when the load reaches a critical value. Hence, metal-to-metal contact occurs and become predominant.

### Crystal structure and compatibility of the metals

Besides the influence of the cleanliness of the contacting surfaces, Buckley made two more statements [Buc71]. Firstly, as nonferrous metals have different crystal structures, he deduced that packed hexagonal metals exhibit lower adhesion than body- and face-centered cubic metals do. Secondly, he showed that chemical reactivity or electro-positivity exerts an additional influence on the forming bonds as more chemically active metals exhibit stronger bond when compared to other metal with the same crystal structure and comparable cohesive energy. The compatibility of the metal elements of the contacting surfaces influence adhesion considerably [Law11]. In the case when oxygen is present on the surface of the nonferrous metals, bonding still forms between the metals and the oxygen. The measured adhesive forces to fracture could be related to the metal to oxygen chemical bond energy.

### Boundary layers

When lubricant oil is applied at the contacting interface, the coefficient of friction falls considerably from 0.6 – 0.7 in dry clean contact of copper – steel to about 0.15 under the same contact parameters [Bow45]. Effectively, in the presence of lubricant, the so called boundary layers form at the metal surfaces. They are fundamentally meant to protect the surfaces against any solid – solid contact in boundary lubrication regime [Viz04].

They are formed as a result of the interaction (physical – chemical, colloidal – chemical, or chemical) between the rubbing surfaces and the lubricant. They promote decrease in wear of rubbing parts and prevent seizure of friction units [Buy04]. The detailed description of the formation of boundary layers is very complex and out of the scope of this work. However, it is important to mention the basic step [Hsu01; van06b]:

1. Oxidation of the base oil hydrocarbons which results in the formation of hydrocarbon radical with polar heads (e.g. aldehydes, ketones, alcohols).
2. Physical adsorption of the polar heads of the oxidation products to the atoms of the contacting surfaces.
3. Chemical adsorption of the polar heads of the hydrocarbon chains in some occasions to form stronger bonds
4. Adsorption or reaction of the additives (complex compounds based on phosphorus, sulfur, barium and chlorine) contained in the lubricant with the contacting surfaces.

The nature of the lubricant, the nature of the contacting surfaces, the compatibility between the lubricant and the surface and the environmental conditions especially the thermal conditions are the most dominating factors in the formation and the subsequent effectiveness of boundary layers of lubricant [Shr16; Hsu01]. The lubricating boundary film between the two surfaces is no longer a liquid/semiliquid layer but only a very thin film of molecular dimensions [Kaj04]. Hardy provided the first assumption that the molecules of the lubricant are oriented by the attraction fields of the solids so that their long axes are at right to the solid faces [Har22]. Thereby, they form a high-viscosity carpet-brush-like layer which aims to reduce wear and friction. The viscosity of boundary layers essentially differs from the bulk viscosity of lubricating media [Der52]; these layers possess some real elasticity and can be considered as quasi solid and quasi crystalline bodies [Akh63].

There is a claim that the formation of the atomic junctions is strongly impeded and adhesion can be neglected during the sliding contact in sheet metal forming as lubricant is involved [Kar13]. It is true that the amount of adhered particles decreased but adhesion still occurs nonetheless according to Bowden [Bow45]. By means of a radioactive method, Sackmann *et al.* [Sac44] was able to measure the pick-up of metal in lubricated contact. The measurement was made on a small curved surface of a slider after it has traversed a certain distance. Although the results may differ of his, Bowden stated that the measurement of Sackmann has shown the evidence of metallic adhesion through the lubricant film [Bow45].

## 2.4.2 Plastic interaction of asperities

### 2.4.2.1 Description

In frictional contact where the coefficient of friction is less than 0.1, the lubricant boundary film is assumed to be effective. The parameters such as the chemical structure of the lubricant substance, its chain length, and the nature of the substrate surface material influence considerably the effectiveness of the boundary films. By the increase in the effectiveness of boundary film, the effects of adhesion become small. Therefore, non-adhesional mechanisms such as the so-called "ploughing" become more dominating in the frictional process [Dor85]. Ploughing relates the degree of plastic deformation occurring as a result of the asperity interaction [Bow50; Men13]. Effectively, during sliding, interaction of two rough surfaces may result in mechanical inter-locking.

Firstly plastic deformation and displacement of the interlocking surface asperities primarily occurs. If one of the sliding surfaces is harder than the other, the asperities of the harder surface penetrate the softer ones. If shear strength is exceeded the asperities of the harder material plough the surface of the softer one via plastic deformation which results either in grooves or in fracture, tearing, or fragmentation.

Secondly ploughing may also occur as the result of impacted or entrapped wear particles. Ploughing not only increases friction, but also creates wear particles, which, in turn, increase subsequent friction and wear [Sah05].

### 2.4.2.2 Quantitative estimation

The quantification of ploughing is usually performed by means of experimental and mathematical models. In many cases, the ploughing coefficient of friction  $\mu_p$  is related to the measured value from nano-scratch tests as a single asperity experimental model. For the test, a tip with a given geometry ploughs a sample surface. This method has the main disadvantage that the indenting tip is not perfectly perpendicular to the scratch surface which may lead to big errors in the measured values [Liu15a]. Another disadvantage of such model is that it does not allow to make definite conclusion on ploughing contribution for an entire surface which has many asperities. This question was already developed in detail earlier by Blau [Bla91a].

By means of the slip line field theory, Challen and Oxley [Cha79] studied the problem of asperity deformation. They limited their study to the case of sliding of a hard surface over a relatively soft one. Ploughing was the focus of the investigation. They proposed models for asperity deformation namely a rubbing model, a wear model and a cutting model which provide a value of the ploughing term  $\mu_p$  in the early model of Bowden with respect to angle between the contacting asperities as one of the roughness characterizations.

One of biggest limits of the models that were proposed above lies in their incapability to describe the ploughing when the elastic recovery is concerned. This is due to the conditions of application of the slip-line field theory. Lafaye [Laf06] proposed an analytical model that incorporates the elastic recovery on the example of a conical tip with a blunted spherical extremity. Effectively, tips that are used in micro- and nanoscratch tests are not perfectly conical but have blunted spherical extremities. The major difficulty in the

development of the model is the consideration of the shape of the contact area with respect to the elastic-plastic behavior of the contact. Barge *et al.* [Bar03] used the FE-simulation for the investigation of the effect of the elastic recovery and the strain hardening on the coefficient of ploughing. Their model showed better prediction than the one of Bowden and Tabor when the comparison was made through experimental scratch test.

Recent models were developed using molecular dynamic simulations. Mishra *et al.* [Mis12] presented an analytical model for the determination of  $\mu_p$  based on a single asperity contact. The model is represented by a conical tip with a spherical extremity indenting and ploughing a flat surface. The model has the main advantage to consider both the elastic-plastic behavior at the contact zone and the influence of the adhesion at that level.

### 2.4.2.3 Influencing factors

Ploughing contribution may or may not be significant; its magnitude depends on the surface roughness and relative hardness of the two surfaces, on the size, shape and hardness of any wear debris and reaction products trapped between them [Bhu01]. More precisely, the surface texture of the harder surface controls the ploughing contribution to friction while its mean surface roughness  $R_a$  is less influential. Furthermore, the hardness of the softer surface impacts the frictional behavior of the tribosystem only under certain texture of the referred surface [Men11].

The shape of the asperities also affects the deformation. Sharp asperities cut the material creating a groove on the ploughed surface and at the same time wear particles are generated in the form of chips. In the case of blunt asperities, material is just shifted to the sides of the created groove. For this purpose, the slip line field theory was extensively used. It is an approach to model plastic deformation in plane strain only for a solid that can be represented as a rigid-plastic body. Elasticity is not included and the loading has to be quasi-static. A detailed description of the mentioned theory as well as its application is given in the original work of Hill [Hil50] and Johnson [Joh70].

## 2.5 Friction modeling

Friction laws are very often interpreted by means of models which take the form of a relationship between coefficient of friction and selected variables and parameters. Those friction models are also used in FE Simulation of deep drawing processes. Depending on the used approach, these selected variables and parameters can have different meanings.

### 2.5.1 Empirical friction models

Empirical or semi-empirical models are not able to include any effective parameters that are involved in tribosystem component interaction [Ema17]. The obtained mathematical formula of the coefficient of friction simply represents certain frictional behaviors of the tribosystem without providing any hint on the actual mechanism behind friction. Among the empirical models, one can enumerate the Coulomb friction model which exhibits a

linear dependence of the friction force to the normal one through constant coefficient of friction. This model is widely used in deep drawing simulation owing to its simplicity. It has, however, been shown to be limited only up to a certain pressure value [Nin17]. Moreover, Roll [Rol08] has explicitly pointed out that more accurate friction models are needed in order to incorporate various aspects of deep drawing process that are not or cannot be reflected through the simple constant coefficient of friction.

Other empirical models have already emerged such as the models proposed by Karnopp (1985) [Kar85], Armstrong-Hélouvy model [Arm91] and Hess and Soom [Hes90; Liu15b]. Other dynamic models have also been developed based on state variables [Rud13] such as Dahl's model [Dah68] [Mar15], the bristle model by Hessig and Friedland (1991) , Bliman-Sorine model [Bli97], LuGre model by Canudas *et al.* [Can95] and Leuven model by Swevers *et al.* [Swe00]. Those models are at least one step more advanced than the Coulomb model where velocity is also considered besides the contact pressure. However, they were developed for compensators and had not found any actual application in deep drawing process simulation. Most of the models also contain many parameters that are not straightforward to determine in practice. In relation to that, it is very difficult if not impossible to measure the real time values of the coefficient of friction directly from real processes [Ptull]. Thereby, model calibration and validation are difficult to process. In addition, these empirical models are not attractive for the investigation of the physics of friction.

## 2.5.2 Physics-based friction models

Constitutive approaches relating stress and strain fields are used to develop physics-based friction model. The employed parameters are extracted from the basic or fundamental behavior of materials [Mel12]. In many cases if not in all, a physics-based model is not a self-sufficient model in itself, but rather a chain of various models which serve as links with specific functions in the whole model.

Bowden and Tabor [Bow50] proposed the first template of a physics-based friction model. According to them, the coefficient of friction  $\mu$  is the sum of two terms namely an adhesive term represented as  $\mu_a$  and a ploughing term represented as  $\mu_p$ . How each term is obtained constitutes the subject of the subsequent researches on friction. The path of friction modeling has taken two different but interdependent ways namely the path of studying adhesion mechanism related to  $\mu_a$  and the path of studying contact mechanics related to  $\mu_p$ . A good review of the most important development in the study of friction exclusively for metal forming from the 40's to our days is given by Nielsen [Nie17]. The main lines of the review show that the study was emphasized on the analysis, interpretation and theoretical determination of the real area of contact between the asperities. In other words, contact mechanics has caught more attention while adhesion was understated. The main reason is the presence of lubricant which is assumed to reduce considerably the adhesion effect as already discussed in 2.4.1.

Physics-based models can span length scales from nanometer to meter, and time scales from microseconds to minutes. Nielsen *et al.* [Nie11] investigated the size effect on friction and lubrication in metal-forming where they showed that friction increases through downscaling. This scale issue was also discussed by Blau [Bla91b; Bla91a] in the early 90's. He described that the choice of scale depends, on the one hand, on the background

of the investigator. On the other hand, the scale refers to the level of accommodation of the friction within the tribological system. Moreover, the presence of the liquid lubricant at the contact interface introduces further parameters into play.

Wilson [Wil95] developed a friction model for sheet metal forming that takes into account the different lubrication regimes at the contact interface. The model represents the friction force as the sum of the adhesion friction, ploughing friction and hydrodynamic friction contributions depending on the occurring lubrication regime. A model similar to that of Wilson was developed by Khonsari [Lu,15; Akb08] where the total friction force is the sum of the asperity contact friction and hydrodynamic friction contributions. The particularity of the model is that the difference between adhesion and ploughing is not made anymore. A general coefficient of friction characterizing the asperity contact is introduced instead. For the hydrodynamic friction, the corresponding shear force is pressure dependent. Hence, the main core of the model comes down to determining the repartition of the total load between the asperities and the lubricant. Here, an additional term is introduced namely the squeeze force of the lubricant.

Baspinar [Bas16] combined both models considering their strengths. He initially puts Wilson's model as the basis of the friction model since it is easier and faster to apply. It is, however, weak in describing the boundary lubrication regime and the early beginning of mixed lubrication regime. This is mainly because it good describes the frictional contact only from a certain lubricant film thickness which is often very small in deep drawing either due to the insufficient lubricant amount or high contact pressure. Therefore he introduced the Khonsari's model which is more accurate despite its requirements to iteratively solve nonlinear equations and its dependence on initial guesses and tolerances. He insisted that since the existing friction models are not perfect, it is recommended to combine them to take advantage of the strength of both. Similarly to the model of Baspinar, Hol [Hol13] and Karupannasamy [Kar13] developed a physics-based friction model for sheet metal forming application combining several sub-models. Their model spans all the lubrication regimes. For the modeling of the boundary lubrication regime, they used the Westeneng [Wes01] contact model for asperity flattening. The growth of the real contact area during sliding is considered using the Tabor's formulation of junction's growth [Tab59]. Ploughing contribution is given by the model proposed by Challen and Oxley [Cha79]. The effect of adhesion is neglected assuming that only shear of lubricant boundary layers occurs. For hydrodynamic lubrication regime, the model is based on the solving of the Reynolds equation considering the effect of surface roughness. They describe the mixed lubrication regime by combining hydrodynamic and boundary lubrication regime models. The effectiveness of their models has been presented in many occasions for the FE-Simulation of car body parts [Sig15; Sig16].

The development of physics-based model provides important knowledge on friction. However, they are still based on hypotheses and approximations. And the lack of realistic experimental data and methods that enable to validate them represents a great obstacle.

### 2.5.3 Estimation of the real contact area

#### 2.5.3.1 Modeling of the rough surface

The determination of the real area of contact is closely associated with the modeling of the rough surface. The first popular model for contact of rough surfaces was proposed by Archard [Arc57]. It consists of superimposed hemispherical asperities of different length scales. The contact model utilizes then the Hertzian contact of a sphere and a plane half space where a nonlinear relationship exists between the real area of contact and the applied load in elastic contact. By incorporating the multi-scale approach in the description of the rough surface, Archard could re-establish a linear dependence between the real contact area and the applied load. The physical significance of the model is that the real area of contact increases either by the enlargement of the existing area or the formation of new contacts.

Later on, the model of Greenwood and Williamson replaced the model of Archard where the asperities were represented as hemispheres without the superimposition approach. They assumed the following: (1) asperities have the same radius of curvature, (2) asperity heights are distributed around an average value, (3) deformations of asperities do not affect each other and (4) contact exhibits an elastic behavior [Gre66]. This allows to extend the Hertzian solution of an individual hemispherical asperity contacting a flat surface to a population of asperity with a probability distribution function.

Using an exponential probability distribution of asperity heights, Greenwood and Williamson predict linearity between the true contact area and the load. In case of Gaussian distribution the linearity was only approximately approached [Giu09]. Replacing the exponential distribution by a normal one and adding an exponential autocorrelation function [Whi70], Onions *et al.* calculated more accurately the real contact area for rough bodies as the rough surface is described in a more complete manner [Oni73].

In the case when the surface roughness resembles to a self-affine fractal over a wide range of length, the Greenwood-Williamson model shows its limit. Furthermore, when the surface is perfectly fractal, the model fails completely since it is not able to detect neither individual asperities on the surface nor its curvature [Gao06]. To cope with the problem, Ciavarella proposed a model which consists of an elastic half-plane pressed against a rigid fractally rough surface with a profile defined by a Weierstrass series (a sum of sinusoidal profiles, with progressively decreasing wavelengths). The results have shown that the contact process exhibits limiting self-affine fractal behavior at small scales and the total contact area is a lacunar fractal. The apparent fractal dimension is load dependent. This can be explained through the deviation from simple power-law fractal behavior at low wavenumbers [Cia00]. Other important works on contact involving fractal surfaces are of Majumdar and Bhushan [Maj91], Warren and Krajcinovic [War95], Willner [Wil04] and Yan and Komvopoulos [Yan98].

Another contact model was developed by Westeneng [Wes01] based on an energy analysis and the volume conservation. Instead of using the summit height distribution as Greenwood and Williamson did, he described the surface roughness rather with the surface height distribution which is, in turn, based on surface points that are obtained from surface measurements. The advantage of this rough surface model is the direct use of the real surface heights instead of the summit based stochastic parameters. The contact

model consists of the modeled rough surface flattened by a smooth rigid tool surface. The material is assumed to behave as ideally plastic which imposes a restriction on the mechanical behavior of the surface material compared to real surfaces. In such model, it is also important to ensure that the measured surface area for the model is really representative of the total area.

### 2.5.3.2 Approaches in the estimation of the real area of contact

Bowden and Tabor (1939) [Bow39] stated the direct proportionality between the applied load and the contact area holds true only when plastic flow is involved at the interfaces of the approaching solids. However, experiment showed that for randomly rough surfaces, even when the contact is purely elastic (i.e., no plastic flow), the area of real contact is proportional to the load as long as the contact area is small compared to the nominal contact area [Per06].

Holm (1959) mentioned that although the overall stresses are in elastic range the contact spots are much higher so that the elastic limit will be exceeded and the contact will yield plastically [Hol99; Gre66]. However, he noticed that since the tips of the asperities are at different levels of their deformation, the stress distributions must differ. Therefore, some of the asperities are under conditions of elastic deformation. In general all contacts can be divided into three groups, depending on the type of deformation, i.e. elastic, plastic and elastic-plastic. Greenwood and Williamson introduced the index of plasticity as a criterion for the transition from elastic to plastic deformation [Kra77; Shi12].

By means of the slip-line field theory, the stress field at the contact between the asperities was studied by Green (1965) considering the different wedge shape joints [Gre54]. The key point here is the introduction of the interdependence of the normal and shear stresses by means of a yield criterion. Tabor (1959) explained that the increase of the real contact area was due to the reduction of the yield pressure by an imposed shear stress during sliding [Tab59]. The surface roughness is, however, not included in the analysis.

Bowden and Tabor (1942) and later on Greenwood (1965) and Fogg (1967) showed also that the bulk strain and the surface expansion have a big influence on the flattening of the asperities and the increase of the real contact area [Bow42][Gre66; Fog67]. This was to emphasize that friction is not only a pure surface effect, but rather a more complex phenomenon in which the influence of the bulk material is also to be considered. However, the bulk material was assumed to be negligible in the first attempt to determine theoretically the real area of contact.

Wanheim *et al.* were able to establish a dependence of the real contact area and the friction stress on the contact pressure based also on the slip line field theory with a corresponding experimental validation. The importance of closed lubricant pockets was also mentioned which are able to take a part of the external normal load in terms of hydrostatic pressure [Wan73; Wan74; Bay76]. Thereby, the normal pressure on the asperities is reduced and so is the real contact area. This has been later exploited in the frame of surface texturing of sheet metals in order to improve the properties of tribosystems involving them [Pod12; Vil17].

## 2.6 Wear

### 2.6.1 Adhesive wear as severe wear

As well described by Stachowiak and Batchelor [Sta93], adhesive wear is a manifestation of severe wear which is easily identified by its high wear rates and an unstable coefficient of friction. In lubricated contact, it is the consequence of the failure of lubrication where the separation of the contacting surface is not ensured anymore.

Strong adhesion between the contacting asperities, plastic shearing of the softer asperity which subsequently adheres to the opposite surface stand behind adhesive wear [Jim11]. Effectively, material in the softer or sharper asperity deforms in a series of shear bands to accommodate the relative movement, i.e. there is no sliding along the asperity contact line. When each shear band reaches a certain limit, a crack is initiated or an existing crack progress till a new shear band is formed. The crack extents across the asperity and eventually a particle detaches from the deformed asperity. The particle of metal detached from the soft asperities remains attached to the other surface. It may subsequently be removed by further asperity contact to form a true wear particle or it will remain on the surface to form a transfer film. The latter and the possible subsequent wear particle generation are characteristic features of adhesive wear which can a dramatic effect on wear rate [Sas81].

In sheet metal forming, adhesive wear is known as galling which is characterized, as already mentioned earlier, by the alteration of the tool surface due to material transfer from the sheet metal causing damage and fracture on the sheet metal surface such as scratching [Sch93]. The mechanism behind galling occurs in three stages namely the initiation, the lump growth and the severe scratching [van06a; Sch93]. Effectively, as material transfers and accumulates to the tool surface, lumps are formed which are at the origin of the initiation of local microscratching of the sheet metal surface. Those microscratchings may become too severe and cause seizure. Experimental study of Attaf *et al.* [Att02] has shown that the die radius is very prone to adhesive wear in deep drawing as it contains the highest pressure zones. The most ordinary model that describes adhesive wear is the Archard model.

Schedin [Sch94] used various combinations of tool and sheet materials in order to observe the galling initiation. His observation concerned in particular the influence of the sheet surface chemistry and topography as well as the tool surface conditions. He concluded inter alias that tool surface defects such as grinding scratches and carbide serve as initiation sites for the sheet material transfer. In a later time, Gaard *et al.* [Gaa09] revealed through their investigation that the amount, size and distribution of carbide enhance the amount of material transfer from the sheet metal. Also, Schedin said that tool surface irregularities facilitate transfer of particle by simple mechanical interlocking. He mentioned that zinc coating is very sensitive to induce galling. Podgornik *et al.* [Pod12] concluded in their work that the removal of the tool asperity peaks provides a plateau-like topography which can improve the galling properties of forming tools. Coating of the tool can also provide a high resistance to galling. The Galling initiation was also investigated by Wang *et al.* [Wan15] with hot-dip galvanized steel where they described the three stages of galling initiation. Thereby, they underlined the importance of the roughness difference between the sheet metal and tool surface topography. In addition, they stated that the

stretch bending can enhance galling further.

The selection of the right lubricant can reduce the effect of galling as Heide *et al.* stated [van06a]. Another very important conclusion of their work consists of the misleading information that may provide the coefficient of friction on galling. Effectively, they said that a low coefficient of friction at the start of the experiment is not a reliable indicator of galling prevention and so the lubrication evaluation is to be done based on long term testing instead of short term ones. This can be related to the difference between friction and wear. Effectively, friction is an instantaneous process with instantaneous measurement value while wear is a progressive process which requires a certain period of time to be measured.

## 2.6.2 Abrasive wear and severe-mild wear transition

Abrasive wear consists of a gradual loss of material and an associated generation of wear debris [Rig88] which takes place when a hard surface or hard particle also known as grit passes over a softer surface [Bhu99].

In his review of the mechanism of abrasive wear, Pintaude [Pin05] revisited the background understanding of the mechanism of abrasive wear. In brief, wear particles are generated through four main modes namely by microcutting, by microfracture, by pull-out of surface grains and/or through fatigue due to repeated deformation.

The mechanism of abrasive wear is generally classified in two categories in literature namely "two-body" and "three-body" abrasive wear. On the one hand, two-body abrasive wear is characterized by the sliding of hard asperities and/or firmly fixed grits over the soft surface causing cutting of the latter. On the other hand in three-body abrasive wear, the grits are loose. They can either roll or slide freely so that they can abrade both contacting surfaces.

The severity of abrasive wear correlates with the ratio of the hardness of the abrasive HA (surface or grit) to the hardness of the abraded surface H [Rab65b]. In their study, Coronado *et al.* [Cor13] showed that while HA/H is less than 1.9, the hardness of the abrasive has a considerable effect on wear rate. However, this correlation is not always verified depending on the nature and properties of the contacting surfaces. Hereupon, Sundararajan [Sun87] proposed an alternative model for the quantitative description of the wear particle generation based on deformation energy. He assumed that the generation of a unit wear volume requires plastic work to bring the surface material from zero strain state to the ultimate strain state at which failure occurs and debris particle is generated. The model validation concerned mostly two-body abrasive wear. Still remaining within the frame of two-body abrasive wear, Challen and Oxley proposed a 2D-model for abrasive wear mode based on the slip-line field theory [Cha84]. The model integrates the critical angle of the rubbing asperity, which was firstly introduced by Mulhearn and Samuels [Mul62]. Depending on this angle of attack, the groove formation on the surface follows different modes namely ploughing mode, wedge forming mode and cutting mode. While the ploughing mode is characterized by material dislodging without particle generation, cutting mode transforms the major part of the removed volume from the groove into wear particles. In the wedge forming mode, some material is removed and some remains on the edge of the groove. The model for two-body abrasive wear is well

discussed in Kato [Kat97]. Microcutting represents severe wear while ploughing is mild.

The three-body abrasive wear mode is not well understood until now compared to the two-body one. However, the work of Zum Gahr came up with the conclusion that the rate of three-body abrasive wear is one order of magnitude lower than that of two-body one [Zum98]. Effectively, the loose particles do not constantly abrade the contacting surface but only during 10% of the sliding time since they are more prone to roll than to slide. They rather leave plastic deformation in the form of multiple indentation groove on the surface [Boz99; Pin05]. Besides the hardness of the particles, the main influencing factors on the rate of three-body abrasive wear include the size, the geometry and the volume fraction of the abrasive particles within the lubricant as well [Kra61; Rab65a; Wil92; Zum98; Sta00; Sta04; Bel07]. In their work, Costa *et al.* [Cos17] show in a reciprocating test on aluminum that large and hard particles act as protuberance leading to abrasive wear. On the contrary, small particles are trapped into the pits of the surface roughness so that their further influence on damaging of the contacting surfaces is reduced. Moreover, Kato [Kat03] has investigated the severe-mild wear transition with respect to the size of the abrasive particles. He found out that small particles accumulate in the pits of the surface roughness to form compact layers leading to a fast transition from severe to mild wear. Many literature are available on the topic of severe-mild wear transition which is already beyond the scope of this work.

In deep drawing, the zinc coating of the sheet metal is considered to be the soft surface and the tool has the hard surface. However, the latter is also very often worn by debris particles. Masen [Mas04] has investigated the abrasive wear of sheet metal forming tool and he also proposed a micromodel for the quantification of the phenomenon.

### 2.6.3 Third body concept

The concept of third body was initially developed by Godet with the intention to bring into convergence the different points of view of mechanical engineers and material scientists about friction and wear within a common unified approach. In the original description, the contact interface consists of two first bodies (i.e. machine elements) and a separating intermediate third body [God98]. As defined within the frame of material science, the main characteristic of third body is its composition and microstructure which significantly differ from that of the first bodies. In the kinematic sense, third body carries out the function of accommodator of the velocity difference between the first bodies through its thickness [God84]. This is accomplished through shearing and the following reformation. Besides, according to Berthier [Ber04], third body fulfills three other main functions namely:

1. Transmission of the normal load which involves the load bearing capacity of the third body;
2. Separation of the first bodies to impede their interaction and thereby their wear;
3. Transformation of the kinetic energy into heat by shearing and then following partial or full dissipation of the generated heat via its flow.

On the one hand, third body can be artificially supplied to the interface as an extra-component from outside such as lubricant for instance. On the other hand, it can be

generated naturally from the direct interaction and degradation of the two first bodies through wear [God98]. Hereupon, according to Dienwiebel and Scherge [Die15], it can be either just a particle between the sliding surfaces or an entire layer with significant property difference from the first bodies. They can consist of oxide and contaminant layers or particles loosened from the first bodies [Ber04].

In addition, depending on its origin or its forming process, third body can have different denotations. It can be from the mechanical mixing of debris and surface contaminants and then named "mechanically mixed layer". It can be also a material transferred from the counterface and then named transfer layer [Kap00]. The latter is considered to be a static view of third body. Its analysis enables to determine whether it is an actual material transfer through adhesion or a static view of flowing film that accommodates the velocity difference between the surfaces [Ber04]. Fayeulle *et al.* [Fay92] described the structure of a near-surface zone in dry friction as shown in figure 2.2. Four different structures are defined after the surface was tribologically loaded namely:

1. detached particles forming a layer at the top surface;
2. debris layer;
3. tribologically transformed structure (TTS) as a new formed structure;
4. DIA (deformed initial alloy) – zone below the TTS.

On the one hand, the DIA–zone consists of deformed initial structure namely deformed grain boundaries, twins and shear bands. On the other hand, the TTS is already a new structure that is equiaxed and made of ultra-fine grains. Chemical analysis has, however, shown that the TTS still conserves the initial chemical composition of the bulk material. In opposite to TTS the detached particles and debris layer exhibit different chemical compositions than that of the initial bulk material. While the former contains a high amount of oxygen as generally made of oxide, the latter consists of a mixture of the two first bodies. All four structures can be considered as third bodies referring to the difference either in their composition or in their microstructure compared to the initial bulk material.

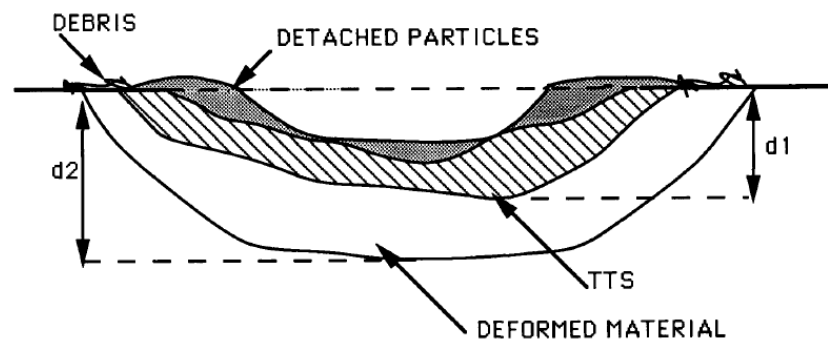


Figure 2.2: Schematic representation of superficial layer of various samples [Fay92].

As mentioned in earlier section, engineering surfaces are covered with either natural or artificial screen which limits adhesion. Therefore, the "clean" (i.e. free of oxide layers) sheet metal and tool surfaces can be defined as the first bodies in deep drawing. All

the involved oxide layers, lubricant film and lubricant boundary layer as well as the resulting wear products theoretically constitute the third body. The debris layer as a mixture of the two bodies i.e. tool and sheet metal coating surfaces can be evaluated with radionuclide-technique by activating the tool surface. In addition, as mentioned earlier, in mild wear a surface change of another kind occurs. The surfaces often become very oxidized. Therefore, the formation of a third body can be associated to mild wear.

## 2.7 Relationship between third-body and friction

Berthier [Ber04] stated that third body stands at the origin of friction. In hydrodynamic lubrication regime where the two surfaces are separated by the thick lubricant film, friction is associated with the rheology of the lubricant as third body in terms of its viscosity. The concept is already well developed. In the case of mixed and boundary lubrication regimes as well as dry friction, knowledge of the rheology of the acting third body is one of the required ingredients in order to predict friction and load based on the analysis of the third-body [God84]. The other requirements are inter alias:

1. the need of precise information on the transverse and longitudinal boundary conditions that apply to the third-body;
2. a general theory of thin film mechanics that enable to consider any potentially occurring rheological condition at the interface zone.

At the present days, there is still a lack of measurement capabilities that enable to record instantaneous contact pressures and the flow of solid third bodies. Therefore, the rheology and flow (or velocity accommodation) of solid third body are only estimated qualitatively by means of visualization tests [Des02]. This gives only a static view of the phenomena involved in the contact. A relative evaluation of the ductility and adhesion capability of third bodies can be achieved nonetheless [Sta04]. Another approach in the study of the rheology of third body is by means of the numerical tools. Cundall [Cun71] proposed a discrete element model that serves as a basis of the analyses of other authors on the mechanical behavior of third bodies as well as the characterization of their rheology as function of local parameters. Renouf *et al.* [Ren11] proposed an extended discrete element approach that they used for the simulation of the flow of solid third bodies. S

# Chapter 3

## Methods and Materials

In this chapter, the applied methodology along with the used materials for the investigation of the influence of the coating type and morphology on the tribological behavior of the corresponding tribosystem is described. The related experiments are performed at two locations namely at "thyssenkrupp steel Europe AG" and at the "Fraunhofer IW MikroTribologie Centrum".

Tribological tests in this work consist of deep drawing test and pin-on-disk test combined with radionuclide- technique. They provide tribological data such as coefficient of friction and wear rate. For chemical analysis, X-ray photoelectron spectroscopy (XPS) and Glow Discharge Optical Emission Spectroscopy (GDEOS) are applied. The main mechanical property of interest is the hardness of the surfaces. Therefore, nanoindentation technics is used. For the observation of the structure and the topography of the surfaces, Scanning Electron Microscopy (SEM) with Focused-Ion-Beam (FIB) feature and whitelight spectrometry are used. The measurements and analyses are performed on worn and unworn specimens.

### 3.1 Description of the tribological tests

#### 3.1.1 Strip drawing

Strip drawing test is one of the most used, if not the most used, experimental model for the determination and assessment of the frictional behavior of a tribosystem in sheet metal forming [Wag97]. In most of the cases, the test aims to investigate the influence of a chosen lubricant and/or the surface characteristics of a sheet metal [Klo06] by evaluating the resulting friction coefficient. The test also reproduces similar conditions in deep drawing as for instance in the flange [Beh17].

There are two principal types of strip drawing test namely the two-sided and the one-sided test. For this work, the two-sided test will be used and it consists of a strip drawn between flat dies. In this case, the sliding contact occurs on both sides of the sheet metal. The testing machine and a schematic representation of the test are shown in 3.1. The basic operating of test machine and the performance of the test are given as follow:

- The lubricated strip is pressed between two flat dies at which a given pressure  $F_N$

### 3.1. Description of the tribological tests

is applied from a hydraulic clamp. Contact pressure can be applied as constant or in an increasing manner.

- At its other end, the strip is gripped by a clamp and then drawn with a predefined constant velocity  $v$ .
- During drawing, the resulting friction force  $F_R$  is measured by means of a friction force measuring element. Together with the applied pressure, they are continuously recorded.
- The coefficient of friction is computed as half of the ratio of the measured friction force to the applied normal force. Half is taken because of the two-sided contact.

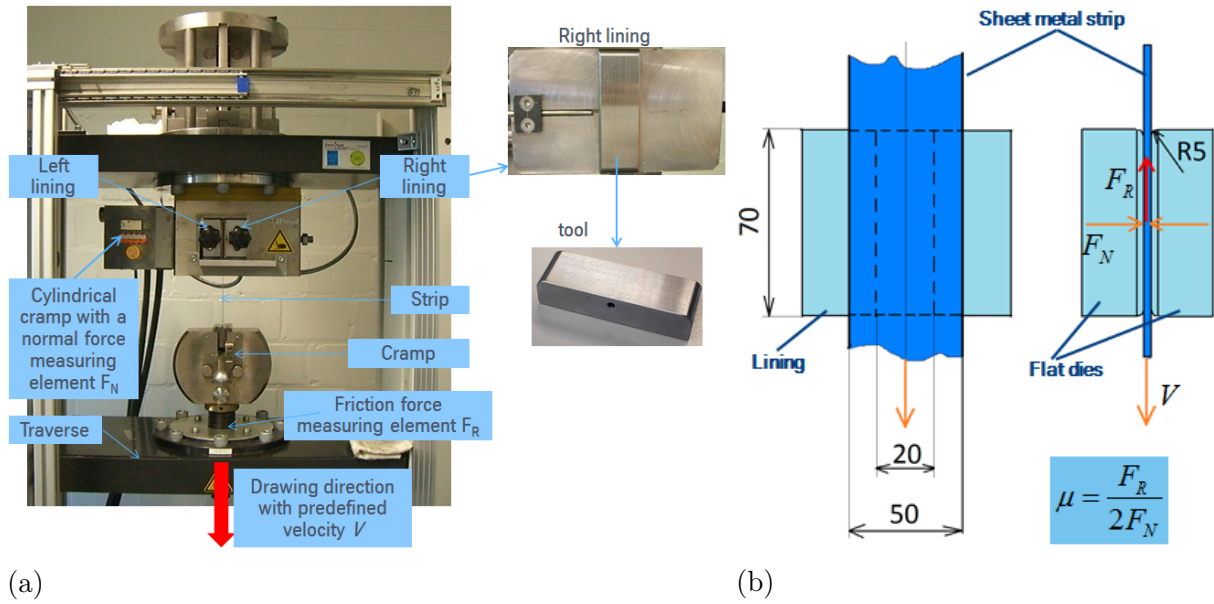


Figure 3.1: (a) - Strip drawing test equipment; (b) - Schematic representation of the strip drawing test with flat dies.

On the one hand, flat dies can be used with different surface areas from 660 ( $33 \times 20$ ) to 2700 ( $60 \times 45$ )  $\text{mm}^2$  with length lying along the drawing direction. They can be grinded or polished depending on the required surface roughness. The surface can be also coated and hardened. On the other hand, the strips have a dimension of  $700 \times 50$  mm and the sliding distance can be set up between 1 and 500 mm. Before the application of the chosen lubricant oil, the strips are immersed first in an ultra-sound bath and then in an acetone bath in order to remove the initially applied corrosion protection oil as well as other impurities and contaminants. Only after that, the chosen oil is smoothly and equally sprayed on the surface of the samples by a special lubrication machine where the desired amount can also be set up.

Scale effect may also influence the obtained results. In a preliminary work, comparison of results from strip drawing test with different tool sizes but under similar contact conditions are performed. The used tools with different sizes as shown in figure 3.2 have similar surface roughness but their surfaces underwent different treatments. The tools with small and big areas (i.e. 660  $\text{mm}^2$  and 2680  $\text{mm}^2$  respectively) underwent a surface hardening through plasma-nitriding process while the tool with area 1200  $\text{mm}^2$

is left unhardened. The hardness of the tool surfaces are given in table 3.10. The investigations of the influence of the tool size and the tool hardness were combined. The results of the tests are provided in figure 3.3, 3.4 and 3.5.

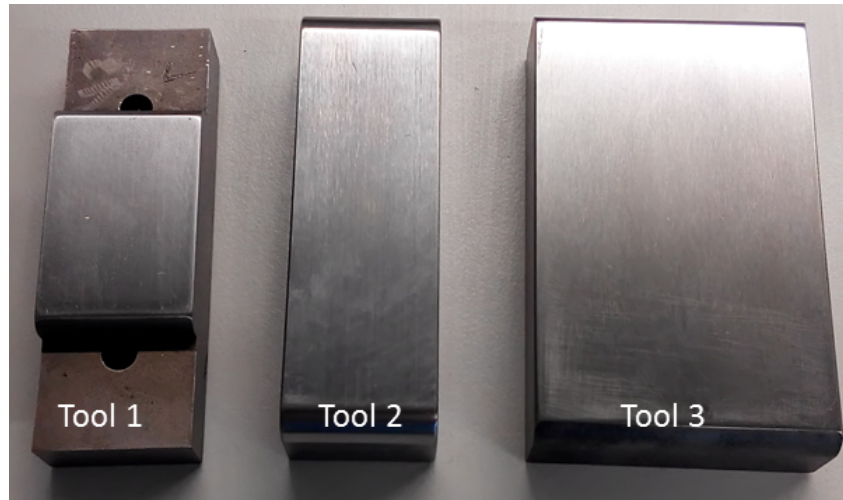


Figure 3.2: Strip drawing tools with different sizes: (a) tool 1 –660 mm<sup>2</sup>; (b) tool 2 –1200 mm<sup>2</sup>; (c) tool 3 –2680 mm<sup>2</sup>.

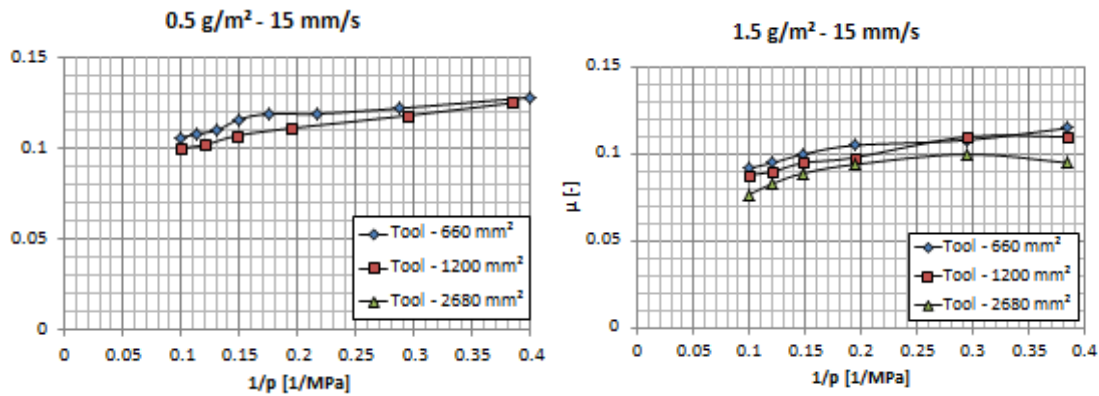


Figure 3.3: Comparison of the frictional behavior of tribosystems with different tool sizes at  $v = 15$  mm/s.

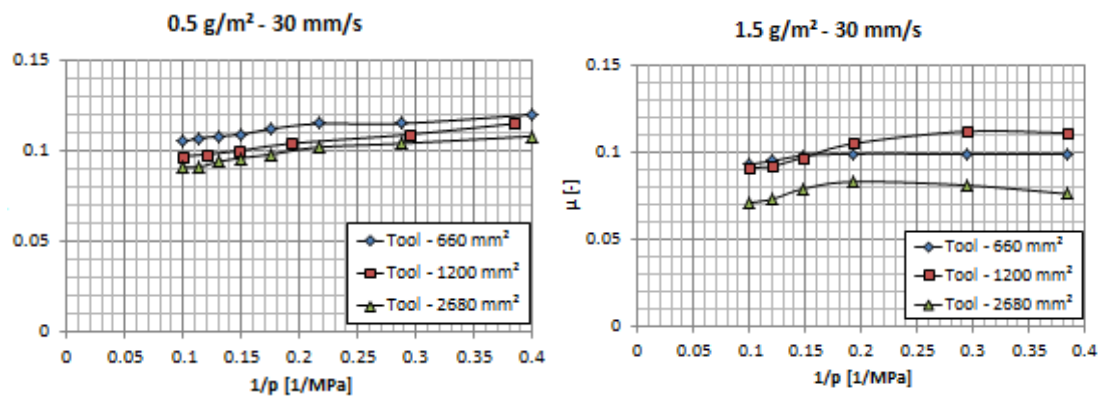


Figure 3.4: Comparison of the frictional behavior of tribosystems with different tool sizes at  $v = 30$  mm/s.

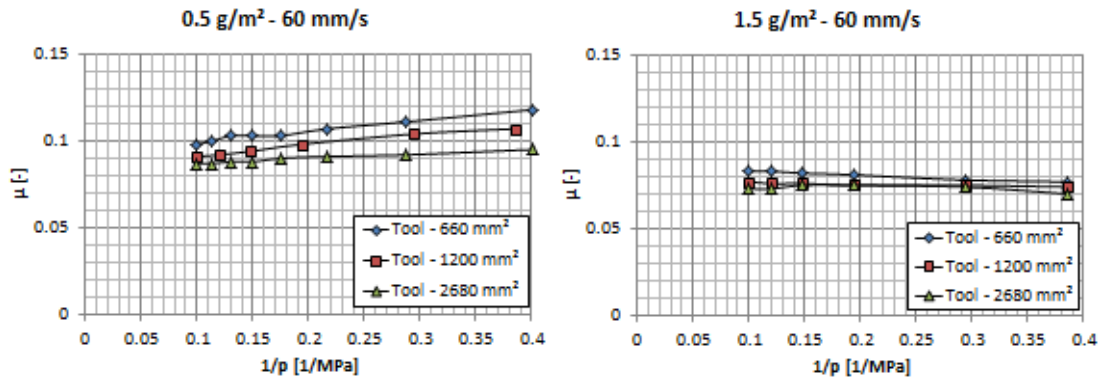


Figure 3.5: Comparison of the frictional behavior of tribosystems with different tool sizes at  $v = 60$  mm/s.

A general behavior of the tribological systems can be deduced from the graphs namely as the tool size grows, the coefficient of friction slightly decreases independently of the drawing parameters. Another comparison can be made between the tools with area 660 and 2688 mm<sup>2</sup>. They have comparable surface hardness and topography parameters. However, the tribosystem with the bigger tool generates lower friction. This confirms the dependence of the frictional response of a tribosystem on the tool size. With the increase of drawing speed and the lubricant amount, the dependence lessens.

The tool with area of 1200 mm<sup>2</sup> has a lower hardness value than the two other tools but still the coefficient of the related tribosystem follows the dependence on tool area i.e. smaller than the coefficient of the tribosystem with the small tool but bigger than that of tribosystem with the bigger tool. Therefore, it can be deduced that the frictional response of a tribosystem is not influenced by the hardness of the tool surface at least as long as the sheet metal coating is softer.

In conclusion, based on those first experiments on different tools, one can assume that the coefficient of friction that is obtained from strip drawing tests depends on the surface area of the used tool. This dependence is not substantial but it is important to keep it in mind all the same for further investigation in this work.

### 3.1.2 Pin-on-disk with radionuclide-technique

A universal pin-on-disk tribometer is further customized for the investigation of the tribological properties of the tribosystem as shown in figure 3.6. While friction force is recorded by the measuring system of the tribometer, the extended installation is measuring wear based on radionuclide-technique. A wide range of normal force and sliding velocity can be investigated. Based on sensibility analysis and finite element simulation of top-hat profile and cup drawing, the chosen nominal pressure lays in the range between 1 and 50 MPa. The sliding velocity spans from 1 to 150 mm/s. The oil temperature during the test remains at room temperature.

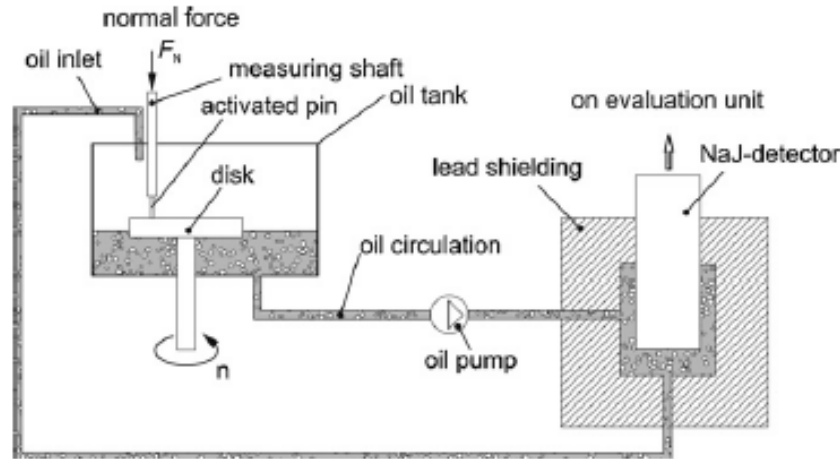


Figure 3.6: Schematic representation of the setup for the pin-on-disk wear testing machine (source: [Ant10]).

Contact occurs between the rotating sheet metal disk (2) with a diameter about 230 mm and a thickness of 0.6 mm, and an adjustable cylindrical pin (3) on which normal load is vertically applied through a spring (4) as shown in figure 3.7 (left). The pin is activated for the use of the radionuclide-technique. The operating principle of the installation is described as follow:

- Disk (2) is centralized and fixed on the platform (1) of the tribometer.
- The activated cylindrical pin is then given a  $(x,y)$  coordinate position in the plane of the disk such that a predefined diameter of the contact/wear track is set up with a good accuracy.
- While the disk rotates, the desired lubricant amount is applied by means of a nozzle linked to a pump such that only the wear track is lubricated.
- The motor M sets up the rotation of the disk with predefined velocity, the controlling of the tribometer is performed via a software.
- The normal force is applied on the pin and the desired circular velocity is given to the disk.
- During the sliding contact, the normal and friction forces are measured with the measuring system of the tribometer.
- After the test, the disk is washed with motor oil which further circulates in the extended installation in order to measure the amount of wear particle from the activated pin by means of the radionuclide-technique. A detailed explanation of the RNT can be found in [Sch03a].
- As a result, the wear rate and the frictional response of the tribological system can be monitored on screen.

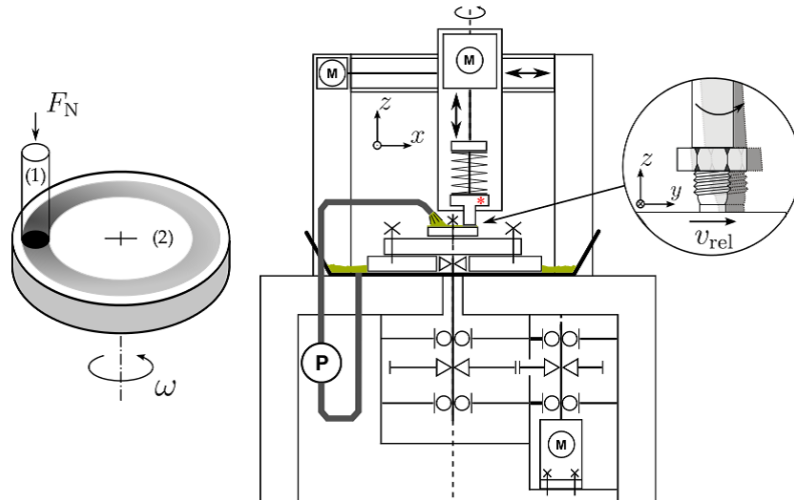


Figure 3.7: Pin-on-disk tribometer. Left: contact principle; right: structure of the tribometer and measurement principle (Source: [Sch14a; Lin16]).

## 3.2 Chemical analysis of surface

### 3.2.1 X-ray fluorescence measurement

Based on the use of X-ray spectrometry, the measuring equipment called Fischerscope X-ray instruments has been developed by Helmut Fischer GmbH & Co [Helllb; Hellla]. The method allows for measuring the coating thickness of metallic coating and to perform materials analysis by measuring the energy dispersive X-ray fluorescence (EDXRF) according to ASTM B568 and DIN EN ISO 3497.

### 3.2.2 X-ray Photoelectron Spectroscopy (XPS)

This method, as its name implies, is also based on the X-ray spectrometry as the EDXRF method. The difference is that the emitted photoelectrons are the analyzed targets instead of the secondary X-ray radiation. Effectively, the method analyzes the kinetic energy distribution of the emitted photoelectrons to evaluate the chemical composition and the electronic state of the surface of interest. The used primary X-ray radiations are monoenergetic Al- $K\alpha$  X-ray and have a photon energy of 200-2000 eV. Detailed information on the method are already well elaborated in many literatures [Hof13; Bri03; Nak18].

### 3.2.3 XPS-depth profiling

The procedure consists of an alternation of etching argon ion gun and XPS measurements. Material of the sample is etched for a predefined period of time by the argon ion gun which results in the exposing of a new surface. Then XPS measurements are performed on the new exposed surface through which its chemical composition is analyzed. The average depth analysis for XPS measurements is usually about 5 nm. This procedure is, therefore, repeated until a certain depth is reached, normally in the order of hundreds of nanometers.

The investigated area over which information is collected is approximately  $1 \times 1$  mm. Thereby, a depth profile in terms of XPS quantities is generated for each sample. It should be kept in mind that the depth profile is calibrated according to silica (silicon dioxide SiO<sub>2</sub>). Effectively, all materials behave differently to the same sputtering conditions so that the etching rates and depths may vary accordingly. The equivalent depth for the well – known silica is then used for a given sputtering energy which does not always correspond to the actual depth on the investigated material. However, discrepancies lie within 10% errors and experiences show well comparable results.

It is a widely used surface analysis technique owing to its large spectrum of applicability in terms of materials and its ability to provide quantitative and qualitative information about the surface of investigation [Phyll]. The main weakness of the method is that it requires high vacuum with a special vacuum chamber which limits the sample size to be only small or forces to cut a piece of the sample from an entire part and destroying it at the same time. Related to the high vacuum requirement, the sample must be cleaned and oil free in the case of deep drawing samples.

### 3.2.4 Scanning Electron Microscopy (SEM)

Scanning electron microscopy is a method that enables to observe the surface of a studied sample with high resolution normally down to the nanometer scale using an electron beam. The used apparatus is the "Scanning Electron Microscope". The path of the electron beam describes a raster which correlates with the grey level pixel on a screen. That is why it is called "Rasterelektronenmikroskop" in German. A detailed guideline for the use of the SEM is given in Beane [Bea16]. SEM has further advantages that it is not just a simple morphology-observation apparatus, but in reality a very resourceful apparatus with broad application capabilities such as elemental and state analyses. The basic principles of SEM are elaborated in details for instance in [Hay68; Oka18]. The basic components of the SEM are an electron gun, condenser and objective lenses, a specimen stage, a secondary electron detector and a display unit.

### 3.2.5 Focused Ion Beam system

A focused Ion Beam system operates in an analogical manner to the Scanning Electron Microscope (SEM) with the major difference that a finely focused ion beam (FIB) is used instead of an electron beam (EB). The ion source is a liquid metal typically gallium. The FIB system can be operated both at low and high beam currents depending on the aim. Low beam current is used for imaging while high beam current is meant for particular purpose such as specific sputtering or milling. Electron and ion dual-beam system is also often applied for non-destructive observation by using the high beam current for milling or micro-machining the surface and EB-SEM for imaging.

Some features of the FIB-SEM are [Sak18]:

- The nature of the image is surface sensitive. In the case of EB-SEM, the primary electrons from the EB penetrate deeper into the bulk material so that the emitted secondary electrons come actually from deeper region. EB-SEM images provide, thus, only averaged information between the topmost surface and beneath the sur-

face. On the other hand, ions from FIB do remain in the near surface layer. Therefore, the emitted secondary electrons are only from the vicinity of the surface and so are the FIB-SEM images.

- Besides surface observation, FIB enables a precise micro-machining and allows, thereby, to make very precise FIB profiles and cross sections at critical locations for further imaging investigations. Moreover, FIB enables the sectioning of a thin film out of the studied sample for further Transmission Electron Microscopy (TEM) sample preparation and observation.
- FIB-SEM has stronger channeling contrast compared to EB-SEM which is very suitable for grain size contrast observation in polycrystalline surfaces. Thereby, it also allows to perform microstructure analysis when combined with micromachining.

### 3.3 Nanoindentation

Nanoindentation test is one of the most used procedures to determine the modulus and indentation hardness of very thin film and surface layers on the basis of measured load-displacement data and the geometry of the indenter. It was initially proposed by Oliver *et al.* [Oli86]. Its popularity was enhanced with the development of high precision machines that can register small displacements at small loads. The most widely used indenter for nanoindentation is the three-sided Berkovich indenter as shown in figure 3.8 as it is much easier to fabricate compared to other popular indenters such as the four-sided Vickers' one [Fen10]. In this work, the Berkovich indenter is used indeed.

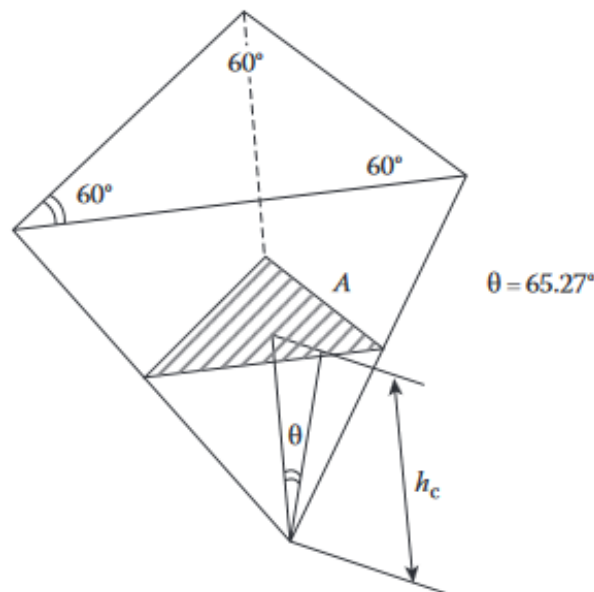


Figure 3.8: Geometry of a three-sided Berkovich indenter [Fen10].

The hardness of a solid material can be interpreted as a measure of its resistance to a permanent shape change under constant compression [Bro17]. It is generally quantified by the indentation hardness that equals the mean contact pressure at the contact zone, which is defined as the ratio of the indenter load to the projected area of contact [Fis11].

Conventional microindentation tests and nanoindentation test differ in the manner of computing the real area of contact. For the former, the contact area is obtained from the measurement of the plastic residual impression as a function of the applied load in microindentation. This is, however, technically difficult in nanoindentation with optical instruments because of the small size of the residual impression which is in the order of few microns only. SEM can cope with the difficulty but it is too unpractical. Thus, the contact area is, instead, computed on the basis of analytical models that use both the measured depth of penetration and the geometry of the indenter. In this sense, Oliver and Pharr [Oli92] developed a method for independent estimations of the contact area from the indenter shape function and combined it with the load-displacement data to provide accurate estimates of the modulus  $E$  and the hardness  $H$ . The main steps of their method are described in [Oli92; Bro17].

Nanoindentation test has the advantage to leave only very small and mostly negligible impression on the surface and thus, can be considered as a non-destructive method. Detail information on the nanoindentation test can be found in [Bro17; Fis11; Kra14; Oli92].

## 3.4 Surface topography measurement

### 3.4.1 Topography characterization

According to Thwaite (1982), topography or surface topography refers to the distribution of heights across a surface, and it is only one element in the characterization of a surface. Microgeometry and roughness are substitute terms for surface topography. Surfaces can be divided into broad classes. The fundamental division is the division into homogeneous (stationary) and inhomogeneous (nonstationary) surfaces. Those divisions are further broken down into isotropic and non-isotropic, deterministic and random, Gaussian and non-Gaussian surfaces [Thw82].

Another term in the characterization of a surface is the surface texture. As described in Song *et al.* [Son92], it refers to the fine irregularities such as peaks and valleys that are produced on the surface during the surface generation process as for instance during the skin-pass rolling. Surface texture is divided according to ISO into roughness, waviness and the unfiltered profile. On the one hand, roughness is the fine irregularities characteristics of the surface generation process itself. They can be impressions left by the rollers during skin-pass rolling process. On the other hand, waviness is generated on the rough surface due to improper manufacture such as vibration of the machine during the surface generation processes and is mostly inevitable but not desired. They are of longer wavelengths compared to roughness. An illustration of the difference between roughness and waviness is given in figure 3.9. Other still longer waves such as the errors of form are also part of the irregularities of the surface. They originate for instance from thermal distortion.

Another term is the so called "lay" that designates the direction of the dominant pattern of a surface texture. This is an important parameter for surfaces that are produced usually by machining processed as they have very strong unidirectional pattern.

As described in [Jen11], with the profile method, an unfiltered profile or P-profile is firstly generated which corresponds to the actual profile of the measured surface. Further by

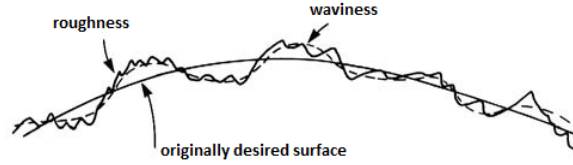


Figure 3.9: Geometric deviations from intended shape [Whi03].

using appropriate filter for instance according to ISO 11562/ISO 16610-21, other profiles namely the waviness or W-profile and the roughness or R-profile are generated. The separation of roughness from waviness is made by means of a sampling length  $l_r$  which corresponds to the cut-off length  $\lambda_{cof}$  of the used filter. The evaluation length  $l_n$  is determined as an average of five sampling lengths. The total length of the measurement is designated by the transverse length  $l_t$  and it must be greater than the evaluation length  $l_n$ .

As surface textures are highly complex, statistical descriptors are often used for the parametrization of the surface. On the one hand, there are the descriptors that describe the surface by means of only a single parameter value and known as the "surface parameters" (e.g. root mean square). On the other hand, more complex descriptors that characterize the surface texture with statistical parametrical functions (e.g. power spectral density).

There exist approximately 100 surface parameters described in standard such as ISO (e.g. ISO 4287:1997, ISO 12085:1996, ISO 4288:1996) for industrial use [Son92] which are categorized as R-parameters, W-parameters and P-parameters. The R-parameters can be further broken down into height parameters, waviness parameters, shape parameters, and combination of these, known as hybrid parameters.

$P_p$	$R_p$	$W_p$	Maximum profile peak height
$P_v$	$R_v$	$W_v$	Maximum profile valley depth
$P_z$	$R_z$	$W_z$	Maximum height of profile
$P_c$	$R_c$	$W_c$	Mean height of profile elements
$P_t$	$R_t$	$W_t$	Total height of profile
$P_a$	$R_a$	$W_a$	Arithmetical mean deviation of the assessed profile
$P_q$	$R_q$	$W_q$	Root mean square deviation of the assessed profile
$P_{sk}$	$R_{sk}$	$W_{sk}$	Skewness of the assessed profile
$P_{Ku}$	$R_{Ku}$	$W_{Ku}$	Kurtosis of the assessed profile
$P_{Sm}$	$R_{Sm}$	$W_{Sm}$	Mean width of the profile elements
$P_{dq}$	$R_{dq}$	$W_{dq}$	Root mean square slope of the assessed profile
$P_{mr}(c)$	$R_{mr}(c)$	$W_{mr}(c)$	Material ratio of the profile
$P_{dc}$	$R_{dc}$	$W_{dc}$	Profile section height difference
$P_{mr}$	$R_{mr}$	$W_{mr}$	Relative material ratio

Table 3.1: Parameters defined in ISO 4287:1997 [De 00].

Table 3.1 gives a summary of the most common surface parameters where the R-, W- and P-parameters are given. The computation of the parameters are well described in [Jenll; De 00; Son92]. Taking the roughness parameters as illustration, the other profile and waviness parameters are determined analogously.

### 3.4.2 Measurement equipment

The surface topographies of the tool and blank in this work are obtained by measurement using the NanoFocus confocal microscope, the principle of which is based on the confocal point sensor from Minsky's patent in 1955. A copy of the patent can be found in [Min88]. Confocal microscope of NanoFocus works according to the basic confocal principle and comprises a LED light source, a dichroic mirror as a beam splitter and a CCD camera. The main improvement was made by the use of a rotating multi-pinhole disk after the beam splitter and the use of piezo-drive on the objective so that the objective moves vertically instead of the sample. Thus, the operating of the Nanofocus microscope also differs accordingly from the basic confocal principle.

## 3.5 Plan of experiments

The aim of the work consists of characterizing wear and frictional behaviors of tribosystem in deep drawing. To do so, the main investigation is divided in two complementary sections. The first one treats the role of surface topography. The importance of topography of both tool and sheet metal is regarded such that sheet metals from a coil with different skin-pass level are taken as well as tools with different surface finish and treatment. The second section assigned to chapter 5 relates the importance of coating structure. Thereby, two types of zinc coating are investigated while the tool and the lubricant are kept the same.

Additional investigation regards the reliability of the experimental results with respect to the used tool and equipment. Effectively, the size of the used tool in strip drawing can be a source of discrepancy since there is no physical reason on the choice of the tool size. It is rather dependent on the used equipment. Also the obtained results by strip drawing and pin-on-disk can differ even when contact conditions are similar.

### 3.5.1 Characterization of wear

Classification of occurring wear as severe or mild requires indices inter alia the resulting material transfer, the amount of generated wear particles, the possible change of subsurface microstructure and chemistry due to plastic deformation and triboloading. All these are influenced by the constituents of the tribosystem as well as the contact conditions. For this purpose, strip drawing test with subsequent surface analyses as well as pin-on-disk with radionuclide-technique are carried out. Since a myriad of treatment exists, the choice is made on the least treated tool surface that can also serve as a reference.

In the first instance, 70 strips are drawn one after another under constant pressure and velocity of 5 MPa and 60 mm/s respectively. Little lubricant amount of 0.5 g/m<sup>2</sup> is applied on the strips in order to limit to minimum any hydrodynamic effect. Variation of the coefficient of friction is recorded for the observation of the running-in behavior of the strip drawing tool. Analogically, pin-on-disk test is also performed with 30 discs. The tool undergoes three rotations on the same wear track before the disk is changed. In order to trace any wear particle from the tool, the latter is activated and the radionuclide-technique is applied. The contact conditions are similar to those of the strip drawing test.

The parameter setup is summarized in table 3.7 and 3.8.

In the second instance, surface analyses consisting of chemical analysis (XPS and GDOES), near-surface microstructure analysis with FIB and SEM, nanoindentation and topography analysis with whitelight interferometry and SEM are performed on both tool and sheet metal strips.

#### 3.5.2 Characterization of friction and lubrication

Investigation of friction mechanics implies the examination of the resulting adhesion and plastic deformation after contact. Thereby, a qualitative estimation of  $\mu_a$  and  $\mu_p$  is included. In order to do so, chemical compositions of contacting surfaces are analyzed to trace any material transfer resulting from adhesion as well as the formation of third body. The possible change of the surface topography as well as the near-surface structure will also give information on the importance of plastic deformation and the real contact area. This investigation complements the subsection 3.5.1.

Since surface topography and lubricant are among the main ingredients of the frictional response of the tribosystem, the interplay between the surface roughness for both tool and sheet metal and the lubricant thickness is to be regarded. In the first instance, Stribeck curve is established by parameter variation namely contact pressure, drawing velocity and applied lubricant amount in strip drawing and pin-on-disk tests. This also allows to compare the two tests under the same parameters. Another characteristic of the tribosystem is the relationship between the coefficient of friction and the pv factor within the concept of friction power density. Strip-drawing test enables to establish this relationship. In the second instance, influence of surface topography of both tool and sheet metal surfaces on friction is investigated by means of strip drawing. On the one hand, sheet metals with the same surface coating but with different surface roughness are tested keeping the tool unchanged. The sheets are taken from a coil with different skin pass level. On the other hand, grinded and polished tools are used with the same sheet metal as illustrated in figure 3.10.

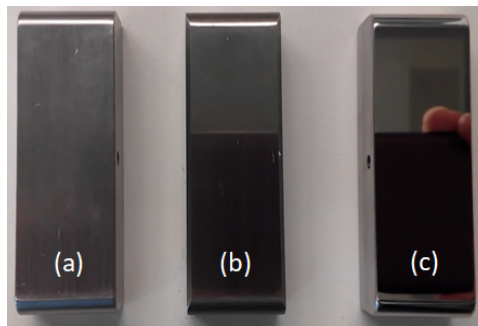


Figure 3.10: Strip drawing tools with different surface finishing: (a) –grinded tool; (b) –plasma nitride treated tool; (c) –polished tool.

Corresponding Stribeck curves are recorded. The parameter setup of strip drawing and pin-on-disk tests are summarized in table 3.2, 3.3, 3.4, 3.5 and 3.6.

### 3.5.3 Summary of parameter setup for tribological tests

material of the sample	type: dual-phase steel DP500 coating 1: zinc (car outer-skin) coating 2: zinc-magnesium thickness: 0.6 mm
nominal contact pressure	2.5 – 10 MPa (increasing)
drawing speed	15/30/60 mm/s
lubricant	type: Fuchs Anticorit PL3802-39s amount: 0.5/1.5 g/m <sup>2</sup>
tool	type: steel tool 1.2379 surface treatment: grinded
temperature	room temperature
surrounding environment	atmosphere

Table 3.2: Setup of strip drawing tests for the establishment of Stribeck curve.

material of the sample	type: dual-phase steel DP500 coating 1: zinc (car outer-skin) coating 2: zinc (multi-purpose) thickness: 0.75 mm
nominal contact pressure	2.5 – 30 MPa (increasing)
drawing speed	15/60 mm/s
lubricant	type: Fuchs Anticorit PL3802-39s amount: 0.5/1.5/4.5 g/m <sup>2</sup>
tool	type: steel tool 1.2379 surface treatment: grinded
temperature	room temperature
surrounding environment	atmosphere

Table 3.3: Setup of strip drawing tests with lubricant amount variation.

material of the sample	type: dual-phase steel DP500 coating 1: zinc (car outer-skin) coating 2: zinc-magnesium thickness: 0.6 mm
nominal contact pressure	5 MPa (constant)
drawing speed	1/5/10/20/40/60/80/100/125/150 mm/s
lubricant	type: Fuchs Anticorit PL3802-39s amount: 0.5/1.5 g/m <sup>2</sup>
tool	type: steel tool 1.2379 surface treatment: grinded
temperature	room temperature
surrounding environment	atmosphere

Table 3.4: Setup of pin-on-disk tests for the investigation of lubrication regime.

material of the sample	type: mild steel DX57D coating: zinc thickness: 1 mm skin-pass level: 1 – 9
nominal contact pressure	2.5 – 10 MPa (ramp)
drawing speed	30/45/60 mm/s
lubricant	type: Fuchs Anticorit PL3802-39s amount: 0.5/1.5/4.5 g/m <sup>2</sup>
tool	type: steel tool 1.2379 surface treatment: grinded
temperature	room temperature
surrounding environment	atmosphere

Table 3.5: Setup of strip drawing test with various skin-pass levels.

material of the sample	type: dual-phase steel DP500 coating: zinc (multi-purpose) thickness: 0.75 mm
nominal contact pressure	2 – 10 MPa (ramp)
drawing speed	30/45/60 mm/s
lubricant	type: Fuchs Anticorit PL3802-39s amount: 0.5 & 1.5 g/m <sup>2</sup>
tool	type: steel tool 1.2379 surface treatment: grinded & polished surface area: 1200 g/m <sup>2</sup>
temperature	room temperature
surrounding environment	atmosphere

Table 3.6: Setup of strip drawing test with grinded and polished tools.

material of the sample	type: dual-phase steel DP500 coating (variant 1): zinc (car outer-skin) coating (variant 2): zinc-magnesium thickness: 0.6 mm
nominal contact pressure	5 MPa (constant)
drawing speed	60 mm/s
number of test pro coating variant	70 (equals 35 m of wear track)
lubricant	type: Fuchs Anticorit PL3802-39s amount: 0.5 g/m <sup>2</sup>
tool	type: steel tool 1.2379 Surface treatment: grinded
temperature	room temperature
surrounding environment	atmosphere

Table 3.7: Setup of the first series of strip drawing for running-in investigation.

material of the sample	type: dual-phase steel DP500 coating 1: zinc (car outer-skin) coating 2: zinc-magnesium thickness: 0.6 mm
nominal contact pressure	5 MPa (constant)
drawing speed	60 mm/s
number of test pro coating variant	30
lubricant	type: Fuchs Anticorit PL3802-39s amount: 0.5 g/m <sup>2</sup>
tool	type: steel tool 1.2379 surface treatment: grinded
temperature	room temperature
surrounding environment	atmosphere

Table 3.8: Setup of pin-on-disk test for the investigation of tool running-in.

## 3.6 Materials

The description of the tribological phenomena during deep drawing process imperatively requires the comparison of the state of the surfaces composing the tribosystem before and after tribological loads are applied. Therefore, at this point, it is important to give as much information as possible on the initial state of the used materials. The basic properties of the materials and the topography, microstructure of the near-surface zone, chemical composition and mechanical properties such as hardness are inter alia the main characteristics to be described.

### 3.6.1 Tool

#### 3.6.1.1 Tool material

Strip drawing and pin-on-disk tests in this work are performed using tool steel 1.2379/X153CrMoV12 according to DIN EN ISO 4957 which exhibits an average microhardness of 60-64 HRC after tempering and a Young's modulus of 210 GPa. It is a high carbon and high chromium type cold steel. Owing to its high content of hard carbide in the steel matrix, it exhibits a high abrasive and adhesive wear resistance. Moreover, the presence of carbide provides the tool steel a secondary hardening quality which enables further treatment such as plasma nitride. It is one of the standard materials for the manufacturing of deep drawing tools especially the punch [HSMII]. Typical chemical composition of the material is given in table 3.9.

C	Si	Mn	Cr	Mo	V	P	S
1.50-1.60	0.10-0.40	0.15-0.45	11.0-12.0	0.60-0.80	0.90-1.10	<0.030	<0.030

Table 3.9: Typical chemical composition of tool steel 1.2379 (mass percentage in % according to DIN EN ISO 4957).

### 3.6.1.2 Tool surface

The topography parameters as well as the surface microhardness of the used tools are summarized in table 3.11 and table 3.10 respectively. The tool surface finish corresponds to grinding and polishing without hardening and grinding with further hardening treatment by plasma nitride.

Tool area [mm <sup>2</sup> ]	surface finish	surface treatment	hardness [HRC]
1200	grinded	untreated	22
1200	grinded	plasma nitrided	57
1200	polished	untreated	21
660	grinded	plasma nitrided	58.5
2680	grinded	Plasma nitrided	62

Table 3.10: Tool surface hardness.

tool area [mm <sup>2</sup> ]	surface finish	surface treatment	$R_a$ [ $\mu\text{m}$ ]	$R_q$ [ $\mu\text{m}$ ]	$R_z$ [ $\mu\text{m}$ ]	$R_p$ [ $\mu\text{m}$ ]	$R_{sk}$	$R_{ku}$	Pda [deg]
in drawing direction									
1200	grinded	untreated	0.0009	0.0015	0.0036	0.001	-1.58	3.12	8
1200	polished	unhardened	0.0004	0.0005	0.0008	0.0002	-0.05	2.03	3.2
660	grinded	plasma nitrided	0.0003	0.0003	0.0005	0.0002	-0.024	2.26	0.8
2688	grinded	plasma nitrided	0.0017	0.0018	0.005	0.0014	-0.97	1.55	6.9
perpendicular to drawing direction									
1200	grinded	unhardened	0.35	0.5	2.59	1.03	-0.7	5.3	11.4
1200	polished	unhardened	0.07	0.09	0.51	0.26	-0.04	3.85	3.06
660	grinded	plasma nitrided	0.13	0.16	0.9	0.48	-0.098	3.32	6.5
2688	grinded	plasma nitrided	0.13	0.17	1.01	0.39	-0.8	6.3	5.73

Table 3.11: Topography parameters of the used tools.

### 3.6.2 Sheet metals substrate

Two types of steel sheet materials are used in this work namely the dual phase steel DP500 and the mild steel DX57D. On the one hand, dual phase steel (DP) represents a family of low-carbon steel with a maximum carbon mass percentage of 0.06. It is characterized by a hard second phase of martensite or bainite usually in the form of islands embedded in a soft ferrite matrix. This enables this type of steel to exhibit a good property combination of high tensile strength, low ratio of the yield point/tensile strength, good formability in cold forming owing to a good strain redistribution and an good welding property. An additional bake-hardening effect leading to an additional increase in yield strength after forming is also achievable during painting. It is normalized according to DIN EN 10152,

10338, 10346 /VDA 239-100. The DP500 used in this work designates the DP-K290Y490T which means a yield point at 290 MPa and a tensile strength of 490 MPa. The letter K represents the production of the steel sheet via cold rolling. Dual phase steels are widely applied in automotive industry more precisely for structural and safety parts such as longitudinal beams, cross members and reinforcements. The DP500 is usually meant for roof outer, door outer, body side outer, package trail and floor panel. Therefore, the quality of its surface after deep drawing is important to preserve. More detailed information on the material can be found in [Thylla].

On the other hand, DX57D belongs to the family of mild steel for cold forming. DX57D itself exhibits extra special deep-drawing quality according to DIN EN 10346. It is applied for the manufacturing of complicated parts where the drawing process requires a sheet metal with high forming behavior at high strain. It is also suitable for high speed workshops and highly automated press lines. Besides the outer skin of car doors and roofs, other example of application of DX57D can be a wheel arch and a crankcase as well. It is characterized by a low-carbon content with a maximum carbon mass percentage of 0.12. It has a yield point between 120-170MPa and a tensile strength between 260-350MPa. The steel sheet is also produced via cold rolling. More detailed information can be found in [Thyllb]

### 3.6.3 Sheet Metal Coating

Both DP500 and DX57D in this work are zinc coated via hot-dip coating process. More precisely, three sorts of materials are used here designated as DP500+Z, DX57D+Z and DP500+ZM. The first two are galvanized meaning the coating consists essentially of pure zinc with a small percentage of aluminum about 0.2 to 0.3%. The presence of aluminum is to interact with the iron present in the zinc bath as well as at the steel substrate and coating interface during the coating process. Thereby, the formation of brittle zinc-iron phase at the substrate-coating interface which decreases the drawability of sheet metal is hindered by the first forming iron-aluminum thin layer. Also, by reacting with the dissolved iron in the zinc bath giving a lower density and easily removable precipitation at the surface of the bath, aluminum eliminates the formation of a sediment of zinc-iron phase at the bottom of the bath which affects the quality of the final product [Hac09]. DP500+ZM is similarly galvanized with the main difference that a small percentage of magnesium about 0.5% is added in the composition of the coating. This addition enables to considerably increase the protection of the sheet metal against corrosion. Besides, the structure of the coating is also changed by the apparition of binary and ternary eutectic separating the wide primary zinc grains and which consist of zinc-rich phase  $\text{MgZn}_2$  and zinc-rich/aluminum rich/ $\text{MgZnAl}$  phase respectively. Thereby, the chemical and mechanical properties of the coating are also changed, and therefore their tribological properties alongside. Micrographs of unworn DP500+Z and DP500+ZM are given in figure 3.11 showing the difference of structure of their coating. Topography parameters of all the used sheet metals are given in figures 3.12 – 3.14 and in tables 3.12.

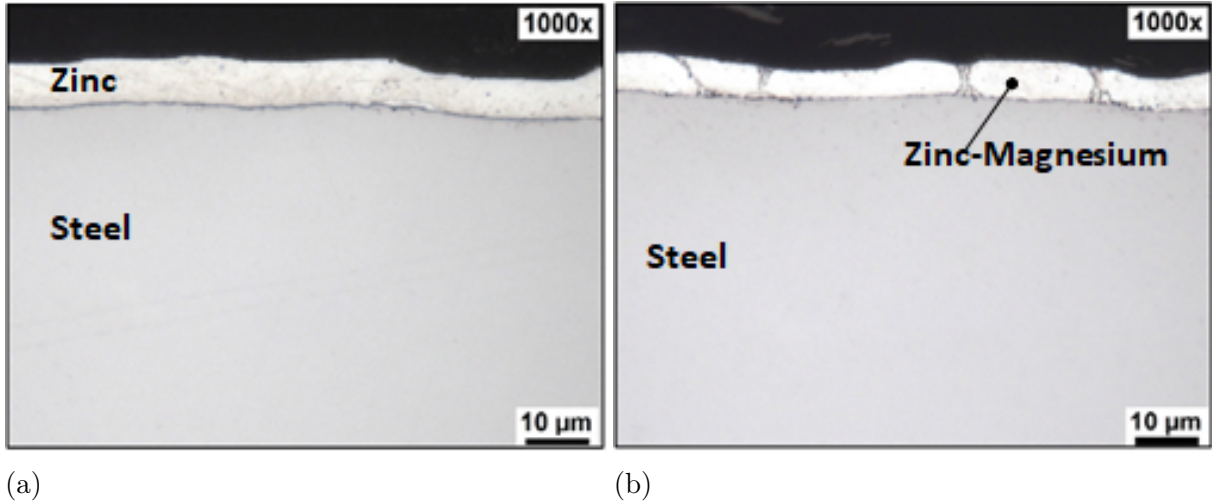


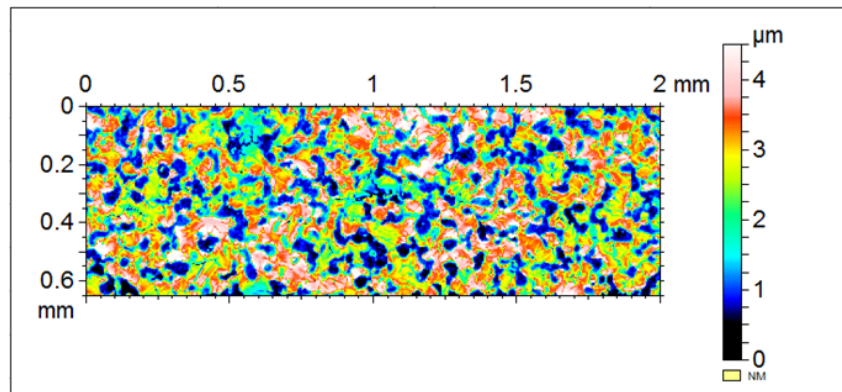
Figure 3.11: Micrographs of: (a) - unworn DP500+Z; (b) - unworn DP500+ZM.

parameters of the roughness profile	DP500+Z (outer-skin)	DP500+ZM (outer-skin)	DP500+Z (multipurpose)	unit
$RP_c$	9.17	11.7	4.17	[1/mm]
$R_p$	1.78	1.77	1.66	[ $\mu\text{m}$ ]
$R_z$	4.15	3.25	3.91	[ $\mu\text{m}$ ]
$R_a$	0.863	0.845	0.782	[ $\mu\text{m}$ ]
$R_q$	1.07	0.930	0.905	[ $\mu\text{m}$ ]
$R_{sk}$	-0.432	0.117	-0.754	
$R_{ku}$	2.35	1.58	2.36	

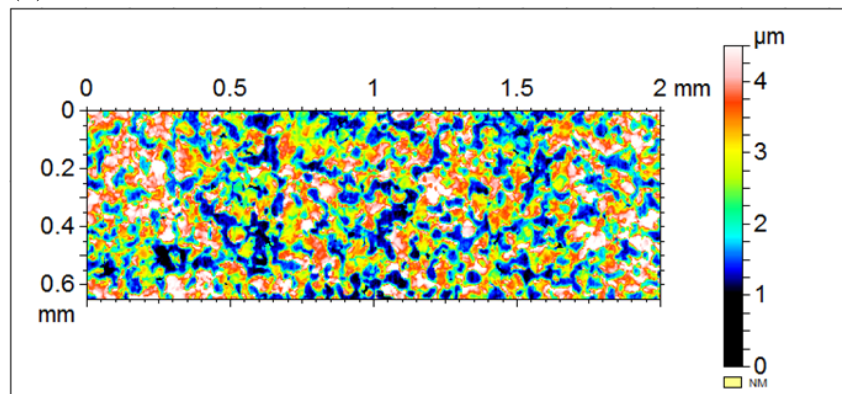
Table 3.12: Roughness parameters of the dual-phase steel with zinc coating DP500+Z and the dual-phase steel with zinc-magnesium coating DP500+ZM according to ISO 4287.

Skin-pass rolling of galvanized steel sheet metal is one of the final steps in cold rolling process by which the mechanical characteristics and the surface quality are improved. More precisely, the process aims to eliminate the yield point elongation also known as Lüders behavior (i.e. upper and lower yield stress behavior) of the steel substrate if it manifests and to adjust the flatness and roughness of the surface [Wic02; Kij07]. While the roughness of the sheet metal surface affects the yield of the deep-drawing process and the adhesion of paints, the strip flatness ensures trouble-free operation of the plant and equipment of industries that will use the product further [SMSII]. In addition, desired roughness and texture also can be transferred to the surface. During the process, sheet metal undergoes a very little thickness reduction (less than 2%). The sheet metal width is much larger than its thickness, and so is the contact length. In turn, the rolling radius is much larger than the contact length [Kij08b; Kij08a]. In general, skin-pass rolling is performed under dry friction conditions.

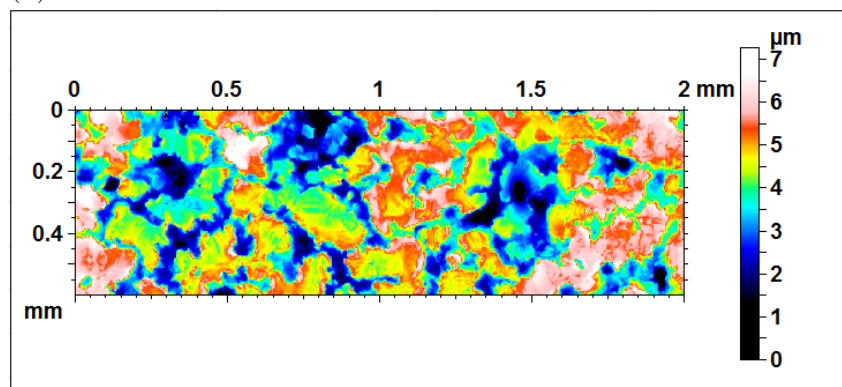
The coil of DX57D, from which the blanks in this work are taken, has nine sections with 9 different skin-pass levels. The roughness of the surface of each section is, thereby, also different as it corresponds to each skin-pass level as presented in figures 3.13 – 3.14.



(a)



(b)



(c)

Figure 3.12: Surface topography of the dual-phase steels: (a) - with zinc coating DP500+Z (outer-skin); (b) - with zinc-magnesium coating DP500+ZM (outer-skin); (c) - with zinc coating DP500+Z (multipurpose).

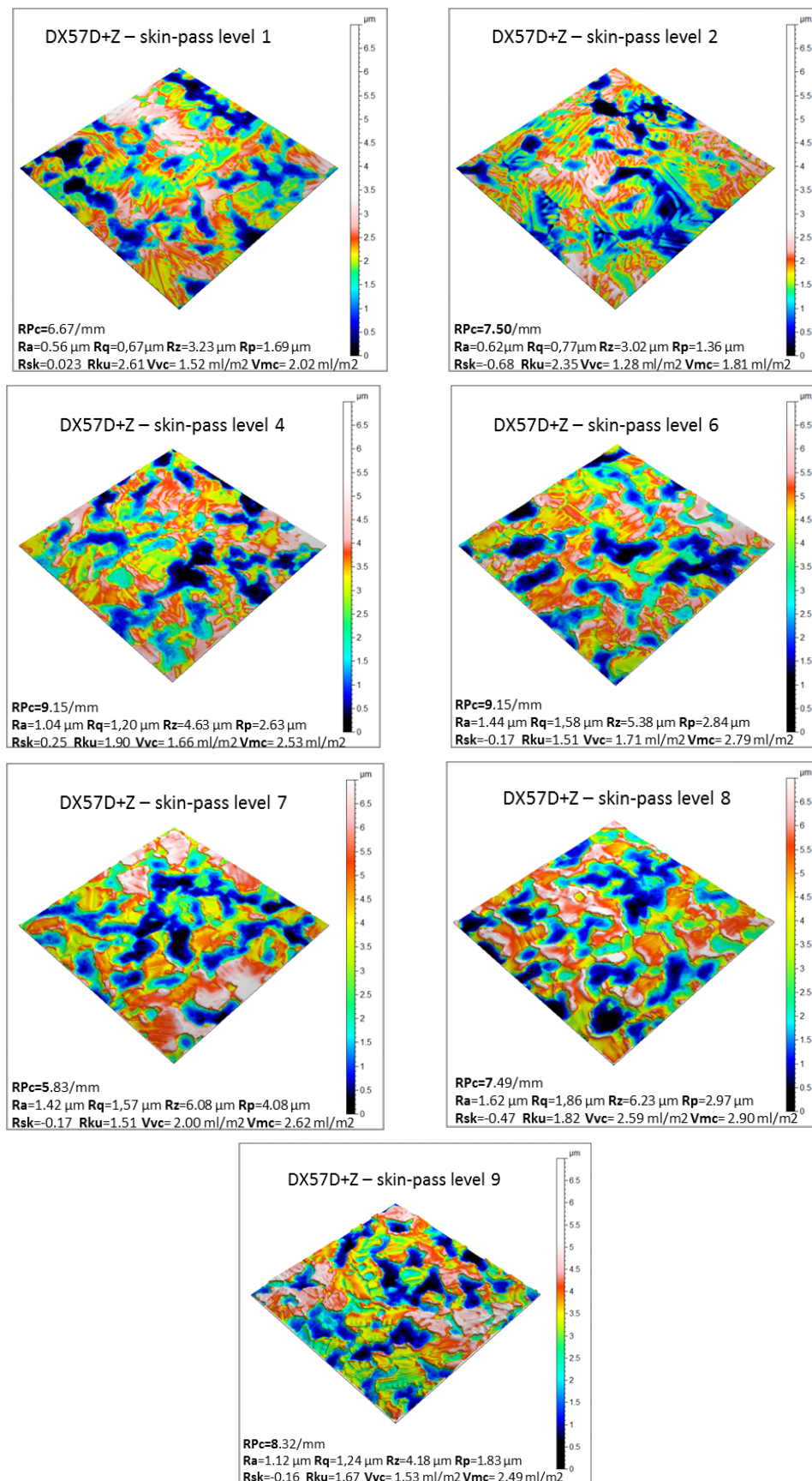


Figure 3.13: Topography parameters of DX57D+Z with various skin-pass levels.

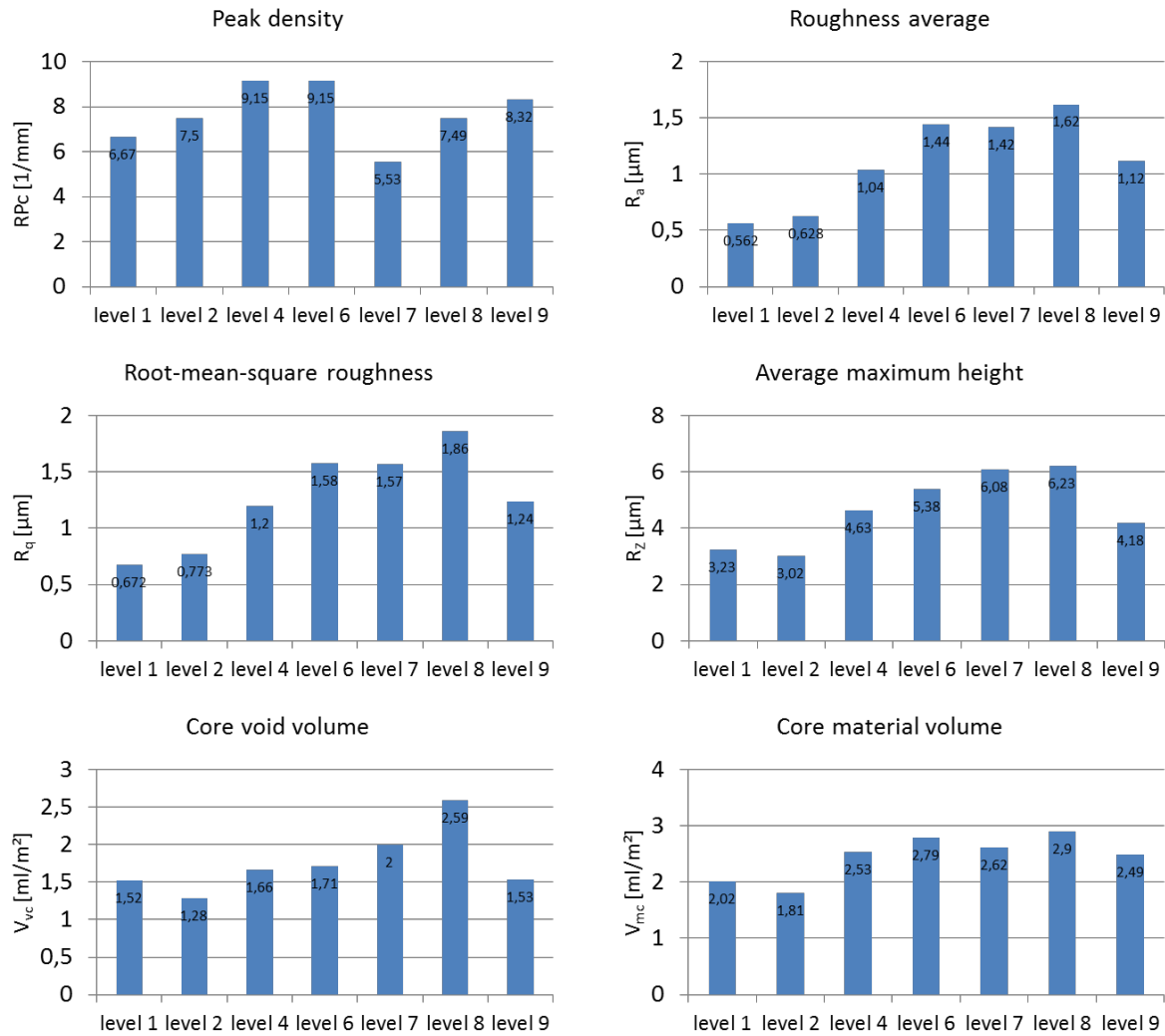


Figure 3.14: Graphical representation of the topography parameters of DX57D+Z with various skin-pass levels.

### 3.6.3.1 Chemical composition

Intensive work was carried out on the determination of the chemical composition of the surface of standard galvanized sheet metal as the DP500+Z and the DX57D+Z. Through very high resolution technics such as GD-OES, EDX line scans and FIB-TEM, it was established that before the skin-pass rolling process, the top layer of the zinc coating consists of a dense and closed layer of aluminum oxide  $Al_2O_3$  which gives the surface a bright appearance [Mar00]. Arndt estimates the thickness of the layer to be approximately 5 nm [Arn12]. When the galvanized sheet metal is skin-passed, the aluminum oxide layer is cracked and the fragments at the contact zone with the skin-pass roller are pressed into the softer zinc layer underneath while the non-contact zones keep their oxide layer intact [Rie11]. It is those intact surfaces that are, in fact, located at the asperity peaks of the sheet metal surface and that enter in contact with the tool surface. The latter is also covered with an oxide layer (iron oxide and chromium oxide). Thus, the tool-sheet metal contact can be characterized as oxide-oxide in the absence of lubricant, at least at the very beginning of drawing.

Analogically, the surface of the zinc-magnesium coated sheet metal is also covered with an oxide layer. The composition of the layer is, however, more complex in this case due to the presence of magnesium. Before the skin-pass process, the oxide layer consists of magnesium oxide  $\text{MgO}$ , aluminum oxide  $\text{Al}_2\text{O}_3$  and a mixture of them i.e.  $\text{MgAl}_2\text{O}_4$  [Rie11]. The layer is smooth and homogeneous. Although the mechanism of formation of those oxide layers has not found a clear unanimous explanation yet, it is assumed that the magnesium and aluminum oxides have formed at different stages of the coating process [Lam17]. After the skin-pass process, this smooth oxide layer is also fragmented and some parts are removed. It is substituted by a new formed layer, the constituents of which correspond exactly to the chemical structure of the metal phases beneath [Arn12].

#### 3.6.3.2 Microstructure

The initial state of the surface of the strips comprises regions that are plastically deformed by compression during the skin pass rolling process and other regions that are indirectly stressed due to the deformation of neighboring regions as shown in figure 5.20. FIB-SEM images show clearly that skin-pass rolling process induces some defect in form of cracks on the surface of the standard zinc coating that propagates within the first micrometer depth. Plastic deformation and buckling can also be distinguished. Those defects and deformations are not encountered in zinc-magnesium coating.

The material of the standard zinc coating is dense while zinc-magnesium coating has a pronounced porosity. Nevertheless, the near surface zone within 500 nm depth is still dense and similar to the standard zinc coating. The diffusion phase between the coating and the steel substrate is also much thicker for standard zinc than for zinc-magnesium coating. The microstructures of the coating are illustrated in figure 5.20 and 5.21.

#### 3.6.4 Lubricants

In this work, the Fuchs Anticorit PL3802-39s is essentially used. It is a first generation Prelube thixotrope according to VDA 230-213. It has a kinematic viscosity of  $60 \text{ mm}^2/\text{s}$  at the temperature of  $40^\circ\text{C}$  and a density of  $910 \text{ kg}/\text{m}^3$  at  $15^\circ\text{C}$ . It ensures additional corrosion protection to the sheet metal as well as it enhances its drawability. It is applied on the specimens at a temperature around  $50^\circ\text{C}$  via a special equipment. The three specimens for strip drawing test are placed on a moving frame. The latter performs a stroke on the horizontal plane inside the machine. On its back stroke to gain its initial position, lubricant is sprayed on the specimens through injection nozzles so that it is optimally distributed on the surface. For the lubricating of the other side, the specimens are just turned over and the same procedure is performed. The machine enables to apply a desired lubricant amount on the specimen. The calibration is carried out by weighing the specimen before and after application of the lubricant by means of micro-weighing machine.

# Chapter 4

## Influence of topology of contacting surfaces on friction

In deep drawing, both sheet metal and tool surfaces exhibit varying surface topographies and can have, therefore, influence on the frictional behavior of the corresponding tribosystem. Hereupon, strip drawing and pin-on-disk tests are performed in the frame of the characterization of friction and wear of tribosystem in deep drawing. The results are presented in the form of Stribeck curve. In relation to that, consistency and comparability of the results deserve also special attention. Effectively, when both tests are performed under the same conditions, the effect of different equipment is still to be considered.

In the first instance, the general form of Stribeck curve is examined through parameter variation i.e. contact pressure, drawing speed and lubricant amount in strip drawing (section 4.1) and pin-on-disk tests (section 4.2). By additional test with more lubricant amount variation in strip drawing (section 4.3), related lubrication regimes are deduced from the observation of the curve behavior.

In the second instance, strip drawing test is performed with tools and sheet metal with diverse surface roughness (section 4.4 and 4.5). The used specimens as presented in section 3.3 are taken from a coil that was submitted to varying skin-pass level. Thereby, it enables to study the influence of the most basic characteristic of sheet metal surface on friction namely its roughness. In turn, tool surfaces are treated to obtain the desired surface quality as mentioned in section 3.3.1. In this work, the tools from the same lot are used. For the topography variation, the first tool is just ground while the second one is polished so that it exhibits a much smoother surface compared to the ground one as already presented in figure 3.10.

### 4.1 Parameter variation in strip drawing test

#### 4.1.1 Experimental results

Sheet metal of DP500 with pure zinc coating were drawn with grinded flat dies for different amounts of lubricants and under increasing pressure from 2.5 to 10 MPa and constant velocities 15/30/60 mm/s. The parameter setup is already provided in table 3.2 of section 3.5. Figure 4.1 and 4.2 present the results.

#### 4.1. Parameter variation in strip drawing test

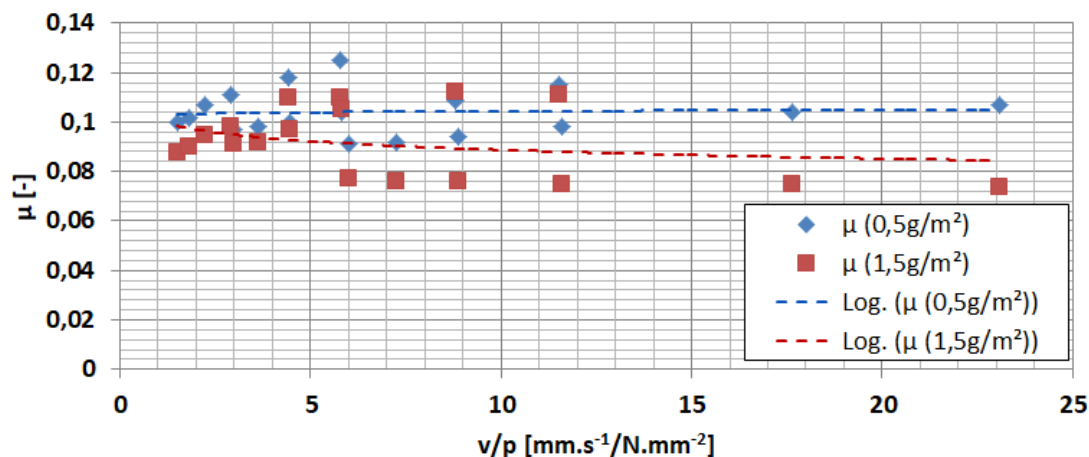


Figure 4.1: General Stribeck curve from strip drawing test with DP500+Z (multipurpose,  $R_a = 0.78$ ,  $RP_c = 4.17$ ).

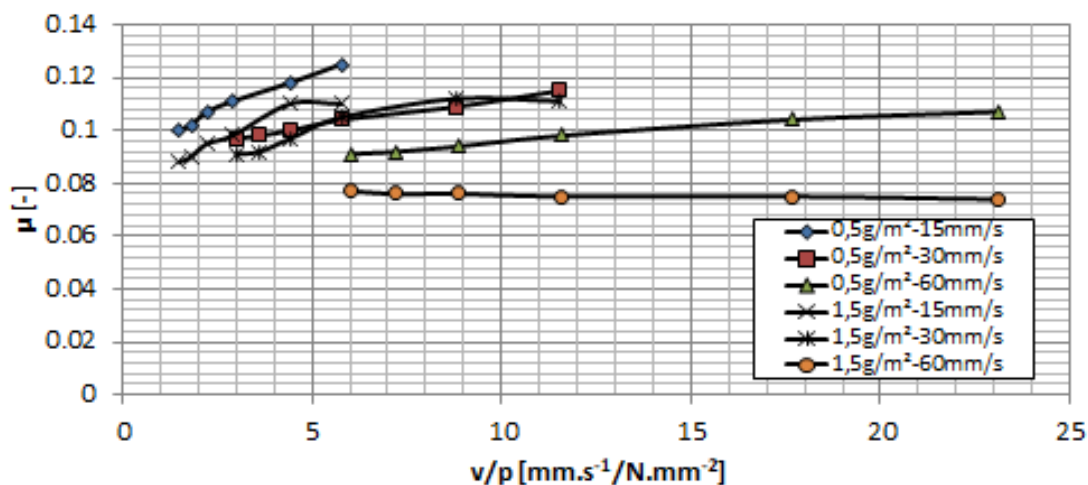


Figure 4.2: General Stribeck curve from strip drawing test with DP500+Z (multipurpose,  $R_a = 0.78$ ,  $RP_c = 4.17$ ). Each curve represents the average curve of three experiments with the same parameters

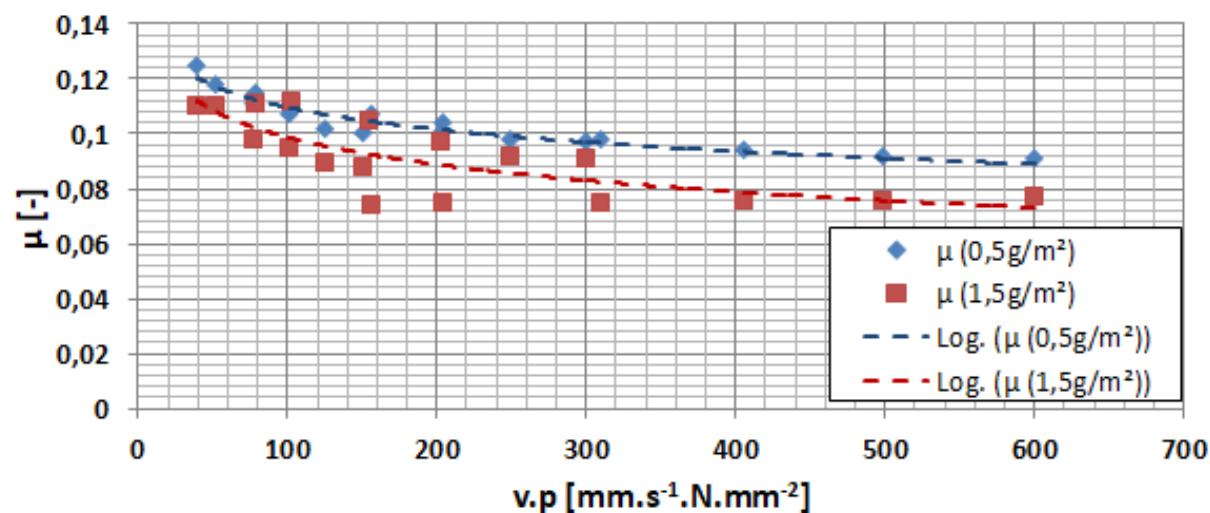


Figure 4.3: Friction power density curve from strip drawing test with DP500+Z (multipurpose,  $R_a = 0.78$ ,  $RP_c = 4.17$ ).

### 4.1.2 Observation

The obtained curves display some characteristics of the regarded tribological system. Firstly, the curves show that the tribological system exhibits more than one value for the coefficient of friction depending on the drawing speed, the contact pressure and the lubricant amount. Thus, the representation of the frictional behavior of a tribological system by a single value of the coefficient of friction is not very accurate. An alternative is to assign a certain range of value which the coefficient can be contained within. In the given case, the coefficient of friction can be allocated in a range of:

$$\mu = 0.1 \pm 0.025 \text{ (25\% of deviation)}$$

Secondly, it can be noticed that the same value of the coefficient of friction can also result from different contact conditions i.e. from different drawing speeds, contact pressures and lubricant amounts. If those conditions are characteristics of a given deep drawing process, then the representation of the coefficient of friction as a single value for the simulation can still hold true. Moreover, if the effect of deviation of the value of the coefficient of friction from the average value (with  $0.5 \text{ g/m}^2$ ) is not significant either in the real process or in FE-simulation, then the assumption about the coefficient of friction as constant is acceptable.

Thirdly, the abscissa of the general Stribeck-curve is the Hersey parameter as the ratio of drawing speed to the nominal contact pressure. It is observed that the same Hersey parameter  $v/p$  that corresponds to different combinations of drawing speed and contact pressure does not provide the same coefficient of friction although the tribological system is similar, i.e. same lubricant amount. Thus, the Stribeck curve cannot be mathematically described by a continuous function where any allowed value of the Hersey-parameter corresponds only to one coefficient of friction. It can be deduced that the curve for the characterization of the lubrication regime is not unique for a specific tribological system.

## 4.2 Parameter variation in pin-on-disk test

### 4.2.1 Experimental results

In analogy to strip drawing, pin-on-disk tests are performed with the same materials for the tribosystem and the experiment setup is summarized in table 3.4. The tests were carried out with only one pressure value (5 MPa) but the speed was varied, the generalized Stribeck curve is simplified as a dependence of the coefficient of friction on the speed only. Figure 4.4 – 4.9 present the results.

### 4.2.2 Observation

The results of the pin-on-disk tests show several information on the behavior of the tribological system. In the first instance, the overall results show that the coefficient of friction is always higher for the first revolution than for the subsequent ones. One possible explanation can be the pile-up effect. Effectively, extra energy is required to flatten the piled-up material in front of the pin in the first revolution as well as the formation

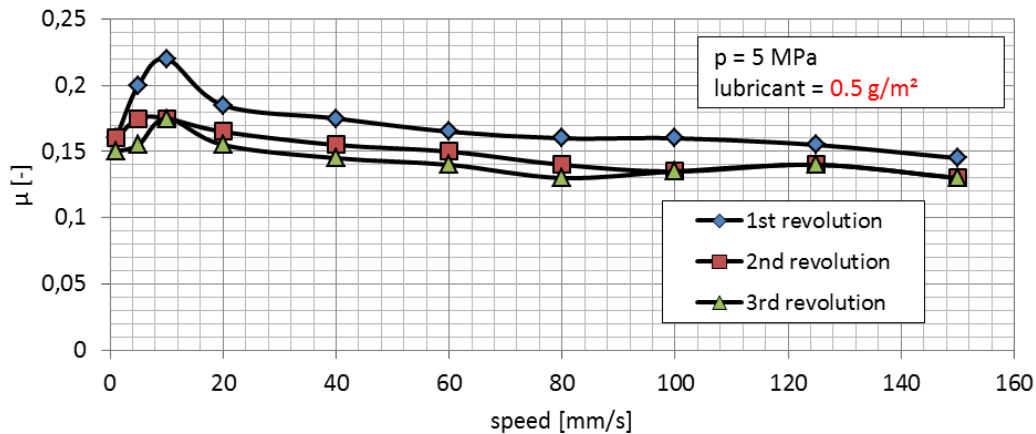


Figure 4.4: Stribeck-curve with DP500+Z(outerskin,  $R_a = 0.86$ ,  $RP_c = 9.2$ ) and lubricant amount =  $0.5 \text{ g/m}^2$ .

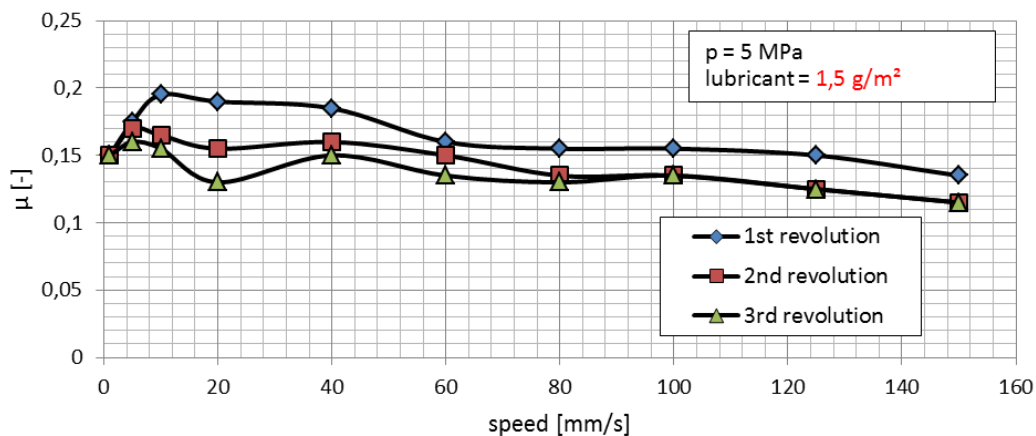


Figure 4.5: Stribeck-curve with DP500+Z(outerskin,  $R_a = 0.86$ ,  $RP_c = 9.2$ ) and lubricant amount =  $1.5 \text{ g/m}^2$ .

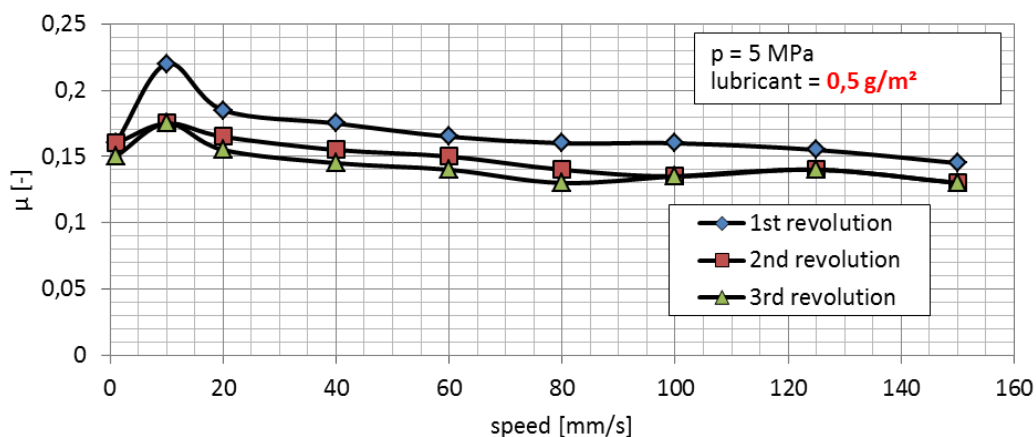


Figure 4.6: Stribeck-curve with DP500+ZM ( $R_a = 0.84$ ,  $RP_c = 11.7$ ) and lubricant amount =  $0.5 \text{ g/m}^2$ .

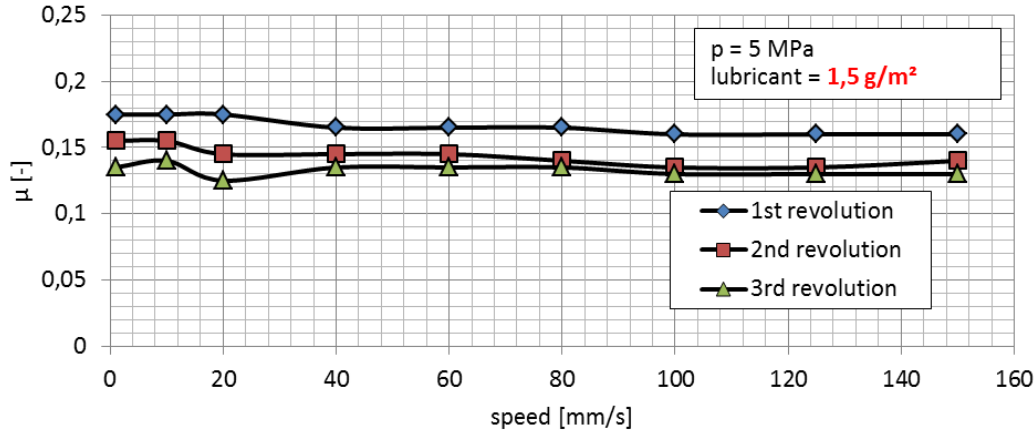
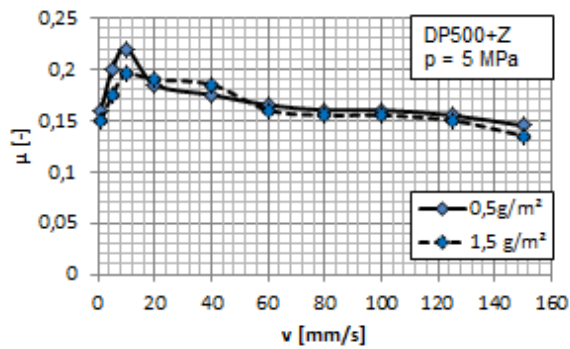
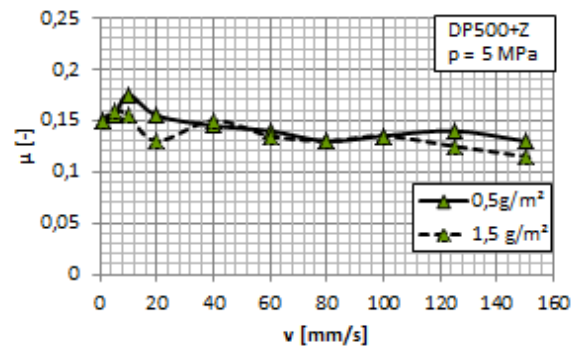


Figure 4.7: Stribeck-curve with DP500+ZM ( $R_a = 0.84$ ,  $RP_c = 11.7$ ) and lubricant amount =  $1.5 \text{ g/m}^2$ .

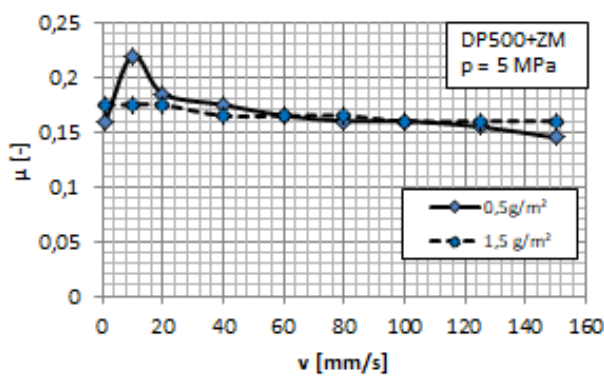


(a)

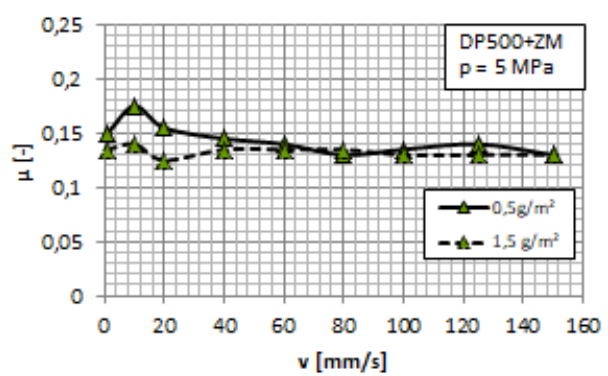


(b)

Figure 4.8: Simplified Stribeck curves for pin-on-disk with DP500+Z (car outer skin,  $R_a = 0.86$ ,  $RP_c = 9.2$ ): (a) – first revolution; (b) – third revolution.



(a)



(b)

Figure 4.9: Simplified Stribeck curves for pin-on-disk with DP500+ZM ( $R_a = 0.84$ ,  $RP_c = 11.7$ ): (a) – first rotation; (b) – third rotation.

of coating chips. An extra pile-up friction force is then generated. In the subsequent rotation, the majority of the piled-up material is already plastically flattened. Therefore, only small energy is required to overcome the elastic recovered piled-up material and so

friction is reduced. This effect is more pronounced in pin-on-disk than in strip drawing because the edge of the strip drawing tool is smoother with a bigger rounding radius than the edge of the pin. This assumption is, however, still to be verified by further experimental investigation out of the scope of this work.

In the second instance, the coefficient of friction decreases with the increase of speed. This is the case either for the first, the second or the third revolution. The values are, however, high in the range of  $[0.11 - 0.19]$  for DP500+Z and  $[0.11 - 0.16]$  for DP500+ZM. Moreover, the difference between  $0.5 \text{ g/m}^2$  and  $1.5 \text{ g/m}^2$  lubricant amounts is almost insignificant especially at high velocity  $40 \text{ mm/s}$  and higher. Therefore, it can be concluded along with table 2.1 that boundary lubrication is the corresponding lubrication regime.

In the third instance, friction shows low sensibility with respect to the lubricant amount in the regarded configuration of the tribological system as shown in figures 4.8 and 4.9. This is even more pronounced at high speed. This is likely related to instantaneous outflow of the lubricant from the contact interface since the nominal contact area is very small ( $\approx 20 \text{ mm}^2$ ). Therefore the tool size effect can play a significant role in the characterization of the corresponding tribosystem.

## 4.3 Lubricant amount variation in strip drawing

### 4.3.1 Experimental results

Figure 4.10 and 4.11 summarize the results of test. Table 3.3 summarizes the parameter setup for the test. The samples are of dual-phase steel DP500 with zinc coating. Two types of DP500 are taken. One with the thickness of  $0.6 \text{ mm}$  is exclusively for car outer skin. Another with thickness  $0.75 \text{ mm}$  is a multipurpose sheet metal.

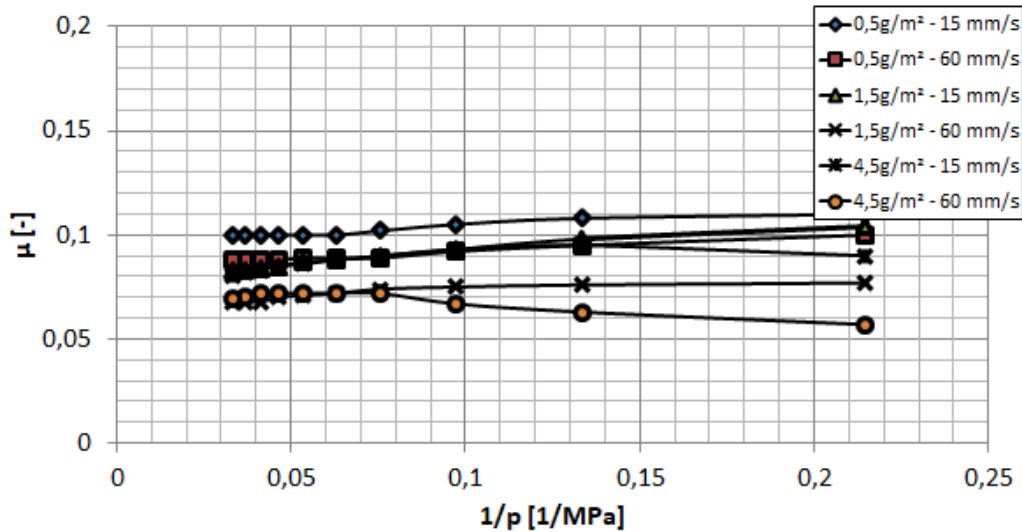


Figure 4.10: Simplified Stribeck curve with DP500+Z (multipurpose,  $R_a = 0.78$ ,  $RP_c = 4.17$ ) and lubricant amount variation.

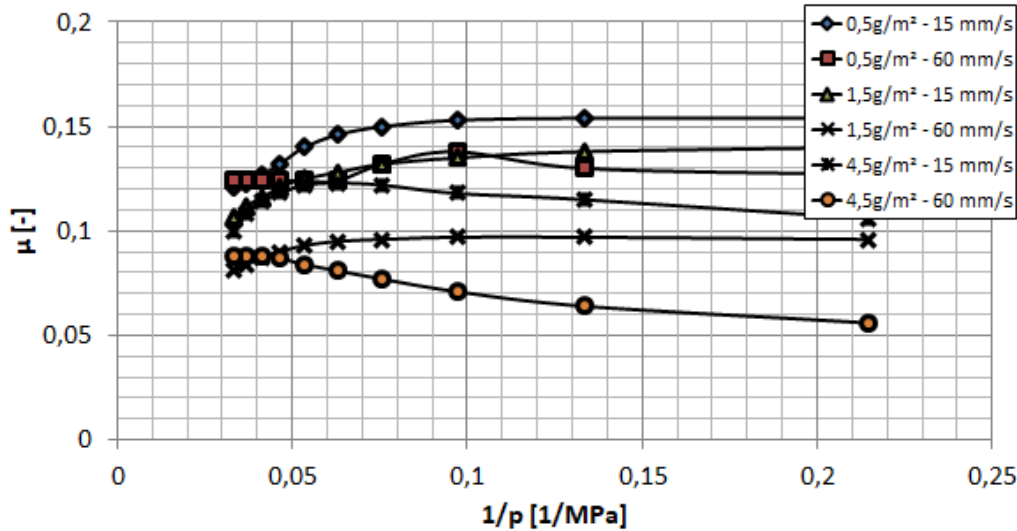


Figure 4.11: Simplified Stribeck curve with DP500+Z (outerskin,  $R_a = 0.86$ ,  $RP_c = 9.2$ ) and lubricant amount variation.

### 4.3.2 Observation

As a general tendency, a decreasing coefficient of friction with increasing contact pressure is observable for the lubricant amount 0.5 and 1.5  $\text{g}/\text{m}^2$  at low (15 mm/s) and high (60 mm/s) drawing speeds for both types of DP500. This is characteristic of boundary lubrication regime although different coefficient of friction corresponds to the same contact pressure and drawing speed. This brings up the question related to the role of the amount of lubricant and the surface topography in boundary lubrication regime.

For the curves (4.5  $\text{g}/\text{m}^2$  – 60 mm/s) for both types of DP500, the coefficient of friction grows with the contact pressure but it is still the lowest among all the regarded cases. The corresponding values lie within the range for a mixed lubrication regime according to table 2.1. After the contact pressure reaches 10 MPa, a transition into boundary lubrication regime is recognized. Thus, mixed lubrication regime occurs at low pressure and high velocity provided that lubricant is in abundance. This is eventually the case in the flange where the contact pressure is low until a certain amount of material has flowed provided that a sufficient amount of lubricant is available.

Hence, it can be concluded that boundary lubrication dominates the deep drawing process albeit mixed lubrication regime can also occur under more restricted conditions i.e. low pressure, high drawing speed and abundance of lubricant. Considering all the curves, a general trend for the Stribeck curve in boundary and mixed lubrication regime can be deduced out of strip drawing test as shown in figure 4.13. While mixed lubrication regime is only characterized by the increase of the coefficient of friction with the growing of the contact pressure as shown in zone A, boundary lubrication is more complex as distinct zones can be observed. The first zone B characterizes a smooth transition from mixed to boundary lubrication. Then, the tribological system develops boundary lubrication with constant coefficient of friction (zone C). The zone D is the final zone where the coefficient of friction decreases until it reaches a final value that is limited by the shear strength of the coating at full contact.

Another observation is that tribosystems with both DP500 with pure zinc coating exhibit

### 4.3. Lubricant amount variation in strip drawing

different frictional behaviors. The one with DP500 for outer skin develops higher friction. Moreover, it can be noticed that the peak density parameter  $RP_c$  of this DP500 for outer skin is twice as great as that of DP500 for multipurpose. Therefore, it can be mentioned forward that the peak density parameter  $RP_c$  can serve a good characteristic as friction might increase with the growth of  $RP_c$ . This will be considered further in the next section.

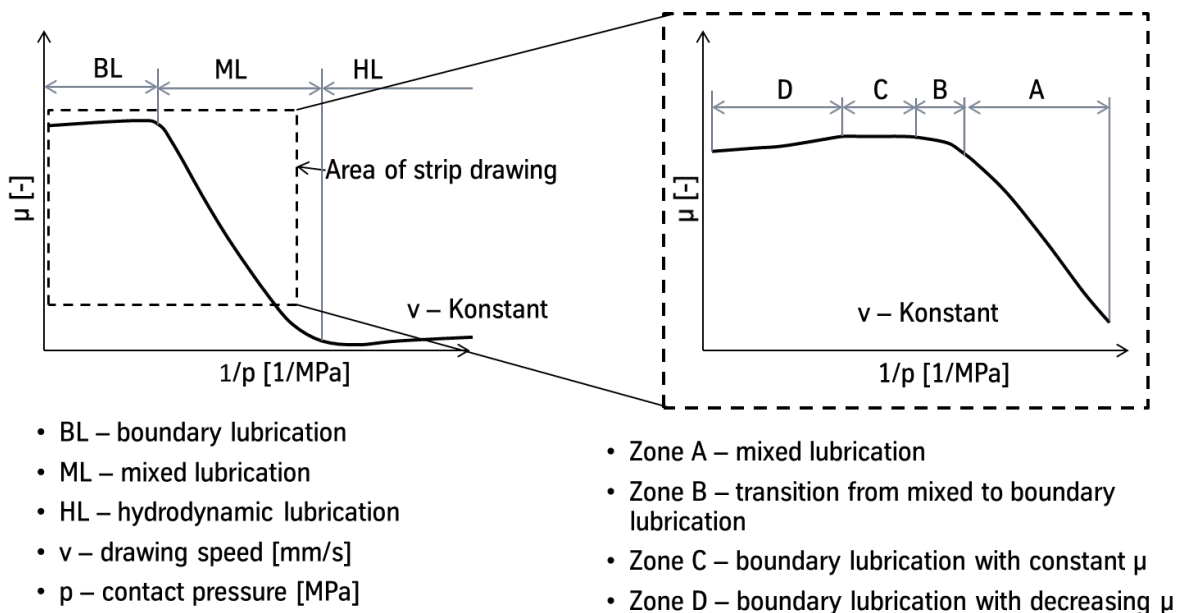


Figure 4.12: Stribeck curve: left – lubrication regime area in strip drawing; right – the different zones of boundary lubrication in strip drawing.

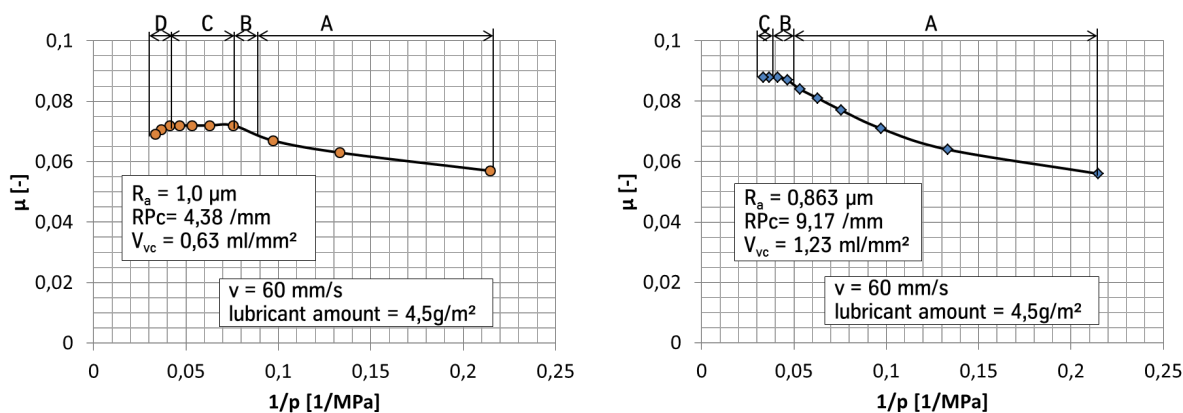


Figure 4.13: Stribeck curve with the different zones of mixed and boundary lubrications: (left) – multi-purpose zinc coated DP500 ( $R_a = 0.78$ ,  $RP_c = 4.17$ ); (right) – car outer skin zinc coated DP500 ( $R_a = 0.86$ ,  $RP_c = 9.2$ ).

## 4.4 Influence of surface topography on friction

### 4.4.1 Experimental results with consideration of blank surface morphology

The results of strip drawing tests with specimens of varying skin-pass levels are presented in the form of Stribeck curve in figure 4.14 and 4.15. The test parameters are described in table 3.5.

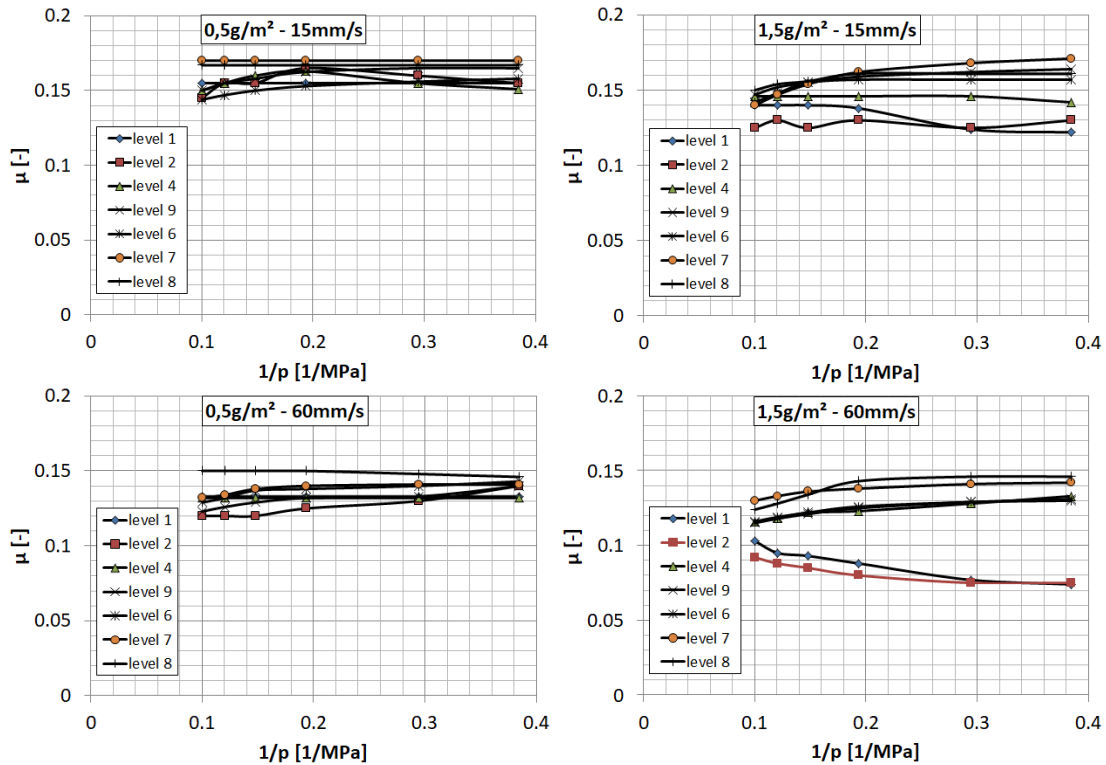


Figure 4.14: Simplified Stribeck curve of the DX57D+Z with different skin-pass levels.

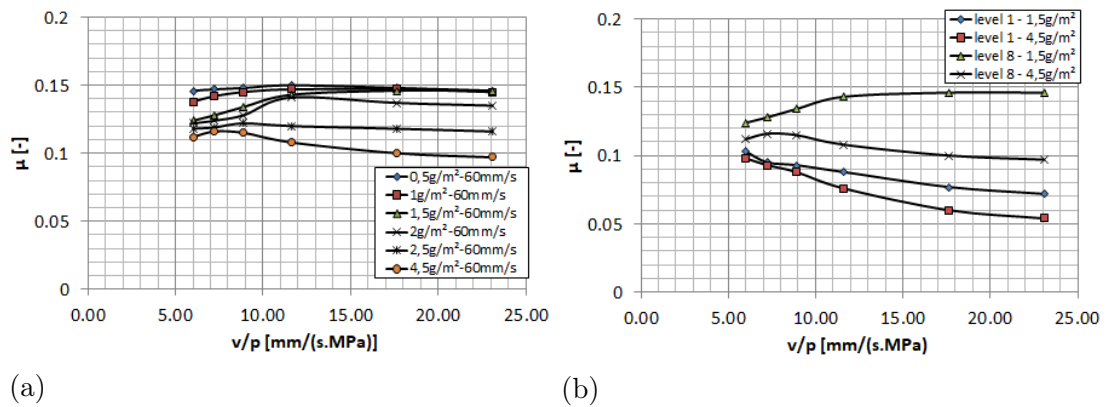


Figure 4.15: Simplified Stribeck curve with lubricant amount variation on DX57D+Z: (a) – skin-pass level 8; (b) – skin-pass level 1 vs level 8.

### 4.4.2 Observation

Figure 4.14 enables to make ascertainment. In the first instance as a generally observed tendency, roughening of sheet metal surface increases the value of the coefficient of friction of the corresponding tribosystem. This behavior is generally independent of the applied lubricant amount and the drawing speed. The roughness average  $R_a$  and root means square  $R_q$  parameters increase and so does the frictional response on the concerned tribosystem. The influence of the peak density parameter  $RP_c$  as mentioned before did not, however, manifest. Therefore, it can be assumed at this point that the surface roughness holds a greater grip on friction than the peak density. Be two surfaces with similar roughness, then the difference in  $RP_c$  will condition the difference in frictional behavior.

In the second instance, when the lubricant amount is low at  $0.5 \text{ g/m}^2$ , the value of the coefficient of friction decreases with the increase of the drawing speed from  $15 \text{ mm/s}$  to  $60 \text{ mm/s}$ . The aforementioned general tendency is preserved as the curves only seem to be shifted down. Hereupon, no particular difference in the behavior of the regarded tribosystems is observed with respect to the skin-pass level and therefore the surface roughness.

In the third instance, when more lubricant is applied i.e.  $1.5 \text{ g/m}^2$ , more significant difference is observed in the behavior of the Stribeck curves with respect to the skin-pass level. Already at low drawing speed, tribosystems with smoother surfaces i.e. lower skin-pass level (level 1 and 2) exhibit lower friction. This effect is even more pronounced with the increase of drawing speed.

In the fourth instance, figure 4.15(b) confirms the above mentioned observation concerning the dependence of friction on surface roughness. Effectively, rough surface incarnated by surface with skin-pass level 8 causes always higher friction even if lubricant is abundantly applied in comparison to smoother surfaces such as the one with skin-pass level 1.

In the fifth instance, complementing the dominant influence of surface roughness on friction, the applied amount of lubricant is alongside a important factor in the frictional behavior of a tribosystem as shown in figure 4.15(a). Effectively, the increase of the applied lubricant amount lowers friction for the corresponding tribosystem. This lubricant amount needs, however, to reach a certain value before its effect can be perceived as here no difference is seen for a lubricant amount lower than  $1.5 \text{ g/m}^2$ .

In the sixth instance, figure 4.15(a) shows another important parameter that enters into play which is the involved contact pressure. Effectively, for any lubricant amount, the Stribeck curve exhibits a constant behavior up to a pressure value around  $5 \text{ MPa}$ . Until here, the effect of lubricant amount is still very explicit. When the contact pressure increases further, the effect of lubricant amount starts to narrow down and gradually vanishes. This is generally observed except for the very low lubricant amount compared to the surface void volume i.e.  $0.5$  and  $1 \text{ g/m}^2$ .

### 4.4.3 Experimental results with consideration of tool surface morphology

The results of strip drawing tests with grinded and polished tools are presented in the form of Stribeck curve in figure 4.16. The test parameters are described in table 3.6.

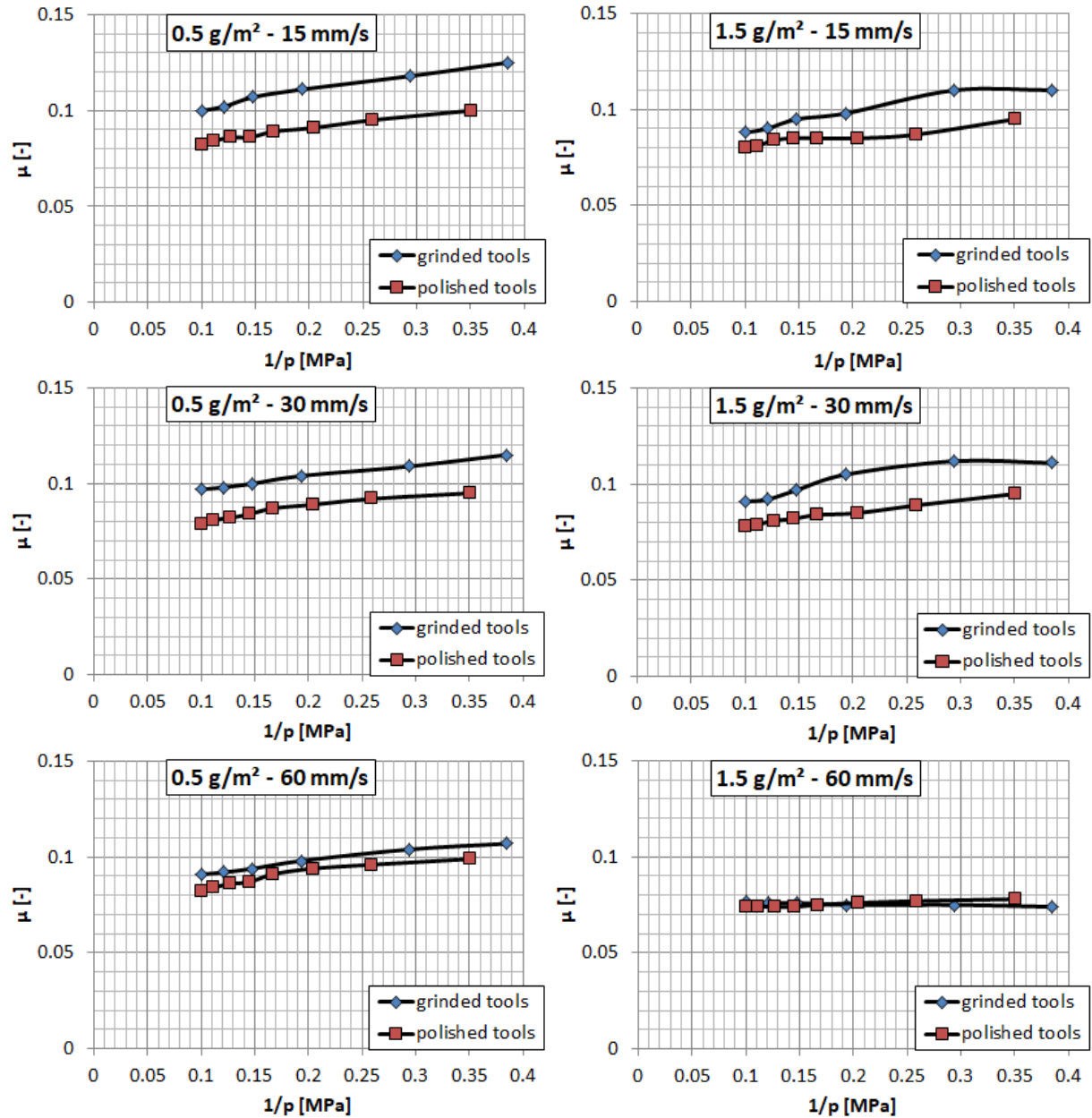


Figure 4.16: Comparison of the frictional behavior of tribosystems with grinded and polished tool surfaces.

### 4.4.4 Observation

A general tendency is observed in figure 4.16 that is polished tool with smoother surface lessens friction of the corresponding tribosystem independently of the lubricant amount

and the drawing speed. This observation complements the observation in section 6.1.1 about the influence of the roughness of the sheet metal surface. A slight difference is, however, to be mentioned namely the influence of the drawing speed. Effectively, the difference between the frictional behaviors of the tribosystems narrows down with the increase of drawing velocity independently of the lubricant amount. This difference practically vanished at 60 mm/s. Another ascertainment is that the curves from the polished tool remain practically unchanged except at 60 mm/s with 1.5 g/m<sup>2</sup> of lubricant. Lubricant amount has also a certain impact by reducing further the difference mentioned above. At high drawing speed (60 mm/s) with enough lubricant (1.5 g/m<sup>2</sup>) to cover the sheet metal surface, the two tribosystems display similar frictional behavior.

## 4.5 Discussion

### 4.5.1 Characterization of lubrication regimes

The obtained Stribeck curves from strip drawing test for the study of sheet metal surface roughness correspond to specific lubrication regimes. Taking in the first instance the reference values from table 2.1, the occurring lubrication is mainly characterized by boundary lubrication regime as the majority of the obtained values of the coefficient of friction lies above 0.1. The only exception concerns the tribosystem with sheet metals of skin-pass level 1 and 2 where the corresponding curves lie under 0.1 at drawing speed of 60 mm/s and a lubricant amount above 1.5 g/m<sup>2</sup>. They are in mixed lubrication regime.

In the second instance, taking complementary into account the curve behavior, the above conclusion can be further accepted. Effectively, the majority of the curves either decreases or remains constant with the grow of contact pressure. Only the cases with skin-pass level 1 and 2 exhibits a steady growth with contact pressure.

In the third instance, the void volumes of the sheet metal surfaces as well as the applied lubricant amount play a crucial role in the determination of the characteristic lubrication regime. Effectively, all the surfaces except those with skin-pass level 1 and 2 have a void volume above the applied lubricant amount. This means the surfaces are not completely covered by lubricant which does not enable to call for at least a mixed lubrication regime. On the contrary, with a  $V_{vc}$  around 1.5 ml/m<sup>2</sup> which corresponds to the minimum of the considered lubricant amount, the surfaces of skin-pass level 1 and 2 are theoretically covered with lubricant so that trapped lubricant in the voids can carry a part of the contact load.

At this point, it can be rigorously accepted that the majority of tribosystems are in boundary lubrication regime except those corresponding to sheet metal with skin-pass level 1 and 2 when the drawing speed is 60 mm/s and the lubricant amount is above 1.5 g/m<sup>2</sup>. They are in mixed lubrication regime. The same might still be assumed for the tribosystem with skin-pass level 8 at lubricant amount equals 4.5 g/m<sup>2</sup> and drawing speed of 60 mm/s. The values of coefficient of friction at low pressure up to 3.3 MPa can be still considered to correspond to mixed lubrication regime but they are already at the boundary. Therefore, the plausibility can be taken but with reserve. One important remark is that macro-hydrodynamic lubrication cannot occur although lubricant is in abundance. Effectively, the drawing speed is too low and a large amount of lubricant has

enough time to squeeze out of the contact interface on the side or directly in front of the tool as shown in figure 4.17 so that not enough hydrodynamic pressure is built up.

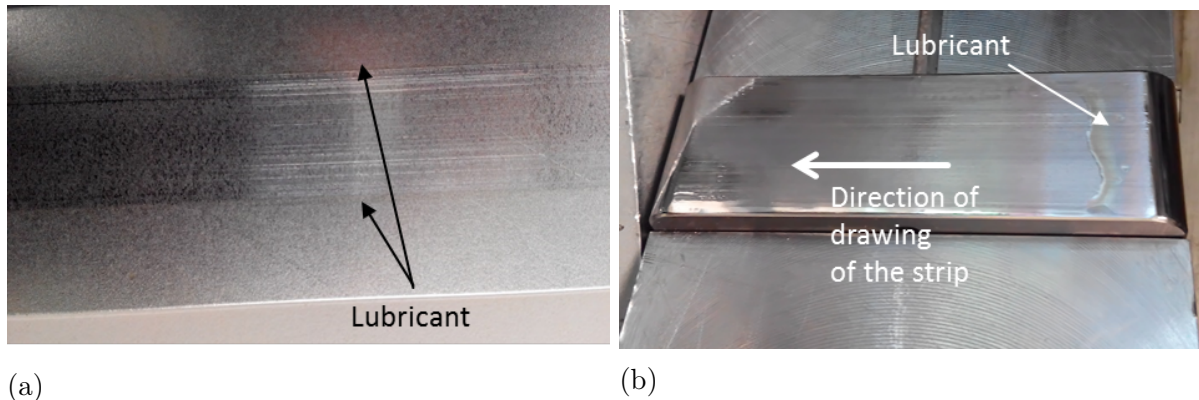


Figure 4.17: Lubricant squeezed out of the contact interface (lubricant amount  $4.5 \text{ g/m}^2$ ): (a) – on the side; (b) – at the entrance into the contact.

Analogically, the Stribeck curves from the study of the influence of tool surface roughness reflects the characteristic lubrication regimes of the corresponding tribosystem. When the applied lubricant amount is  $0.5 \text{ g/m}^2$  which is less than the sheet metal surface void volume ( $V_{vc}=0.63 \text{ ml/m}^2$ ), the sheet metal surface is not fully covered with lubricant and therefore a call for a mixed lubrication regime is practically improbable nay impossible. Moreover, the curves decrease with growth of contact pressure which is more characteristic of the boundary lubrication zone. Although the values of the coefficient of friction lie beneath 0.1 which may indicate the occurrence of mixed lubrication regime according to table 2.1, it is to keep in mind that the given values in the table are just for reference but not strictly binding.

## 4.5.2 Importance of tool surface finishing

The occurring plastic deformation at the asperity contact depends on the average slope of the asperities of the harder surface [Avi86] expressed in terms of the arithmetic mean slope of the raw profile  $P_{da}$ . The polished tool surface has its topography parameters to be much smaller than those of the grinded surface referring to table 3.11. Thus, the resulting contribution to friction is expected to be smaller as well. As shown in figure 4.16, tribosystem with the polished tool exhibits in general a lower frictional resistance than that with the grinded tool. The result was expected since polished tool surface has small asperity slope ( $P_{da}(\text{polished tool}) = 3^\circ \text{ deg}$ ) than the grinded one ( $P_{da}(\text{grinded tool}) = 8^\circ \text{ deg}$ ). Both surfaces have comparable hardness and did not undergo any surface treatment. Thereby, the reduction of ploughing coefficient  $\mu_p$  is seemingly to be the main reason of lower friction. The difference varies, nevertheless, in terms of the drawing speed and lubricant amount while it is insensitive to the contact pressure. Effectively, the drawing speed appears to be the most influencing factor. First at low speed ( $15 \text{ mm/s}$ ), the difference in the frictional resistance of the two tribosystems is very pronounced. As the drawing speed increases, this difference lessens and the influence of the tool surface roughness becomes less and less dominating keeping in mind that the sheet metal surface is still much rougher.

The invariance of the curves with polished tools enables to take the frictional behavior of a tribosystem with very smooth tool surface as a reference. This allows to make the hypothesis that the activation of a desired lubrication regime and the obtaining of desired frictional behavior of a given tribosystem in deep drawing can be achieved also by varying tool surface topography especially the Pda parameter.

### 4.5.3 Role of sheet metal surface topography

As it was already mentioned in section 1.2.4, lubrication has three main principles namely (1) lubricating of the real contact area so that no direct surface to surface contact occurs, (2) generation of micro-hydrodynamic pressure at the surface plateaus in mixed lubrication regime and (3) generation of micro-hydrostatic pressure in lubricant pockets. By varying the lubricant amount in 4.15(a), it is observed that the material void volume is an important parameter of the sheet metal surface. At low contact pressure (less than 5 MPa) by lubricant amounts 0.5/1/1.5 g/m<sup>2</sup> less than the material void volume (V<sub>vc</sub>=2.59 ml/m<sup>2</sup>), the coefficient of friction remains the same. This means that the trapped lubricant in the deep valleys of the surface texture does not have any influence on the course of friction.

With a further increase of the contact pressure, flattening of the surface asperities continues and closed void volumes start to form. Those void volumes generate lubricant pockets which in turn withstand a part of the applied normal force in the form of hydrostatic pressure. Thus, with approximately the same friction force but greater normal force, the coefficient of friction decreases. However, those closed void volumes are still too big (approximately 1.5 g/m<sup>2</sup>) for the 0.5 and 1 g/m<sup>2</sup> of lubricant to fill. In this case, no hydrostatic pressure is generated and the coefficient of friction remains unchanged. For 1.5 g/m<sup>2</sup> of lubricant, the lubricant pockets are now activated so that the coefficient of friction decreases further with the pressure growth. The same behavior as for 1.5 g/m<sup>2</sup> is observed for 2 g/m<sup>2</sup> of lubricant. The only difference is that the coefficient of friction at low pressure is slightly lower. This may be related to the first principle of lubrication i.e. the lubricant may be in the required amount to lubricate the real contact area and to replace efficiently the scrubbed boundary layer in time to impede the direct contact of the surfaces. Above 5 MPa, it operates similarly as described before. When the lubricant amount exceeds the material void volume, mixed lubrication regime may already take place at the low contact pressure. The micro-hydrodynamic pressure can be generated to counterbalance the applied normal force. The lubricant can be more effective as well by replacing the scrubbed boundary layer instantaneously. With the increase of pressure, lubricant pockets form accordingly.

In figure 4.15(b), the difference of the influence of the lubricant for different skin-pass levels is presented. The level 1 has much smaller roughness with smaller void volume (V<sub>vc</sub>=1.52 ml/m<sup>2</sup>) than level 8 (V<sub>vc</sub>=2.59 ml/m<sup>2</sup>). At high lubricant amount i.e. 4.5 g/m<sup>2</sup>, the surface with skin-pass level 1 presents few advantages compared to the surface with skin-pass level 8.

Firstly, the overall material void volume is smaller. Therefore, a thicker pure lubricant film corresponding to approximately 3 g/m<sup>2</sup> covers the surface in comparison to 2 g/m<sup>2</sup> for that of skin-pass level 8. During drawing, this lubricant layer will squeeze out of the contact surface. Thus, the contacting surfaces may stay longer separated by the lubricant

layer or the real contact spots are more lubricated as well.

Secondly, skin-pass rolling process enforces the surface to have a certain roughness. The greater the skin-pass force gets, the more pronounced the surface roughness is. This is seen through the increase of the peak numbers, the average roughness and average roughness height. The plateaus become rougher and do not provide favorable conditions for the micro-hydrodynamic pressure to build up.

Thirdly, surface with skin-pass level 1 has shallow valleys. In the case of abundant available lubricant amount, the flow of lubricant from the valley to the plateau and back is easier. Therefore, the lubricant is more efficient in fulfilling its tasks.



# Chapter 5

## Influence of surface coating type on friction and wear

Figure 3.13 shows that zinc and zinc-magnesium coatings exhibit clear difference in terms of microstructure and chemical composition. The dissimilarity of the frictional as well as the wear behavior of the corresponding tribosystems has risen many questions at thyssenkrupp Steel. It is often observed that the zinc-magnesium enhances to a certain extent the drawability of the sheet metal compared to the traditional pure zinc coating. However, the precise tribological phenomenon that lies behind is not well understood yet. Moreover, zinc-magnesium coating appears to cause less wear of the tool especially galling. The reasons are assumed to be closely related to the microstructure of the coating, the mechanical properties including the hardness and the chemical compositions especially that of the near-surface zone. Thereby, the main hypothesis is that by adding a certain amount of magnesium in the zinc bath, the resulting surface coating which exhibits different properties and characteristics compared to pure zinc coating enhances also the drawing properties of the sheet metal. In order to verify the aforementioned assumption, dual-phase steels with zinc and zinc-magnesium coatings are used for friction and wear (running-in) experiments by strip drawing and pin-on-disk tests.

### 5.1 Running-in test by pin-on-disk with radionuclide-technique

Running-in is the phase when two different tribosystems can exhibit the most dissimilar frictional and wear behavior. For this reason, pin-on-disk test was performed with a special setup of the tribometer as already described in section 3.1.1.2. Figure 5.1 and 5.2 summarize the results of the test in the form of a dependence of the coefficient of friction with respect to the number of performed tests. Additionally, figure 5.3 and 5.4 show the results of the radionuclide-technique for the tracing of tool wear particles which are expressed in the form of a dependence of the mass of the wear particles [mg] with respect to time [s]. The highlighted red points correspond to the time when a disk is measured.

Friction measurement shows for both investigated tribosystems that the first revolution always yields a higher coefficient friction which decreases with further rotations. For pure zinc coating, this difference is even around 80 - 90 percent between the first and third

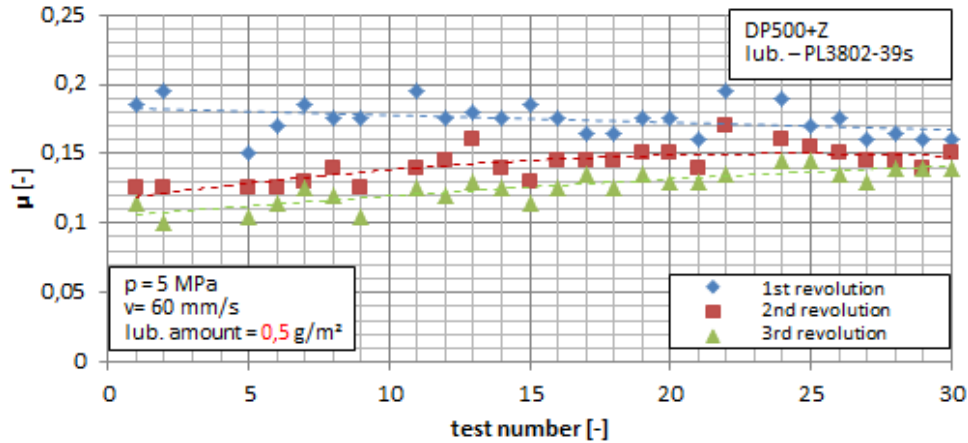


Figure 5.1: Result of pin-on-disk for the investigation of running-in behavior of tool with DP500+Z (one test consists of three revolutions).

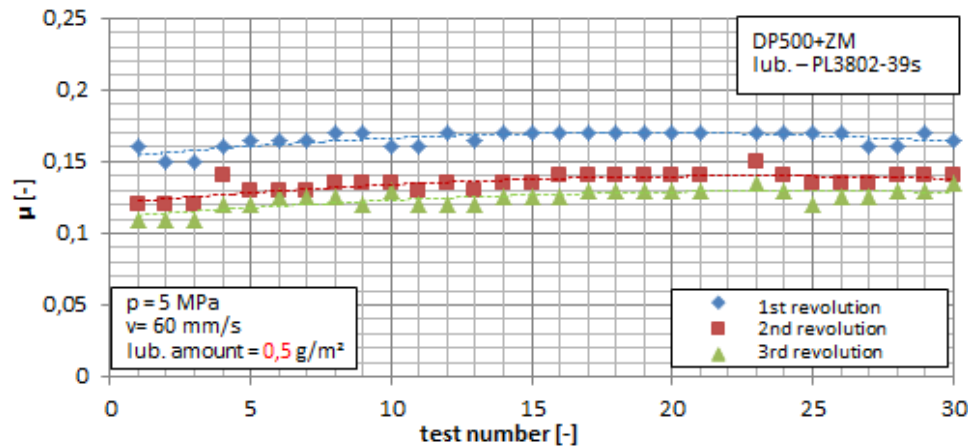


Figure 5.2: Result of pin-on-disk for the investigation of running-in behavior of tool with DP500+ZM (one test consists of three revolutions).

rotation during the first tests. The discrepancy between the values gradually diminishes, however, with the number of test and stabilizes around 0.15 from test number 25. This means that when the pin passes over the same wear track over and over again, the resulting friction decreases. This difference is very pronounced at the first tests for the tribosystem with pure zinc coating. The discrepancy between the values gradually diminishes with the number of test and stabilizes from test number 25. The same decrease of the coefficient of friction with respect to the revolution number is also observed for the tribosystem with zinc-magnesium. The difference is, however, preserved so that the coefficient of friction is independent of the test number. A general trend for both case is that the coefficient of friction slightly increases with the test number especially from the second and third revolutions. At the end of the experiment, the average values of the coefficient of friction for both tribosystems are assimilable.

For wear particle measurement by means of radionuclide-technique, the result shows that no wear particle was detected from the pin. In turn, wear particles from the surface coatings of the sheet metals are seen for both regarded cases. However, since only the tool was activated, their amounts could not be estimated by means of the radionuclide-technique. From this follows that wear particles as a third body resulting from the

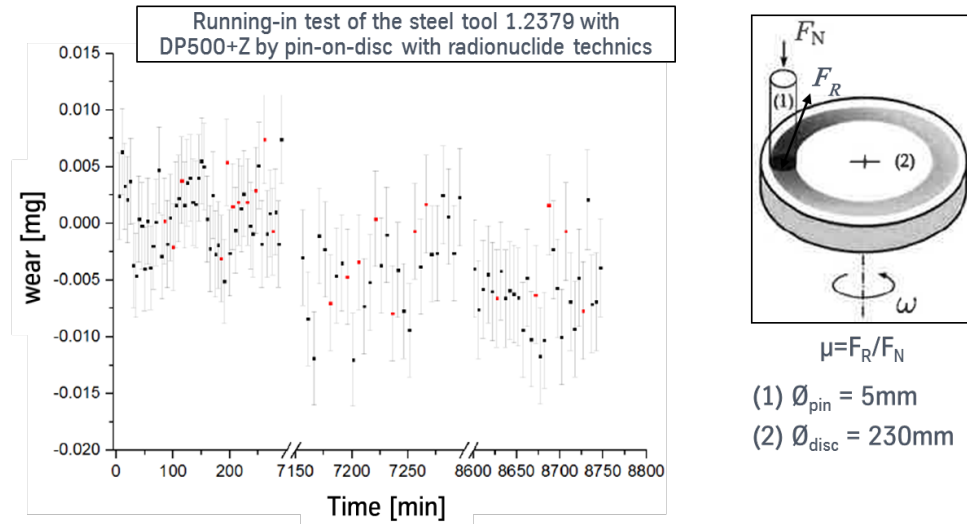


Figure 5.3: Result of radionuclide-technique for running-in test of the tool steel with DP500+Z.

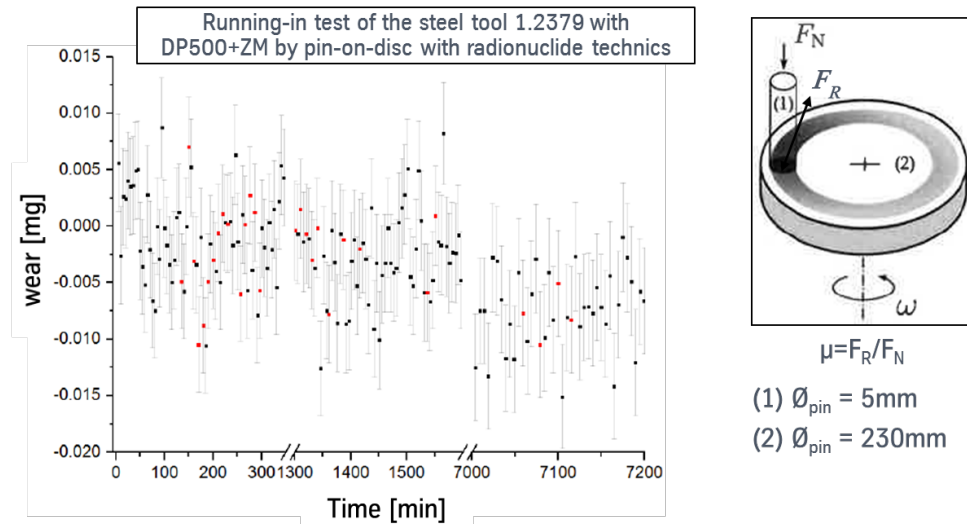


Figure 5.4: Result of radionuclide-technique for running-in test of the tool steel with DP500+ZM.

reaction of the two first bodies were not detected either.

## 5.2 Running-in test by strip drawing

Analogically to pin-on-disk experiment, strip drawing tests were also performed with DP500+Z and DP500+ZM with the same contact conditions i.e. with a lubricant amount of  $0.5 \text{ g/m}^2$  at a drawing speed of  $60 \text{ mm/s}$  and under a pressure of  $5 \text{ MPa}$ . Taking a fresh tool with grinded surface as shown in figure 3.10 (a) in section 3.2.4, 70 strips of DP500+Z are drawn one after another with a lubricant amount of  $0.5 \text{ g/m}^2$  at a drawing speed of  $60 \text{ mm/s}$ . The coefficient of friction for each test is recorded. Figure 5.5 summarizes the results as a dependence of the coefficient of friction  $\mu$  with respect to the

number of drawing test. The same procedure is performed with 70 strips of DP500+ZM.

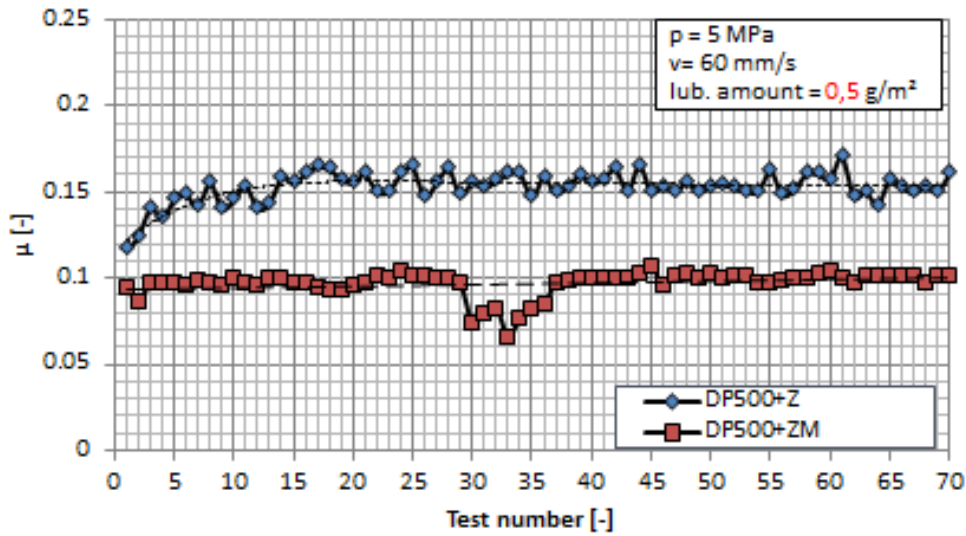


Figure 5.5: Result of strip drawing test for the investigation of the difference of frictional and running-in behaviors between DP500+Z and DP500+ZM.

Tribosystem with pure zinc coating exhibits higher friction than that with zinc magnesium coating. The difference in the coefficients of friction is all the more about 0.05 which is not negligible. The little oscillation of the measurement results around the average values for both tribosystems confirms that the tribosystem with zinc-magnesium surface coating exhibits indeed lower friction. For the tribosystem with pure zinc coating surface, the value of coefficient of friction smoothly increases during the first 20 experiments before it stabilizes around 0.16. This shows that the system requires a certain period of time or more precisely a certain drawing distance to find an equilibrium state. Since the strip is always new at every stroke, it is the tool that is in a need to adjust to the new in-coming surface. This effect is not observed for the system with zinc-magnesium coating surface as the value of the coefficient of friction remains unchanged with respect to the number of experiments. At this point, it is not obvious yet to pronounce about a possible running-in behavior of either of the regarded tribosystems.

Since the tools for the tests were manufactured together, an investigation of the tool surfaces after the experiments is the next step to obtain more information on the dissimilarity between an interaction with pure zinc coating and zinc-magnesium coating.

## 5.3 Analysis of the surface of strip drawing tool

### 5.3.1 Topography analysis

The surface topography of the tools is measured using a confocal microscope which was already described in 3.1.2.3 before and after the tests. Figure 5.6 presents the results while table 5.1 provides the corresponding parameters. Figure 5.7 also provides SEM pictures of the tool surface.

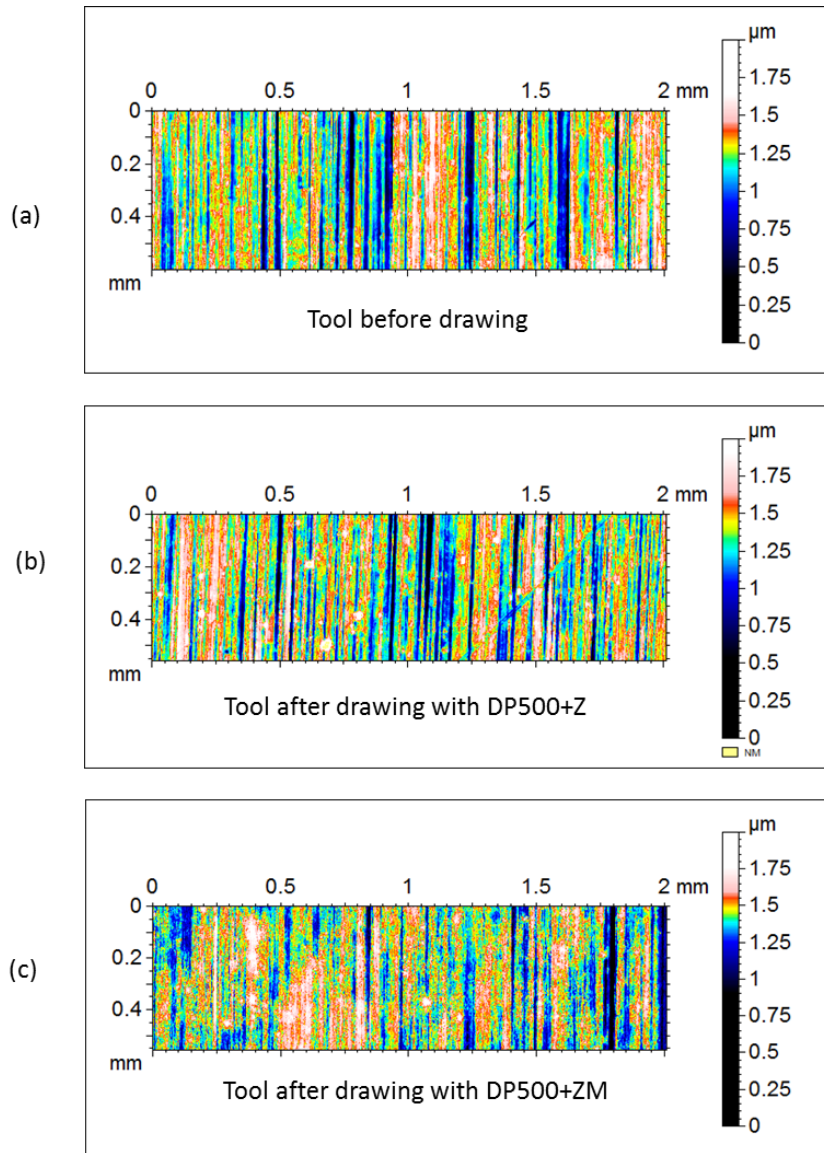


Figure 5.6: Topography of the tool before (a) and after drawing with DP500+Z (b) and DP500+ZM (c) with the corresponding height distribution (not at the same location).

parameters of the roughness profile	initial state	with DP500+Z	with DP500+ZM	unit
$RP_c$	21	23.1	22	[1/mm]
$R_p$	0.552	0.7	0.54	[ $\mu\text{m}$ ]
$R_z$	1.5	1.61	1.25	[ $\mu\text{m}$ ]
$R_a$	0.183	0.203	0.142	[ $\mu\text{m}$ ]
$R_q$	0.246	0.261	0.188	[ $\mu\text{m}$ ]
$R_{sk}$	-1.04	-0.516	-0.15	
$R_{ku}$	4.96	4.07	4.82	

Table 5.1: Topography parameters of the tool before and after drawing with DP500+Z and DP500+ZM.

Figure 5.7 as SEM pictures shows that both DP500+Z and DP500+ZM surfaces change

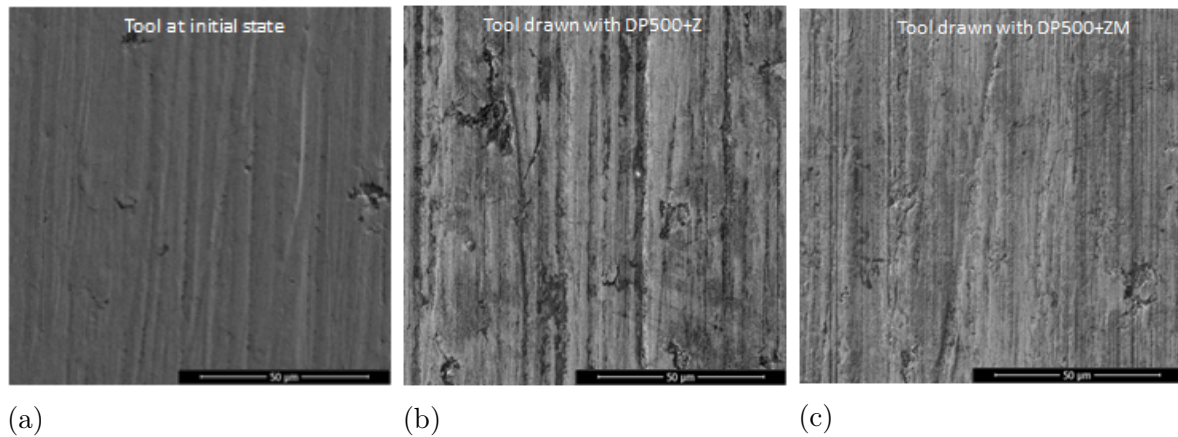


Figure 5.7: SEM picture of the strip drawing tool surface: (a) - before drawing; (b) - after drawing with DP500+Z and (c) - after drawing with DP500+ZM.

the morphology of the tool surface. It could be assumed, in a first instance, that the tool surface which interacted with pure zinc coating is subject to abrasive wear. However, pin-on-disk with RNT could not detect any wear particles from the tool which automatically discards the made assumption. Therefore, the surface change is merely a result of plastic deformation.

The deviation of the tool surface from its initial shape is around 10% and 20% for the cases corresponding to DP500+ZM and DP500+Z respectively. This can be seen by the value of roughness parameters in table 5.1. DP500+Z appears to induce a roughening of the tool while DP500+ZM tends to smoothen it. In spite of that, the roughness of the tool surface still remains much lower than that of the sheet metal surface. It is, however, important to mention that a only slight roughing or smoothening of the tool may lead to a more conspicuous increase or decrease of the coefficient of friction. Effectively, Kirkhorn *et al.* [Kir13] stated that friction reduces with the smoothening of the surfaces.

#### 5.3.2 Analysis of the microstructure of near-surface zone

The analysis of the near-surface zone enables to obtain further information on the possible transformation of the microstructure due to tribological loading and the resulting plastic deformation. This can, indeed, have an important role in the resulting friction and wear. For the analysis, the Scanning Electron Microscopy with Focused Ion Beam or FIB (on Zeiss XB 1540) is used. The advantage in the application of FIB consists of the possibility to accurately position the investigated area so that the smallest structure in the cross section can be also visualized. In other words, by means of FIB, it is possible to see the real microstructure of the near surface in Z-direction. Figure 5.8 shows the results of the measurement.

Few ascertainments can be pulled out of the observation of the FIB profiles of the tool when comparison is made between the microstructure of the peripheral zones:

- A nanocrystalline microstructure is observed directly under the surface up to a depth of 200-500 nm.
- A refinement of the microstructure is observed from the surface to the depth of

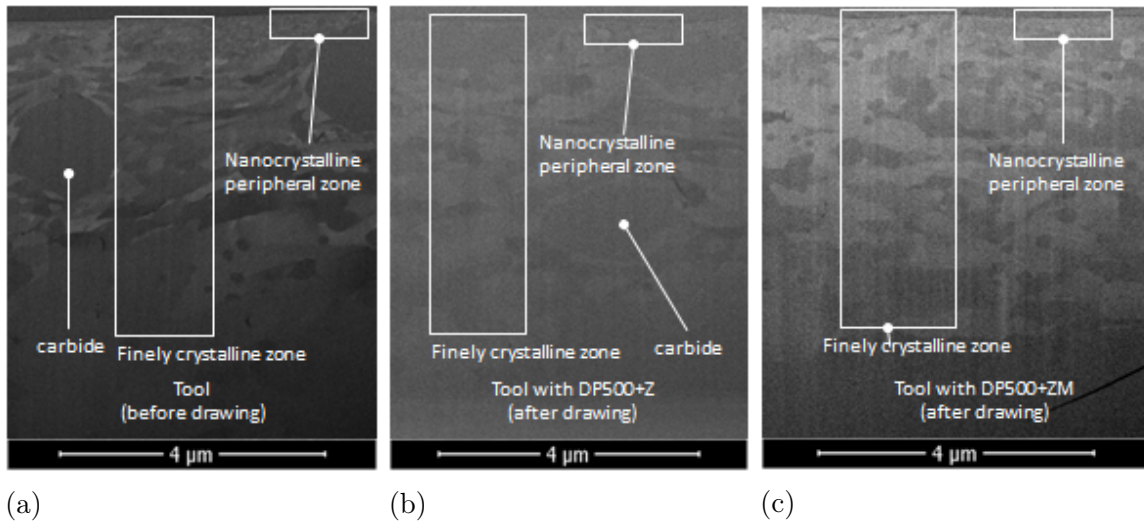


Figure 5.8: SEM picture of FIB profiles of the tool from secondary electrons: (a) - before drawing; (b) - after drawing with DP500+Z and (c) - after drawing with DP500+ZM.

approximately  $6 \mu\text{m}$ . Figure 5.8 enables to clearly observe material shift around the carbides.

- Carbide is observed at the fine crystalline zone of  $6 \mu\text{m}$ . The absence of observable carbide in the case of the tool drawn with DP500+ZM may solely due to the inhomogeneity of the subsurface microstructure.

From the aforementioned observations, no significant change in the subsurface structure due to tribological loading is found.

### 5.3.3 Analysis of the chemical composition of the surface

For the chemical analysis of the surfaces, X-ray Photoelectron Spectroscopy (XPS) and Glow-discharged optical emission spectrometry (GDOES) are applied. The basic principles are already discussed in section 3.1.2.1.

#### 5.3.3.1 XPS-Analysis - Depth profiling of the tool surface

Figures 5.9 - 5.14 give the results of depth profiles of the samples. A first comparison between unworn (initial) and worn (drawn) states of the tool shows only a superficial change in the chemical composition of the near surface zone up to 80 nanometers depth.

Figure 5.9 enables to observe a high oxygen content on the tool surface at the unworn state up to 40 nanometers depth. This is due to the grinding process during which high contact temperature enhances an oxidation process. Therefore, the metal constituents of the matrix especially the iron (Fe) and chrome (Cr) oxidized. After drawing, figure 5.11 and 5.12 show that the oxygen content increases to almost twice the amount at the unworn state. This is due to further oxidation of iron on the surface since the content of metallic iron has also dropped in the same zone (up to 80 nanometers).

The presence of zinc and calcium oxides on the tool surface through tribological contact

### 5.3. Analysis of the surface of strip drawing tool

is also an additional contribution to the high oxygen content.

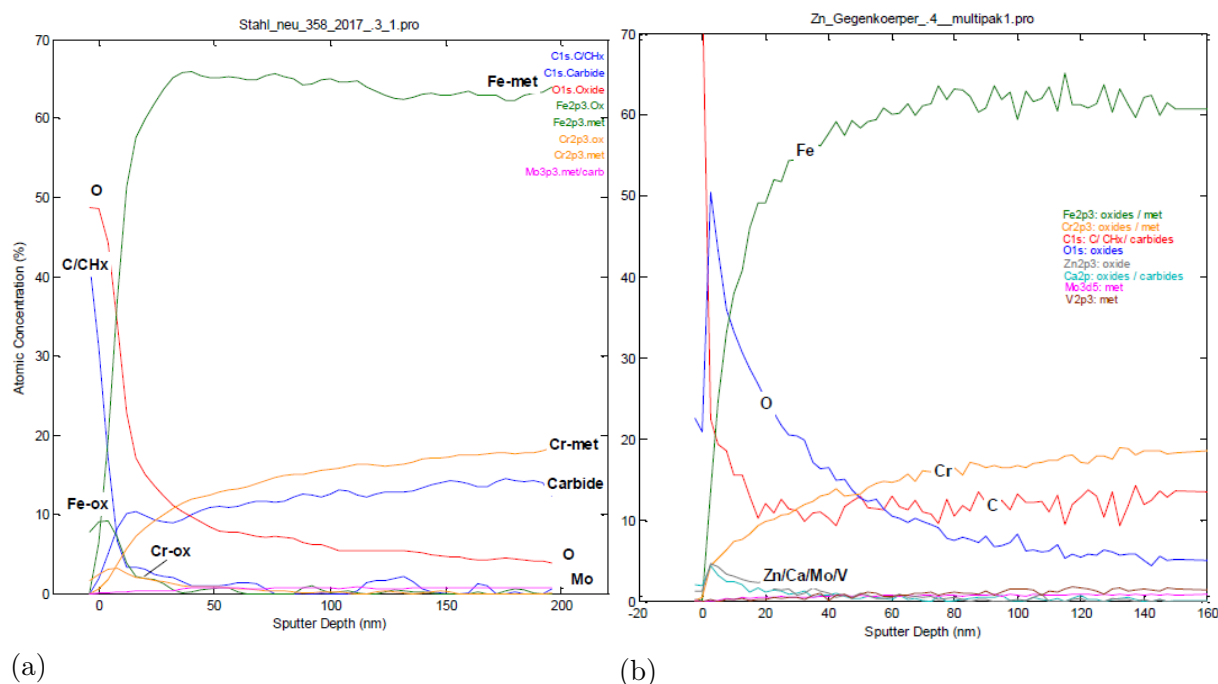


Figure 5.9: XPS depth profile of tool surface drawn with DP500+Z (in original format): (a) – before drawing; (b) – after drawing with DP500+Z.

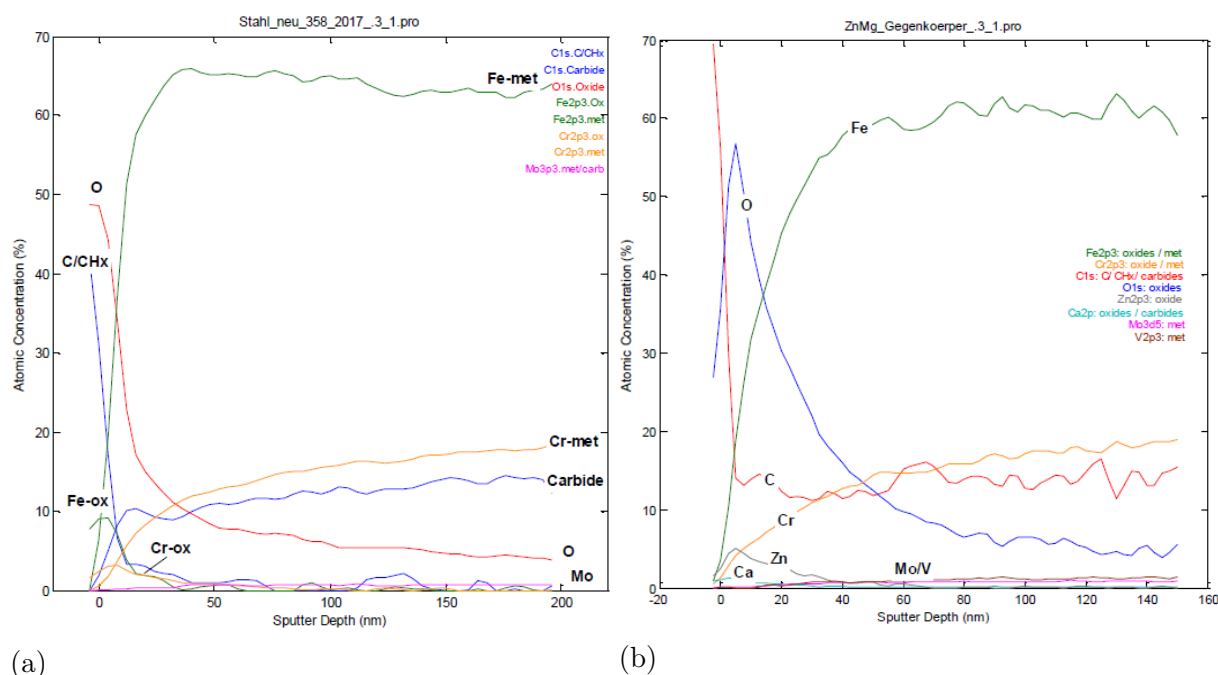


Figure 5.10: XPS depth profile for the tool drawn with DP500+ZM (in original format): (a) – before drawing; (b) – after drawing with DP500+ZM.

Similar amount of Fe-oxide on the tool surface for both drawing cases with DP500+Z and DP500+ZM shows that the big difference in the values of the coefficients of friction (0.15 for DP500+Z and 0.10 for DP500+ZM) is not caused by the oxidation process of the metals on the tool surfaces.

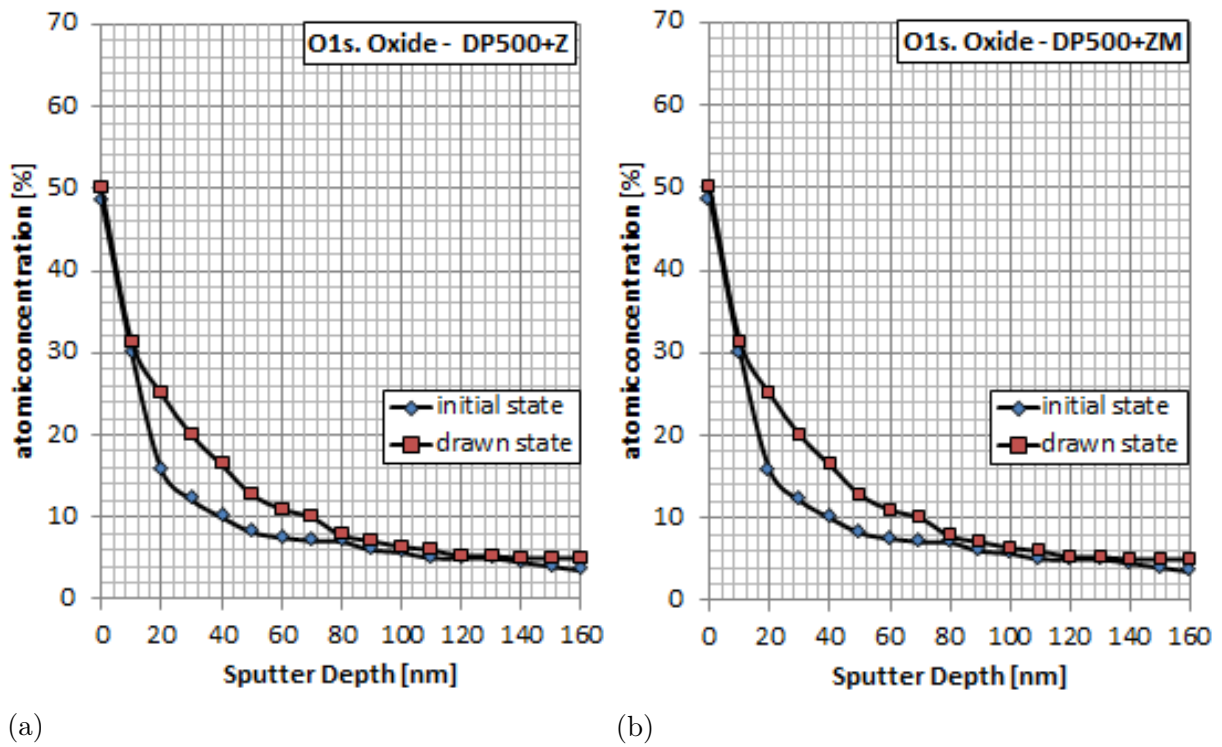


Figure 5.11: XPS depth profiles of O1s.Oxide for the tools: (a) – drawn with DP500+Z; (b) – drawn with DP500+ZM.

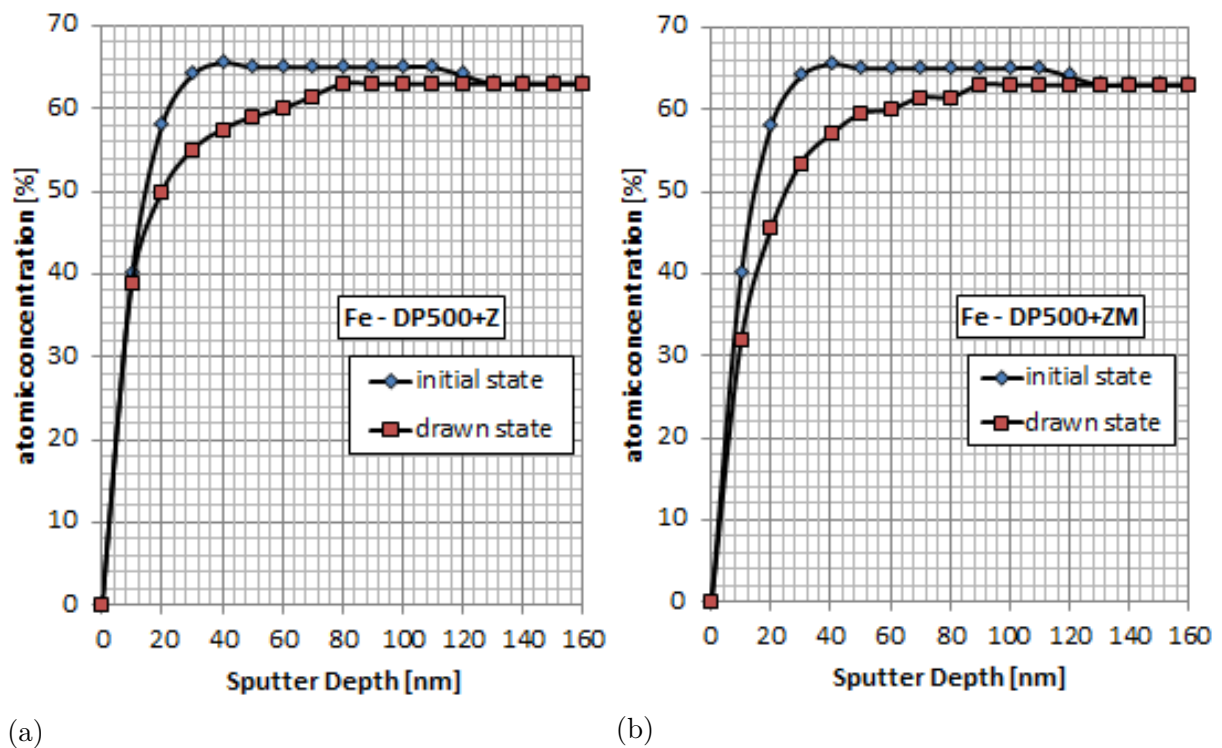


Figure 5.12: XPS depth profiles of Fe-metal/oxide for the tools: (a) – drawn with DP500+Z; (b) – drawn with DP500+ZM.

Concentration of carbon on the tool surface at the unworn state is high in the vicinity of

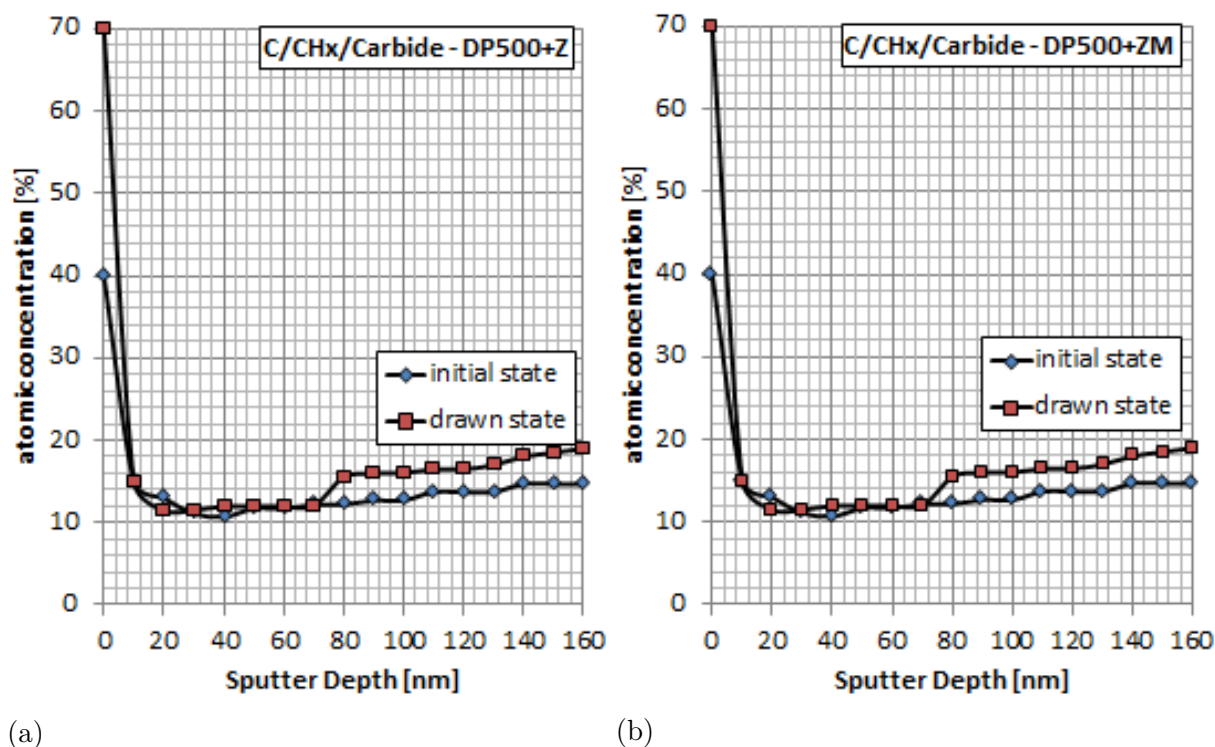


Figure 5.13: XPS depth profiles of C/CHx for the tools: (a) – drawn with DP500+Z; (b) – drawn with DP500+ZM.

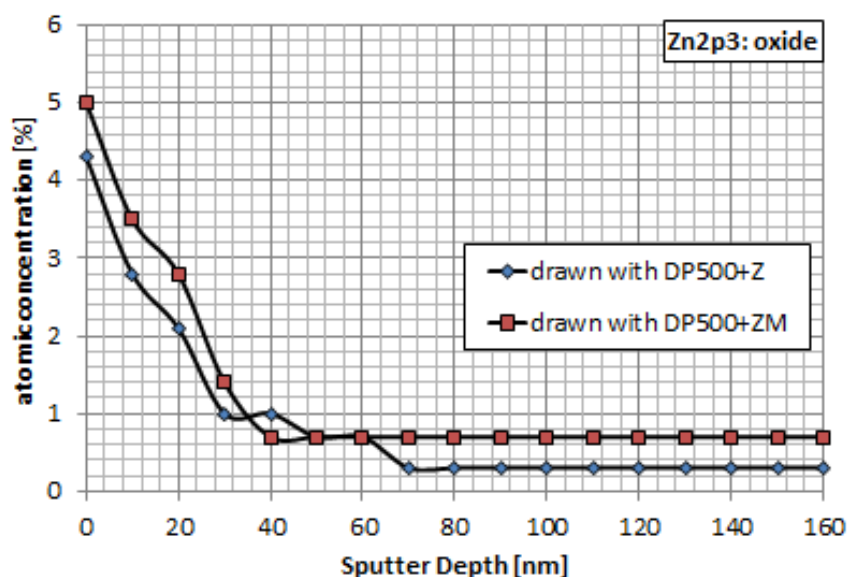


Figure 5.14: Comparison of XPS depth profiles of Zn2p3-oxide on tools.

the surface up to 10 nanometers. This is most probably related to the carbide enrichment as shown in figure 5.8, the formation of which originates from the finishing stage of the grinding process of the tool surface.

Through tribological loading, oxidation of the lubricant which contains a great deal of hydrocarbon also takes place which further contributes to the enrichment of carbon on the top layer of the tool surface.

Figure 5.14 enables to observe a clear transfer of zinc material on the tool surface either the tool was drawn with zinc or zinc-magnesium coated steel strips. The amounts of material transfer for both cases are, moreover, similar. This shows that the presence of lubricant does not completely impede the adhesion of zinc on the tool surface. However, at this point, the similarity of the transfer amount for both cases with zinc and zinc-magnesium coatings does not justify the big difference in the values of coefficient of friction. The GDOES may provide more detail on the material transfer.

### 5.3.3.2 Glow-discharged optical emission spectrometry of tool surfaces

Figure 5.15 provides pictures of the tools where the measurement spots are marked. For the comparison of the result with the unworn state, measurements were also done on the side of the tools where no contact with the strips took place. Table 5.2 gives the surface coverage of the transfer material in the first 100 nm of the tool surface.

	measurement area	Zn	Al	Mg	Unit
tool	side	2.2	<1	<1	mg/m <sup>2</sup>
tool with DP500+Z	middle	24.3	5.4	<1	mg/m <sup>2</sup>
	edge	20.4	3.4	<1	mg/m <sup>2</sup>
tool with DP500+ZM	middle	8.7	5.2	5.2	mg/m <sup>2</sup>
	edge	8.4	4.1	3.5	mg/m <sup>2</sup>

Table 5.2: Surface coverage of the transfer material on the tool.

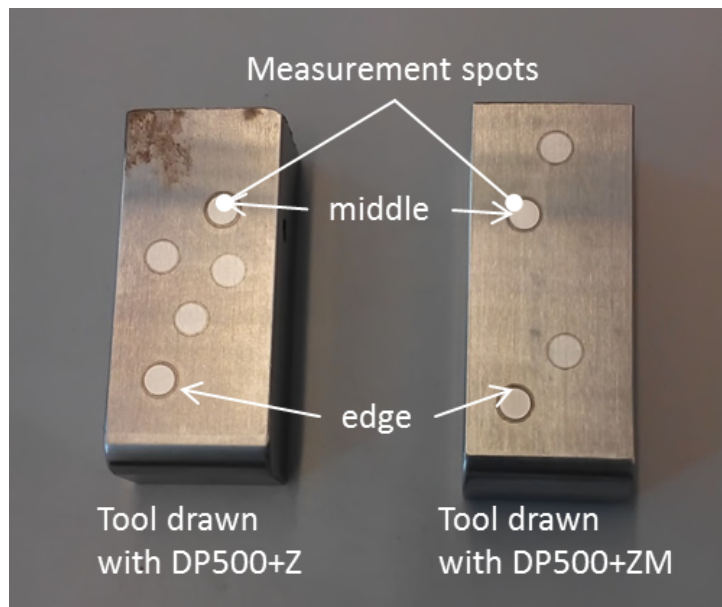


Figure 5.15: Tools (cut) from the running-in test analyzed with GDOES with the measurement spots: left – drawn with DP500+Z; right – drawn with DP500+ZM (N.B: the tools are not in their full size anymore).

The results show that material transfer takes place in the first 100 nm of the tool surface. The total amounts of transferred material are approximately 26.75 mg/m<sup>2</sup> and 17.55

mg/m<sup>2</sup> for the tools drawn with DP500+Z and DP500+ZM respectively with already 50% difference. The amount of transferred aluminum is similar while the transferred zinc is also three times more for DP500+Z. There is no magnesium in DP500+Z which justifies the absence of magnesium transfer. The similarity of the values obtained at the edge and in the middle allows to assume that the contact between the tool and the strips took place evenly all over the tool surface.

## 5.4 Analysis of the sheet metal coating surface

### 5.4.1 Topography analysis

Surface topography analysis enables to estimate the change of the surface morphology through tribological loading. Thereby, the real area of contact can also be given an estimate. Figure 5.16 and 5.17 give the surface topographies of DP500+Z and DP500+ZM at the unworn and worn states.

At the unworn state, the surface of DP500+Z is smoother than the DP500+ZM as the latter has higher peak density (11.7/mm) than the former (9.17/mm). This can also be seen by the range of values of the height distributions. It is up to 5 μm for DP500+Z while it varies up to 6 μm for DP500+ZM. Due to this difference, pure zinc surface presents smaller core material and core void volumes compared to that of zinc-magnesium. The corresponding ratios of the core material volume to the core void volume  $V_{mc}/V_{vc}$  are, however, 1.71 and 1.76 respectively which are very similar. Moreover, the roughness parameters namely  $R_a$ ,  $R_q$  and  $R_z$  are, similar for both surfaces. At this point, the topographies of both surfaces can be considered to be comparable and they do not present any particular difference.

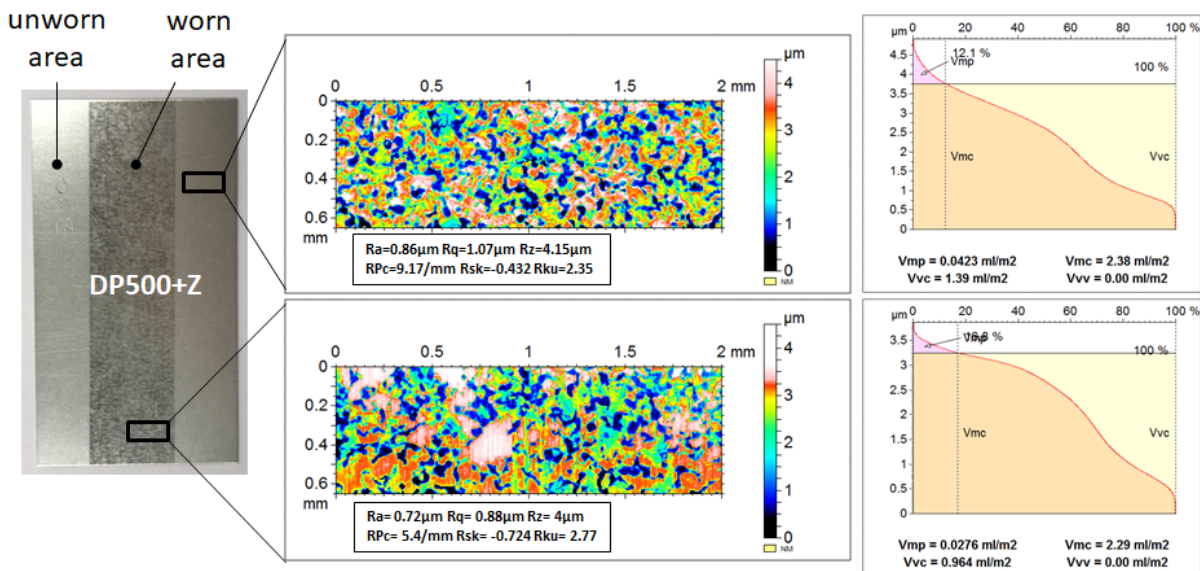


Figure 5.16: Surface topography of DP500+Z with the corresponding volume parameters ( $V_{vc}$ : core void volume,  $V_{mc}$ : core material volume).

After drawing, the tallest asperities are flattened and the overall height distribution is cut off up to 1 μm for both surfaces. The real contact area can be evaluated within the height

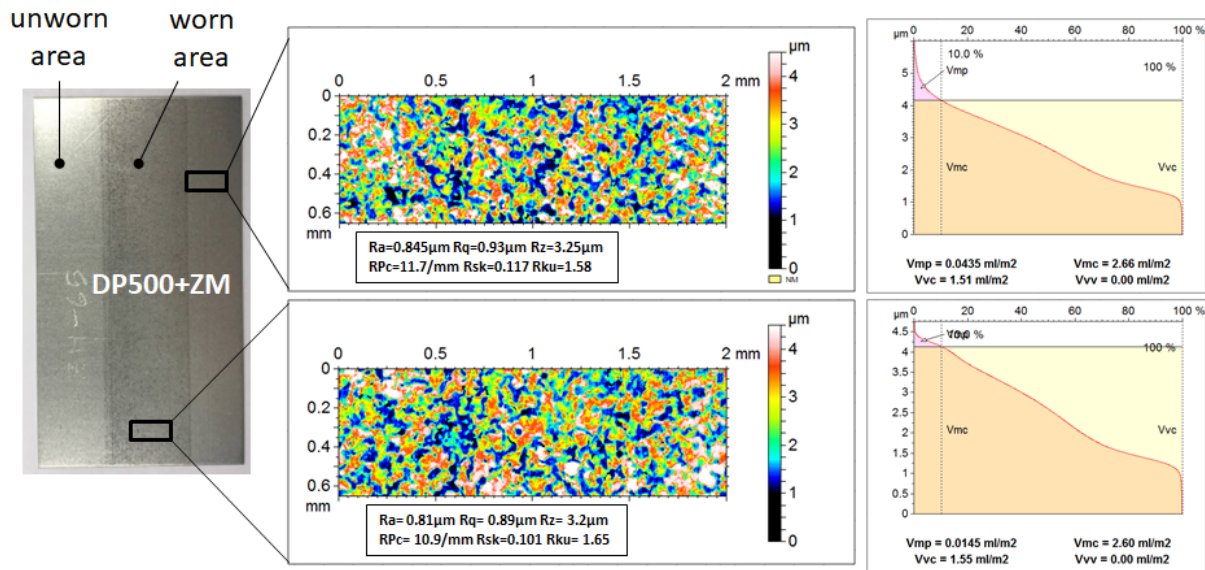


Figure 5.17: Surface topography of DP500+ZM with the corresponding volume parameters ( $V_{vc}$ : core void volume,  $V_{mc}$ : core material volume).

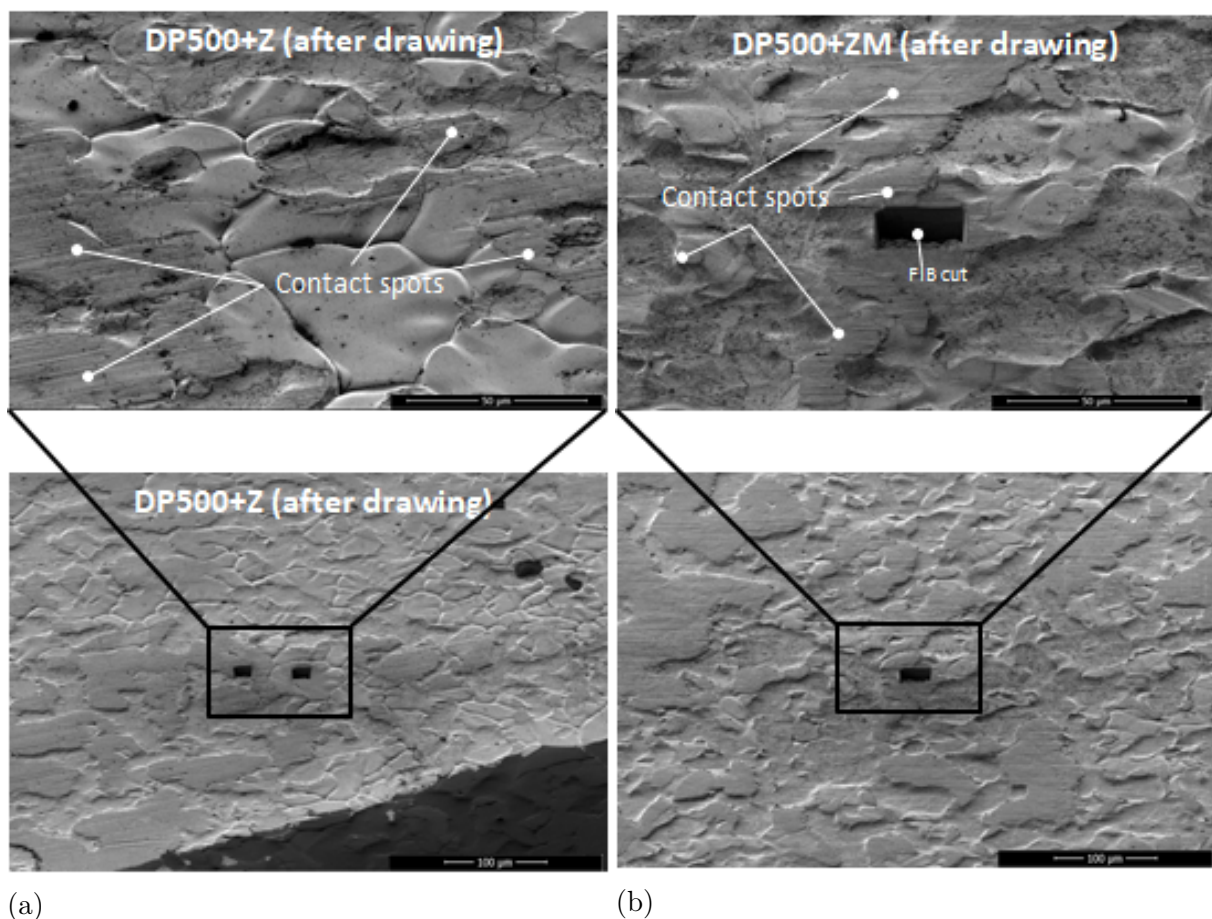


Figure 5.18: Surface topography of the strips with the corresponding volume parameters: (a) – DP500+Z; (b) – DP500+ZM.

range of [3 – 3.5 μm] for DP500+Z and [3.25 – 4.5 μm] for DP500+ZM. The obtained values are then situated within the range of [16 – 37%] and [10 – 33.5%] respectively. This

shows a difference of 5% between the surfaces as zinc-magnesium exhibits more resistance to compression and contact area growth than pure zinc. This can be later on verified by measuring the hardness of both surfaces. The surface roughness parameters of the pure zinc coating were also reduced to 15% while the ones of zinc-magnesium barely changed. In addition, pure zinc coating loses up to 30% of its core void volumes and therefore of its lubricant reserve during contact.

Figure 5.18 gives SEM images of the surfaces. The real contact zones are clearly observable on those images. The pure zinc surface appears to be rougher and it has seemingly undergone abrasion where the ploughing micro-stripes are very manifest with some micro-holes alongside. Zinc-magnesium coating surface is, on the contrary, smoother. Ploughing micro-stripes are also noticeable but not as manifest as for the pure zinc coating. Moreover, the micro-holes do not practically exist.

The grains are distinguishable for the standard galvanized zinc coating with an average size of 40 – 50 nm while they cannot be discerned for zinc-magnesium coating. Based on this picture, the real contact area can be estimated to be approximately 30%. A difference between pure zinc and zinc-magnesium coatings is, however, not very distinguishable.

## 5.4.2 Analysis of microstructure of near-surface zone

### 5.4.2.1 Before drawing

Based on the observation of SEM images in figure 5.19, the unworn state of the surface of the strips comprises regions that are plastically deformed by compression during the skin pass rolling process and other regions that are indirectly stressed due to the deformation of neighboring regions.

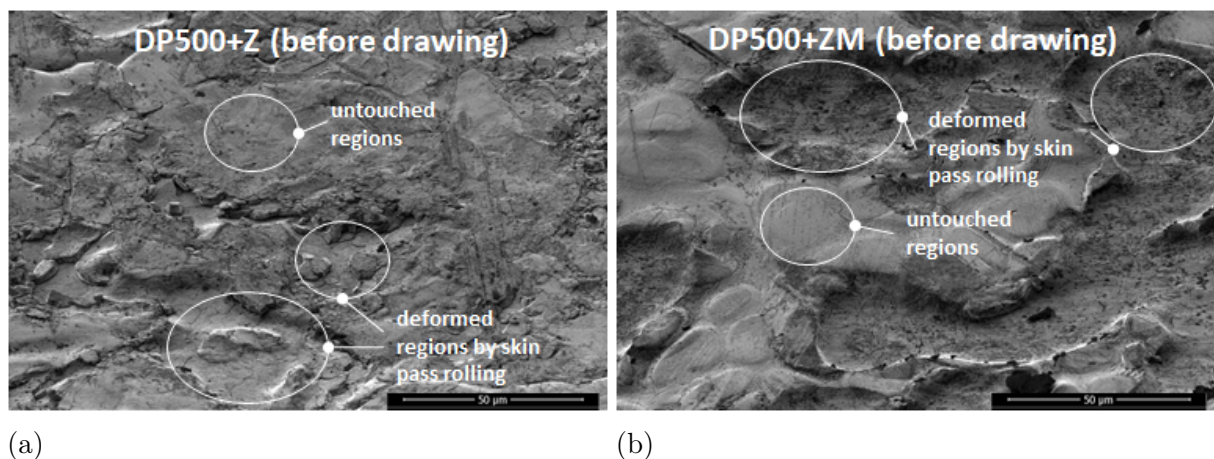


Figure 5.19: Surface topography of the strips with the corresponding volume parameters: (a) – DP500+Z; (b) – DP500+ZM.

Figure 5.19 and 5.20 represent FIB-SEM images which show clearly that skin-pass rolling process induces defects in form of cracks on the surface of the pure zinc coating that propagated within the first micrometer depth. Plastic deformation and buckling can also be distinguished. Those defects and deformations were not encountered in zinc-magnesium coating.

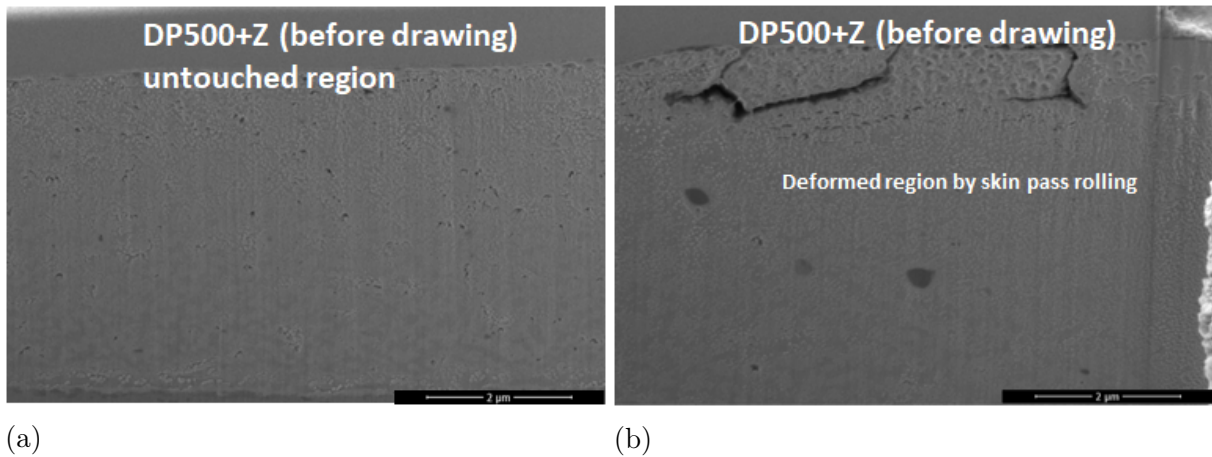


Figure 5.20: FIB-SEM images of the section of the coating of DP500+Z: (a) – untouched region; (b) – deformed region by skin pass rolling.

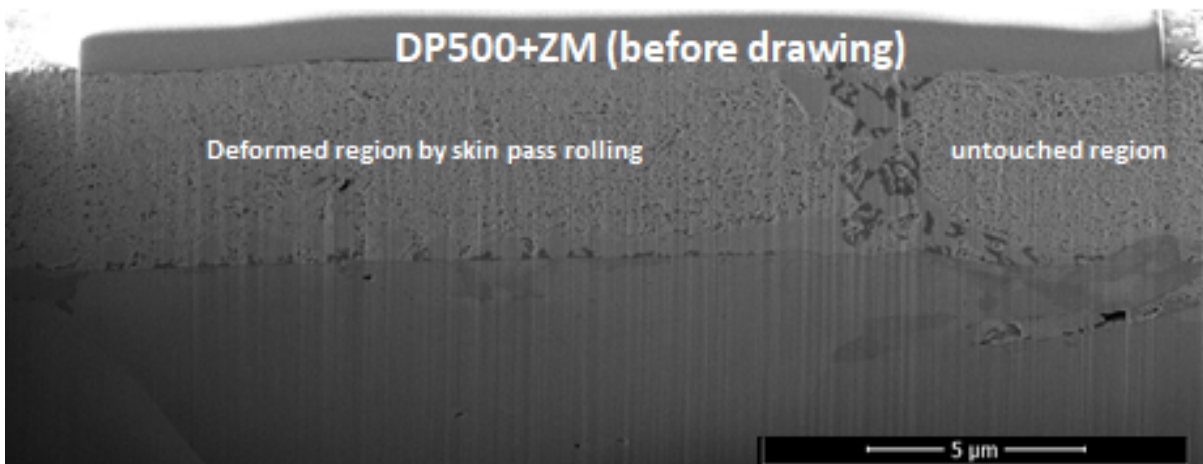


Figure 5.21: FIB-SEM images of the section of the coating of DP500+ZM before drawing.

The material of the pure zinc coating is dense while zinc-magnesium coating has a pronounced porosity. Nevertheless, the near surface zone within 500 nm depth is still dense and similar to that of pure zinc coating. The diffusion phase between the coating and the steel substrate is also much thicker for pure zinc than for zinc-magnesium coating.

#### 5.4.2.2 After drawing

Figure 5.18 shows that some asperities are worn through flattening and subsequent ploughing where the contact areas are also visible. Figure 5.22 presents FIB-SEM images at those locations.

The near surface zone is plastically deformed right at the contact zone in the first 100-200 nm depth for pure zinc coating. In addition, a roughening of the surface is observed at the non-contact zone which is associated to the plastic deformation of the related grain. The latter is affected by the shearing of the neighboring grains which are subjected to contact. In turn, this effect is not observed for the zinc-magnesium coating. The presence of the

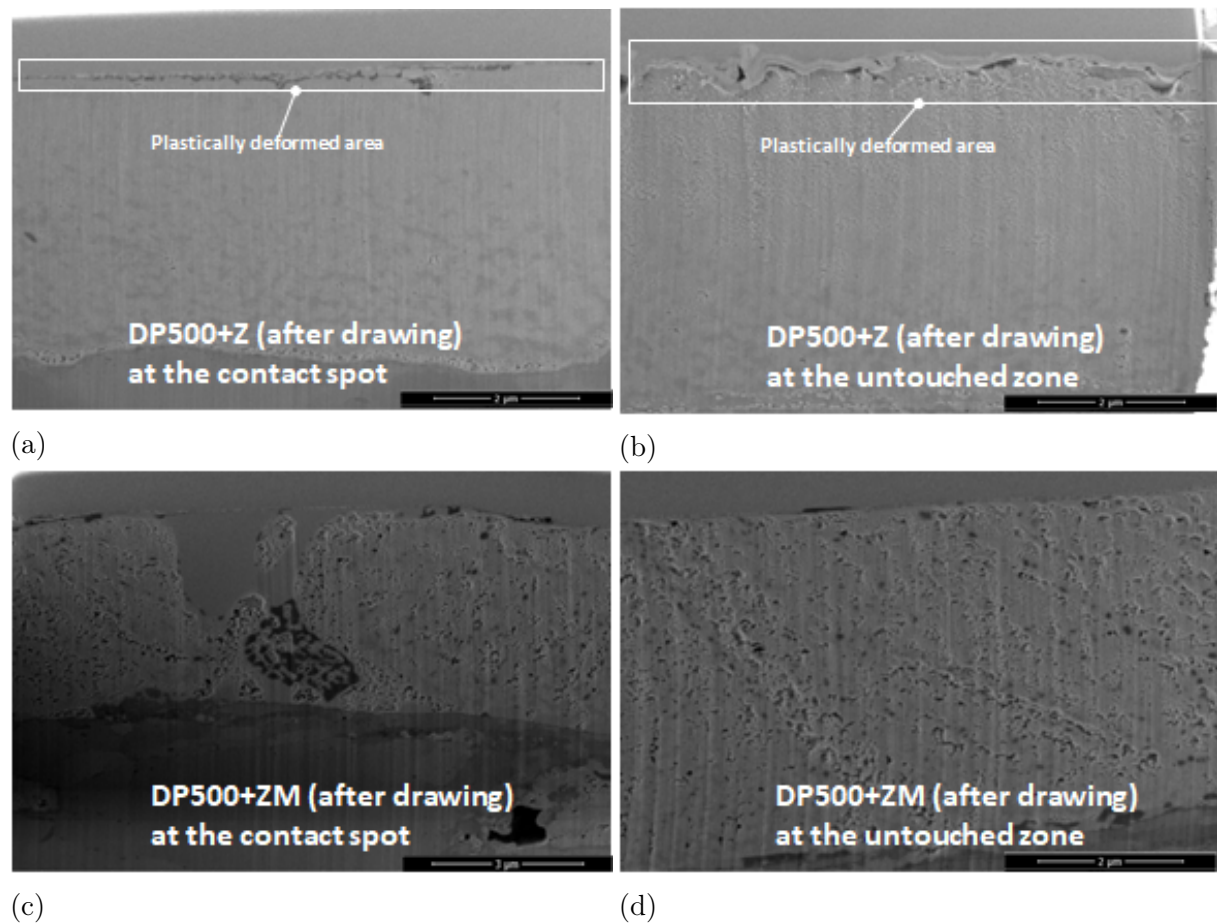


Figure 5.22: FIB-SEM images of the profile of the surface coatings after drawing: (a) – DP500+Z at the contact zone; (b) – DP500+Z at the untouched zone; (c) – DP500+ZM at the contact zone; (d) – DP500+ZM at the untouched zone.

eutectic phases that are orthogonal to surface impedes the shearing or the propagation of the shearing of the neighboring grains. Thereby, these eutectic phases may serve as an armature grid that separates the big zinc grains and then consolidates the cohesion of the constituents of the surface. Instead, a thin layer of approximately 100 nm resulting from the tribological loading is observed at the contact zone. Since the real contact occurs at the thin layer level, this may be one of the reasons of the lower friction compared to the zinc coating.

The porosity of the zinc-magnesium coating may also play a significant role in the reduction of friction through reduction of the plastic wave propagation as it promotes higher energy consumption [Coh15]. This requires further investigation in the future.

### 5.4.3 Analysis of chemical composition

Metal surfaces may undergo a change in chemical compositions after drawing. Moreover, the difference between the compositions of zinc and zinc magnesium coatings may enhance this change especially at the near surface zone where the tribological loading takes place and therefore influences the frictional behavior of the tribosystem. XPS depth profiling analyses on the sheet metal surfaces that were drawn during the running-in test are

performed.

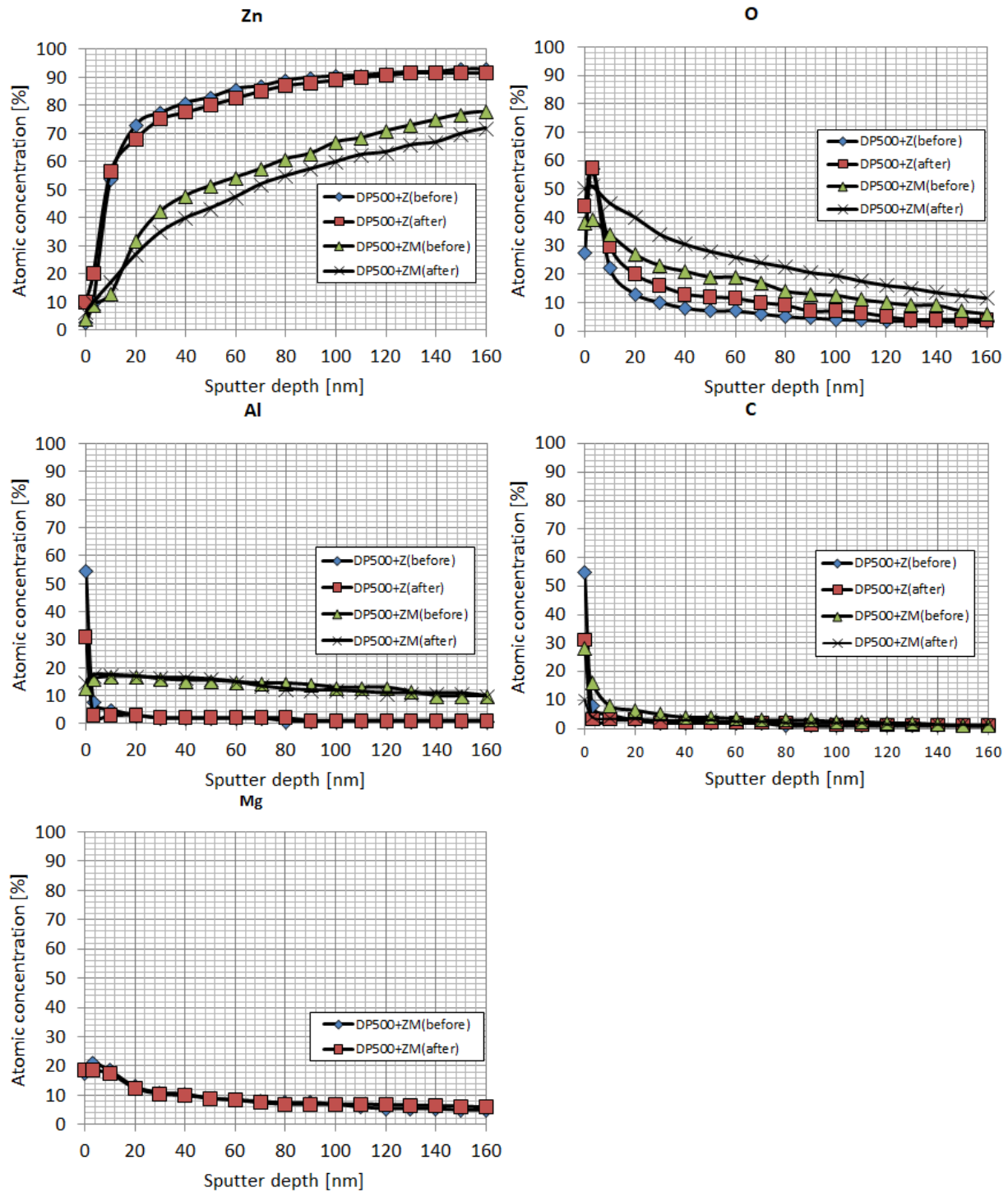


Figure 5.23: XPS-depth profile of the strip surfaces before and after drawing.

Additional XPS measurements of the very superficial part of the surface of the strips are also made in order to obtain a quantitative estimation of the chemical composition of it as well as the thickness of the covering oxide layers as shown in figure 5.24. The strips number 1, 46 and 70 of DP500+Z and DP500+ZM were analyzed. The measurements were performed on several points marked as green on the worn (darker zone) and unworn (brighter) zone of the strips. An estimate of the corresponding oxide layer thickness is

given by relating to the equivalent silicon oxide thickness. This is not an absolute value but rather only a rough approximation. The ratios of magnesium, aluminum and zinc in the oxide layer are also estimated. The results are provided in table 5.3 and 5.4.

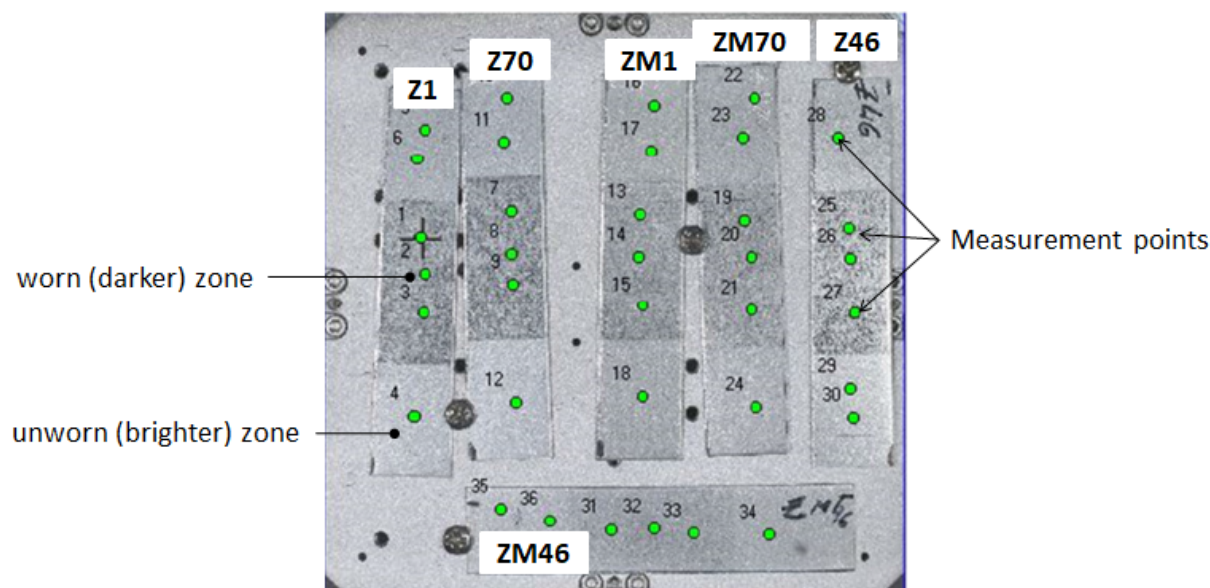


Figure 5.24: Specimens from the strips for xps measurements.

Chemical composition of the surface in Atom %												
	Zn		O		Al		C		Mg		Oxide layer thickness (nm SiO <sub>2</sub> )	
	unworn	worn	unworn	worn								
Z1	4	6	39	33	12	7	45	53	-	-	41	48
Z46	3	4	26	24	6	5	66	67	-	-	38	34
Z70	5	8	42	38	13	7	38	46	-	-	47	40
ZM1	4	5	40	42	6	6	43	41	6	5	56	82
ZM46	4	5	40	40	7	6	41	43	7	5	44	58
ZM70	5	4	40	40	6	6	41	44	6	5	39	53

Table 5.3: Chemical composition of the surface and the corresponding oxide layer thickness.

Ratio of Mg, Al, Zn within the oxide layer in %									
	Zn		Al		Mg		Oxide layer thickness (nm SiO <sub>2</sub> )		
	unworn	worn	unworn	worn	unworn	worn	unworn	worn	
Z1	23	47	77	53	0	0	41	48	
Z46	33	45	67	55	0	0	38	34	
Z70	27	52	73	48	0	0	47	40	
ZM1	24	31	35	36	41	33	56	82	
ZM46	22	30	38	39	41	31	44	58	
ZM70	30	27	37	40	33	33	39	53	

Table 5.4: Ratio of Mg, Al and Zn within the oxide layer.

Figure 5.23 presents XPS-depth profiles which show a high concentration rate of oxygen and aluminum in the first 5 – 10 nm depth near the surface for DP500+Z before drawing.

After that, their rates reduce progressively while the rate of zinc increases alongside. Moreover, table 5.3 shows a high percentage of aluminum as well (approx. 70%) within an oxide layer of 40 nm. These results are in a good agreement with the aforementioned presence of a dense closed aluminum layer covering the surface and a zinc layer underneath in chapter 3. After drawing, the rate of aluminum decreases up to 10% according to the depth profile while the rates of zinc and oxygen remain unchanged. Table 5.3 also shows a decrease of 20-30% in aluminum content and an increase of 20-25% in zinc content within the oxide layer. Effectively, due to the tribological loading, a part of the aluminum oxide is abraded and the zinc underneath is in turn oxidized. Some aluminum oxide can be crushed into the zinc and losing its ability to inhibit the oxidation of the zinc which can be seen through the increase in oxygen content. In either case, the oxide layer loses about 5% of its thickness and change happens only within the first 100 nm depth region of the zinc coating.

The case of DP500+ZM is analogous to that of DP500+Z. The aluminum oxide and magnesium oxide can cover the coating surface. After sliding, the rate of magnesium within the oxide layer sunk up to 10% and the rate of zinc increases up to 7% while the rate of aluminum remains practically unchanged. The same explanation can be valid here where the oxide layer could be abraded or crushed into the zinc layer underneath. In comparison to the standard zinc coating, the thickness of the oxide layer for zinc-magnesium coating grows within the range of 14 – 20% after tribological loading.

The oxide layer on the zinc-magnesium coating surface is in principle thinner but denser and much more difficult to abrade than the aluminum oxide on standardized galvanized sheet metal surface [Hac09]. This means the occurrence of a fresh zinc surface that is susceptible to oxidation, cold welding and adhesion is more likely for the standard galvanized coating. This explains why the amount of material transfer on the tool surface that was drawn with DP500+Z is 50% more than that with DP500+ZM as shown in table 5.2 and the oxide layer loses in thickness.

In conclusion, the oxide layer on the surface of the zinc-magnesium coated sheet metal seems to be more resistant to the tribological loading than that of the standard galvanized sheet metal. This ensures a higher resistance to tribological loading, a better resistance to cold welding and then restraining adhesion. Moreover, the contact pair tool surface oxide – zinc-magnesium surface oxide can exhibit less friction than tool surface oxide – standard zinc surface oxide. Therefore, this may contribute significantly to the reduction of friction in boundary lubrication regime.

#### 5.4.4 Nanohardness measurement

The hardness of the sheet metal coatings are measured by means of nanoindentation principle which was already described in section 3.1.2.2. The measurements were performed on both worn and unworn regions of the strips. Figure 5.25 presents the specimens where the dark stripes are the worn contact regions.

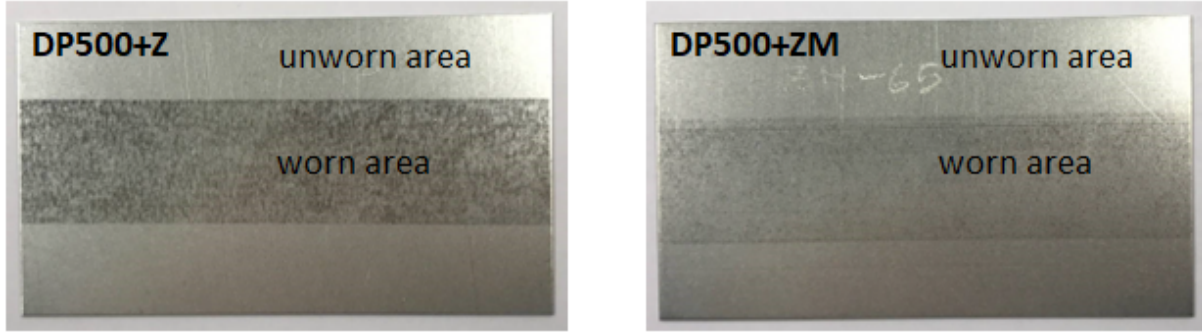


Figure 5.25: Specimen for nanoindentation from DP500+Z (left) and DP500+ZM (right).

Specimen	Metallic composition	Hardness $H$ [GPa]	Elastic modulus $E_r$ [GPa]
DP500+Z (unworn)	Zn	$0.8 \pm 0.1$	$100 \pm 8$
			$70 \pm 5$
			$60 \pm 6$
DP500+Z (worn)	Zn	$0.8 \pm 0.2$	$67 \pm 16$
DP500+ZM (unworn)	Zn	$1.1 \pm 0.1$	$101 \pm 12$
			$70 \pm 8$
	Eutectic phase	$1.5 \pm 0.2$	$104 \pm 14$
DP500+ZM (worn)	Zn	$1.1 \pm 0.4$	$85 \pm 16$
			Eutectic phase

Table 5.5: Hardness and reduced elasticity modulus of the specimen coatings.

For each specimen i.e. DP500+Z and DP500+ZM and for each zone i.e. worn and unworn, indentation on the surface was performed at 6 to 8 locations with an indent-grid of  $4 \times 4$  with varied indenting forces ranging between 200 and 10000  $\mu\text{N}$ . Thereafter, atomic force microscopy (AFM) measurements of each indent-grid with the indenter tips are taken. Attempts to distinguish the indentation spots at different grains and other regions with different metallographic constituents were made. Figure 5.26 shows an example of the AFM measurements.

Figure 5.27 illustrates the results of the measurements on DP500+Z. The hardness and the reduced elastic modulus are plotted with respect to the indentation depth for both unworn and worn zones. It appears that a higher hardness was determined at the unworn zone when the applied indentation depth is small. With further growth of the indentation depth up to a certain value  $h_c = 190$  nm, hardness value decreases until it stabilizes at about  $0.8 \text{ GPa} \pm 0.1 \text{ GPa}$ . At the worn zone, on the contrary, the hardness did not exhibit a high value at low indentation depth and the average hardness value equals  $0.8 \text{ GPa} \pm 0.2 \text{ GPa}$  which is comparable to the stable value of the unworn zone. Concerning the reduced elastic modulus, three distinct values are observed at the unworn zone while only one value corresponds to the worn zone but with a greater dispersion. This is most likely related to the fact that the tribological loading enforced a rearrangement of the polycrystalline structure of the zinc grains since it has a hexagonal closed pack crystal structure which is anisotropic in itself.

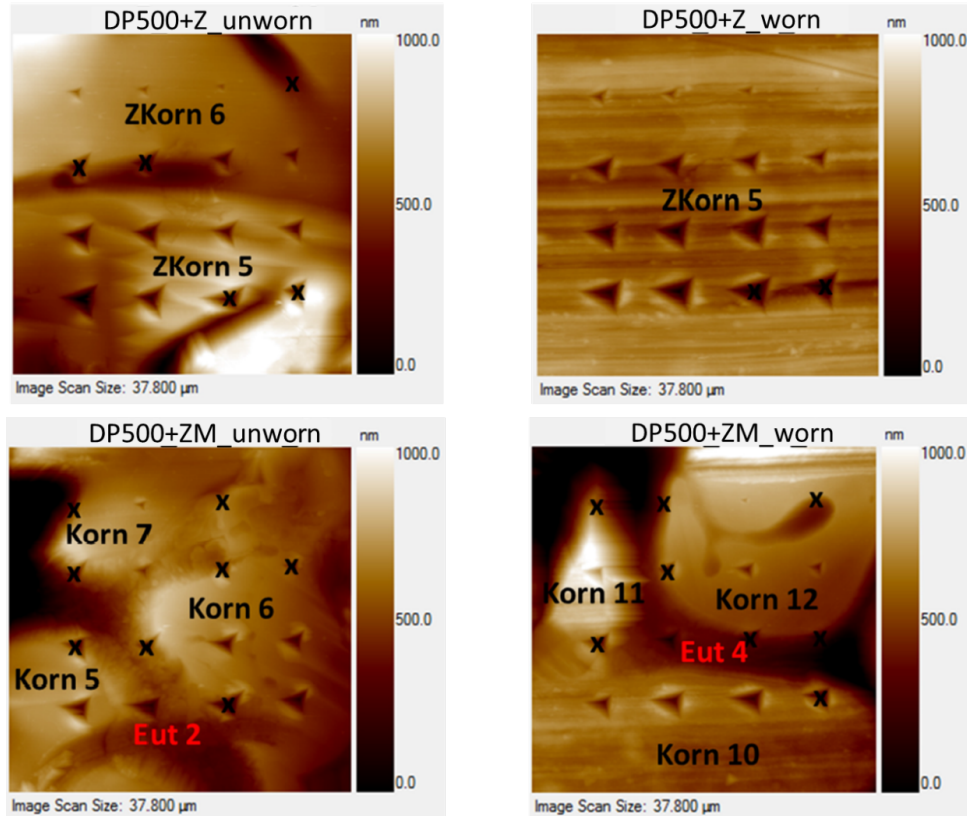


Figure 5.26: AFM measurements of four showcase measurement locations (Korn: grain; Eut: eutectic phase; x: impression where a quantitative evaluation was impossible).

Analogically, figure 5.28 presents the measurement results for the DP500+ZM from the unworn and worn zones. The AFM measurements allowed to identify not only the different indentation marks on the grains but also the indentation marks on the eutectic phases between the zinc grains. The average value of the hardness of the zinc grains is estimated to equal  $1.1 \text{ GPa} \pm 0.1 \text{ GPa}$ . It is, however, not possible to pronounce on the existence of a high value at lower indentation depth since indentation spot with indentation depth  $h_c < 100 \text{ nm}$  did not meet the zinc grains during measurements. For the eutectic phases, only few measurements are available as well. At small indentation depth (less than  $100 \text{ nm}$ ), high hardness values are detected nonetheless and the average value of the hardness at indentation depths above  $100 \text{ nm}$  is approximately  $1.5 \text{ GPa} \pm 0.2 \text{ GPa}$  at the unworn zone. A large discrepancy is observed for the worn zone with the same average value. Concerning the reduced elasticity modulus on the unworn zone, two different but close values were found for the zinc grains while the eutectic phase exhibits a unique but higher average value ( $104 \text{ GPa} \pm 14 \text{ GPa}$ ) than the zinc grains. The worn zone shows only one average value ( $85 \text{ GPa} \pm 16 \text{ GPa}$ ) for the zinc grains but a lower value ( $79 \text{ GPa} \pm 9 \text{ GPa}$ ) for the eutectic phase this time. All the values are given in the table 5.5.

For both specimens with different surface coatings, the measured hardness values are higher at small indentation depth ( $< 100 \text{ nm}$ ). The presence of the thin oxide films which are in general harder than zinc may influence the results. As the tip indents the surface deeper, the influence of the oxide films lessens since they are very thin. Moreover, the indentation size effect can also interfere in those results.

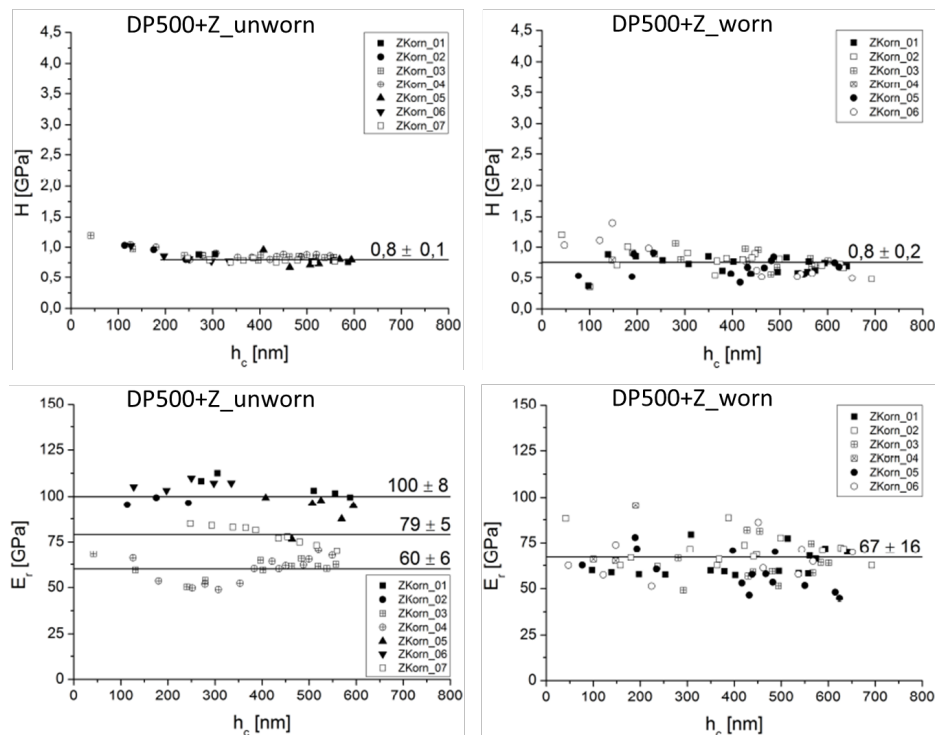


Figure 5.27: Diagrams of the measured hardness  $H$  and reduced elastic modulus  $E_r$  of the pure zinc coating with respect to the indentation depth  $h_c$ . The average values are represented by the horizontal lines.

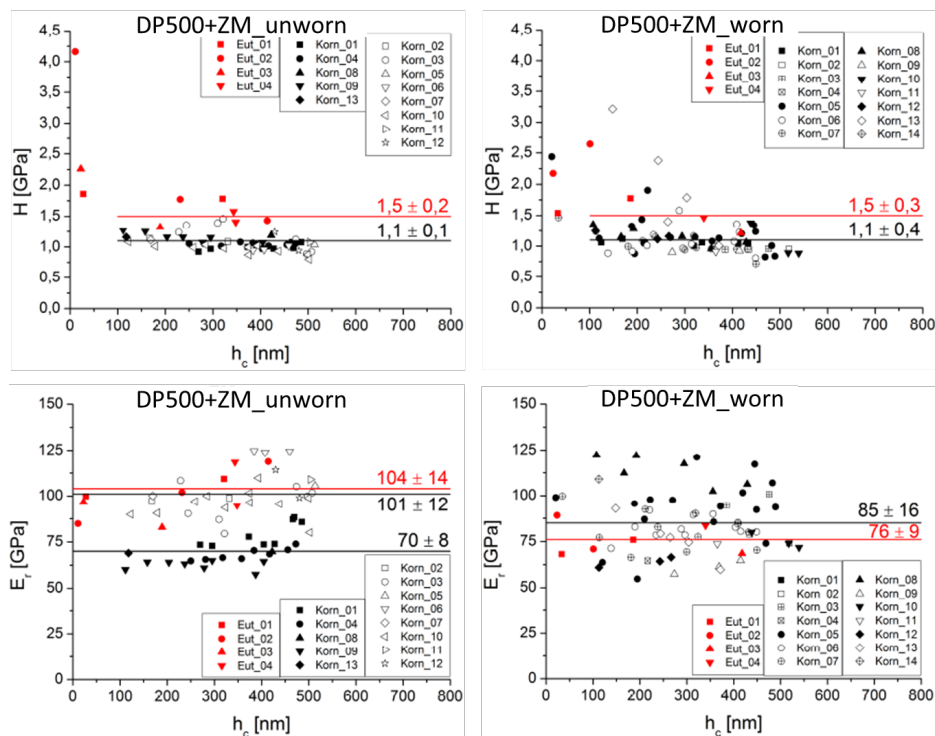


Figure 5.28: Diagrams of the measured hardness  $H$  and reduced elastic modulus  $E_r$  of zinc-magnesium coating with respect to the indentation depth  $h_c$ . The average values are represented by the horizontal lines. The values of the indentation on the eutectic phase between the zinc grains are marked in red.

The zinc grains of the zinc-magnesium coating exhibit greater hardness than their homologues from the pure zinc coating owing to their different size. Effectively, hardness decreases with the growth of the grain size [Hak07] also for polycrystalline structures [Jun13]. And from the photomicrograph, it is clearly observable that the zinc grains of DP500+Z are much bigger.

For both coatings, different levels of the reduced elasticity modulus were also found. This most likely originates from the different crystal orientation of the zinc grains. During drawing, the tribological loading might have enforced a rearrangement of the polycrystalline structure of the zinc grains.



# Chapter 6

## Inference

### 6.1 Summary

#### 6.1.1 Influence of type of surface coating

Tribological test in section 5.1 and 5.2 shows that the used tool steel requires a certain time to adjust to the zinc coated sheet metal. A growth of the coefficient of friction is observed before it stabilizes at a certain average value. This behavior is not observed using zinc-magnesium coated sheet metal. The coefficient of friction is steady and independent of the test number. The radionuclide techniques did not detect any wear particle from the tool with the chosen test parameters. This means tool is not subject to abrasive wear. A measurement of the topography of strip drawing tool surfaces in section 5.2 has shown that an interaction with pure zinc coating causes a roughening of the tool while zinc-magnesium coating tends to smoothen it. SEM images has confirmed this tendency. However, no change was observed in the near surface microstructure. Further analysis of the chemical composition of the worn surfaces has shown that oxidation of iron and other elements such as calcium and zinc occurred on both tool surfaces whether it was drawn with pure zinc coated steel sheet or with zinc-magnesium one giving comparable quantities of oxide. A transfer of zinc from the sheet metal coating is also determined in spite of the presence of lubricant. Pure zinc coating generates 50% more material transfer than zinc-magnesium coating which contributes to the increase of friction.

In a similar manner, analyses of the sheet metal coatings are also performed. At the initial state, both surfaces exhibit similar roughness. Pure zinc coating is practically dense while zinc-magnesium coating shows some porosity especially at the near surface zone. Skin-pass rolling process also induces defects in the pure zinc coating in the form of microcracks which is not observed in zinc-magnesium coating. After drawing, it was observed that pure zinc coating surface was rather abraded and ploughed and its surface roughness parameters were reduced. Plastic deformation at the near surface zone of pure zinc coating accompanied by a roughening of the surface is observed. On the contrary, zinc-magnesium coating has barely changed but a very thin tribological layer is observed which is majorly composed of oxides on the top. Additionally, as both coating surfaces are covered with a thin oxide layer, it appears that the oxide layer of zinc-magnesium coating is more resistant to abrasion which may contribute considerably to lowering of friction along with the mentioned porosity. The contact area is also 5% smaller for

zinc-magnesium coating that for pure zinc one which is justified by the lower hardness of the latter. This is an additional factor that influences the frictional response of the tribosystem.

### 6.1.2 Influence of surface topography

The investigation in chapter 4 on the influence of surface topography on the friction response of the tribosystem as well as the developed lubrication regime allows to enumerate several important facts. Boundary lubrication is the main lubrication regime that the tribosystem develops within the frame of strip drawing and pin-on-disk for deep drawing study. Mixed lubrication occurs only at low pressure, high speed and significant lubricant amount. The latter has to be more than the material void volume. The real contact area must be well supplied with lubricant to reduce friction. That is why at low drawing speed when mixed lubrication regime is excluded, the surfaces which are covered with lubricant ensure lower friction. In this case, lubricant can always overflow the valley and lubricate the contact area close by. In order to ensure a more effective lubrication, the surface roughness is desirable to be low and the valleys to be shallow. Hydrostatic lubrication takes place due trapped lubricant in the pockets. It must be mentioned, however, that it was not explicitly observed in the experimental results.

As a general trend, the coefficient of friction increases with the surface roughness especially at low drawing speed. The roughness average  $R_a$  and root means square  $R_q$  parameters increase and so do the frictional response on the concerned tribosystem. The influence of the peak density parameter  $R_{Pc}$  manifests mostly when the two surfaces exhibit similar roughness. Therefore, it can be assumed at this point that the surface roughness holds a greater grip on friction than the peak density. In addition, for similar sheet metal surfaces with small roughness, a combination of the average maximum height  $R_z$  and the void volume  $V_{vc}$  is a characterizing tribological factor. A smooth tool surface also helps in reducing friction where the ploughing contribution is the most affected. The arithmetic mean slope  $P_{da}$  of the the tool surface represents an important reference parameter for tool surface finish with respect to frictional behavior of the corresponding tribosystem. With the increase of drawing speed, the influence of tool surface roughness becomes, however, less significant.

### 6.1.3 Source of error in tribological tests

Tribological tests are performed at various locations with different equipments. It is, therefore, important to ensure the consistency and reproducibility of the obtained results for the same parameter setup. In this work, a comparison between strip drawing and pin-on-disk tests was performed with the same contact parameters i.e. contact pressure, drawing speed and lubricant amount. It was seen that pin-on-disk develops greater coefficient of friction. Moreover, the latter is very dependent on the rotation number. Formation of wear debris from the sheet metal coating is also very pronounced compared to strip drawing. This can be related to the sharpness of the pin edge since die radius is generally very blunt in strip drawing. Higher friction in pin-on-disk is also related to the size effect. Effectively, pin surface area is too small so that lubricant instantaneously flows out of the contact interface. Therefore, lubricant has practically no influence on

the test results. This behavior is enhanced by the low speed that is characteristic of deep drawing.

In strip drawing, tool size also can be a liability for the evaluation of the results. As a general behavior, coefficient of friction slightly decreases as the tool size grows independently of the contact pressure. This is in agreement with the aforementioned observation for pin-on-disk. Tool surface treatment is also another factor to be considered. With the increase of drawing speed and the lubricant amount, the difference lessens. Treatment of tool surface such as nitride hardening has been regarded as well. It has been seen that the frictional response of a tribosystem is not influenced by the hardness of the tool surface at least as long as the sheet metal coating is softer.

## 6.2 Conclusion

### 6.2.1 Friction mechanics

Investigation in chapter 4 and 5 has shown that both adhesion and ploughing constitute the main mechanics of friction in deep drawing. The amount of transferred materials through adhesion is dependent on the type of coating of the sheet metal as well as the lubricant amount and efficiency. The lubrication effect is tightly related to the sheet metal surface roughness. This can be seen by the role the material void volume plays. The form of the valleys are to consider as well. In turn, ploughing depends mostly on the roughness of the surface of the used tool. The role of the real contact area is primordial which depends mainly on the roughness and hardness of the sheet metal coating.

Another very important factor that plays a fundamental role in the friction is the developed oxide layer on the sheet metal surface. It depends mainly on the type of coating which leans on the chemical composition of the said coating. The oxide layer is preferred to be resistant to abrasion which will prevent a further abrasion or ploughing of the coating surface. This reduces considerably the resulting friction and provides a certain stability to the overall tribosystem.

### 6.2.2 Friction modelling

The general model of friction in deep drawing is the use of coefficient of friction as a single constant value. This has been seen to be very inaccurate as the frictional behavior of a tribosystem is generally not steady with respect to contact parameters. The value of  $\mu$  varies most of the time in a given range. There is, however, a certain opening for the use of a single value for  $\mu$  if the latter is contained in a narrow range. In this case, the average value can be used as a compromise.

A proposed model of friction is the dependence of the friction coefficient on  $p$  $v$  and  $v/p$  factors. The model represents the main dissipative character of friction as well as the influence of surface roughness and lubricant film thickness within the concept of Stribeck curve. The model is empirical but it allows to generalize many of the involved factors of influence. A general form of the model can be expressed as:

$$\mu = f(pv, v/p) \quad (6.1)$$

A difficulty occurs, however, in the use of the model. Effectively, different values of  $p$  and  $v$  may give comparable  $p v$  and  $v/p$  factors which correspond to different  $\mu$ . It is without mentioning the amount of applied lubricant. An alternative model is the use of a simplified model in form of:

$$\mu = f(v, 1/p)|_{V_{lub}} \quad (6.2)$$

In this simplified model, the concept of Stribeck curve is conserved as well as the dissipative nature of friction. Moreover, the initial amount of lubricant is considered as an external parameter.

### 6.2.3 Wear behavior

In the pin-on-disk with radionuclide-technique, no wear particle from the tool was found. This shows that abrasive wear does not take place. SEM graphics have displayed only superficial plastic deformation on the near surface zone. SEM-FIB analysis did not show any change of the microstructure in the near surface zone. This enables to exclude the occurrence of severe wear.

In turn, chemical analysis has shown that oxidation intensively occurs at the contact zone so that both sheet metal and tool surfaces develop thicker oxide layer after drawing compared to the initial state. The oxide layer serves as a separator between the primary surfaces where the frictional energy is dissipated, the velocity gradient is accommodated and the contact loads are transferred. In brief, it plays the role of a third body and the occurring wear can be characterized as mild.

## 6.3 Future research possibilities

It has been seen that this work treats the fundamentals of lubricated friction in deep drawing. The used materials are widely used in industries but are also simultaneously subjected to further investigation and optimization. On the one side, texturing methods are intensively investigated mainly for the purpose of exploiting the advantage of hydrostatic lubrication. Parameters such as  $P_{da}$  of the tool surface, the void volume  $V_{vc}$  and roughness of the sheet metal coating can be used to characterize friction.

It has been seen, however, that the oxide layers at the contact interface play primordial roles in the control of friction. At the present time, this concept of oxide layer has not been intensively developed with the aim of controlling friction in deep drawing. This can lead to a further understanding of the occurring tribological phenomenon.

It has been seen in this work that boundary lubrication regime is the most characteristic regime in deep drawing even if lubricant is in abundance. Mixed lubrication regime can occur at some time and location of the process. There is still, however, little information on the actual mechanism during boundary lubrication including in deep drawing. Many possible explanations have been provided in this work including the lubricating

mechanism during sliding and lubricant boundary layer. However, more proof is still required.

Friction models for deep drawing have been described in this work with their advantages and imperfections. Some of the models include the hydrodynamic lubrication. Others imply that boundary lubrication is mainly mechanical which depends only on ploughing. It has been seen, however, that smooth and rough tools can generate very comparable coefficient of friction in boundary lubrication. Therefore, theory of friction mechanics in boundary lubrication is to be further sharpened before a rational physics-based friction model can be developed.



# Bibliography

- [Akb08] Akbarzadeh, S. S.; Khonsari, M. M.: “Performance of Spur Gears Considering Surface Roughness and Shear Thinning Lubricant”. In: *ASME J. Tribol.* 130.2 (2008), pp. 021503–10.
- [Akh63] Akhmatov, A.S: *Molecular Physics of Boundary Friction*. Moscow: Fizmatgiz, 1963, p. 472.
- [And98] Andreasen, J.L.; Bay, N.; de Chiffre, L.: “Quantification of galling in Sheet Metal Forming by Surface Topography Characterization”. In: *Int. J. Mach. Tools. Manuf.* 38.5–6 (1998), pp. 503–510.
- [Ant10] Antusch, S; Dienwiebel, M.; Nold, E.; Albers, P.; Spicher, U.; Scherge, M.: “On the tribochemical action of engine soot”. In: *Wear* 269 (2010), pp. 1 –12.
- [Arc53] Archard, J.F.: “Contact and Rubbing of Flat Surfaces”. In: *Journal of Applied Physics* 24.8 (1953), p. 981.
- [Arc56] Archard, J.F.; Hirst, W.: “The wear of metals under unlubricated conditions”. In: *Proc. Roy. Soc* 236 (1956), pp. 397–410.
- [Arc57] Archard, J. F.: “Elastic Deformation and the Laws of Friction”. In: *Proc. Roy. Soc of London* 243 (1957), pp. 190–205.
- [Arm91] Armstrong-Helouvry, B.: *Control of machines with friction*. New York, USA: Springer Science+Business Media, LLC, 1991.
- [Arn12] Arndt, M.; Duchoslav, J.; Itani, H.; Hesser, G.; Riener, C.K.; Angeli, G.; Preis, K.; Stifter, D.; Hingerl, K.: “Nanoscale analysis of surface oxides on ZnMgAl hot-dip-coated steel sheets”. In: *Anal Bioanal Chem* 403 (2012), pp. 651–661.
- [Att02] Attaf, D.; Penazzi, L.; Boher, C.; Levallant, C.: “Mechanical Study Of A Sheet Metal Forming Dies Wear”. In: *Proceedings of the 6th International Tooling Conference: The Use of Tool Steels : Experience and Research*. Ed. by Bergström, J; Fredriksson, G.; Johansson, M.; Kotik, O.; Thuvander, F.: Karlstad University, 2002, pp. 209–221.
- [Avi86] Avitzur, B.; Nakamura, Y.: “Analytical determination of friction resistance as a function of normal load and geometry of surface irregularities”. In: *Wear* 107.4 (1986), pp. 367–383.
- [Azu12] Azushima, A.: “Micro-Contact at Interface Between Tool and Workpiece in Metalforming”. In: *Tribology in Manufacturing Technology*. Ed. by J.P.: Davim. Berlin Heidelberg: Springer-Verlag, 2012, pp. 151–173.
- [Bar03] Barge, M.; Kermouche, G.; Gilles, P.; Bergheau, J.M.: “Experimental and numerical study of the ploughing part of abrasive wear”. In: *Wear* 255 (2003), pp. 30–37.

- [Bar13] Bart, J.C.J.; Gucciardi, E.; Cavallaro, S.: *Biolubricants: Science and Technology*. Series in Energy. Cambridge, UK: Woodhead Publishing Limited, 2013.
- [Bas16] Baspinar, M.; Akkök, M.: “Modeling and Simulation of Friction in Deep Drawing”. In: *Journal of Tribology* 138 (2016), pp. 021104–1–7.
- [Bay76] Bay, N.; Wanheim, T.: “Real area of contact and friction stress at high pressure sliding contact”. In: *Wear* 38.2 (1976), pp. 201–209.
- [Bea16] Beane, R.: “Using the Scanning Electron Microscope for Discovery Based Learning in Undergraduate Courses”. In: *Journal of Geoscience Education* 52.3 (2016), pp. 250–253.
- [Beh17] Behrens, B-A; Huebner, S.; Gnass, S.; Gaebel, C.M.: *Bewertung von Zieh- und Schutzfolien für die Umformung von organisch bandbeschichteten Feinblechen*. Bamberg, 2017 (called up on 02.09.2018). URL: [https://www.umformtechnik.net/binary\\_data/3246315\\_2016-05-13-whitepaper.pdf](https://www.umformtechnik.net/binary_data/3246315_2016-05-13-whitepaper.pdf).
- [Bel07] Bello, J. O .; Wood; R. J. K.; Wharton, J. A .: “Synergistic effects of micro-abrasion corrosion of UNS S30403, S31603 and S32760 stainless steels”. In: *Wear* 263 (2007), pp. 149–159.
- [Ber04] Berthier, Y.: “Third-Body Reality – Consequences and Use of the Third-Body Concept to Solve Friction and Wear Problems”. In: *WEAR — MATERIALS, MECHANISMS AND PRACTICE*. Ed. by G.W.: Stachowiak. West Sussex, England: John Wiley & Sons Ltd, 2004. Chap. 12, pp. 291–316.
- [Bhu01] Bhushan, B. (Ed.): *Modern Tribology Handbook*. Boca Raton, USA: CRC Press LLC, 2001.
- [Bhu99] Bhushan, B.: *Principles and applications of tribology*. New York, USA: John Wiley & Sons, Inc., 1999.
- [Bla08] Blau, P.J.: *Friction science and technology: from concepts to applications*. Boca Raton, USA: CRC Press (2nd. ed.), 2008, p. 370.
- [Bla91a] Blau, P.J.: “Scale Effects in Steady-State Friction”. In: *Tribology Transactions* 34.3 (1991), pp. 335–342.
- [Bla91b] Blau, P.J.; DeVore, C.E.: “Sliding friction and wear behavior of several nickel aluminide alloys under dry and lubricated conditions”. In: *Tribology international* 23.4 (1991), pp. 226–234.
- [Bli97] Bliman, P.-A.; Sorine, M.: “Friction modelling by hysteresis operators: application to dahl, stiction and stribeck effects”. In: *Proceedings of the Conference 'Models of Hysteresis', Trento, Italy* (1997), pp. 10–19.
- [Blu16] Blumenau, M.; Zocher, U.; Moll, O.; Meyring, H.; Steinebrunner, J.: “New surface structure of cold-rolled and coated steel strip to improve paint appearance for automotive applications”. In: *10th International Rolling Conference and the 7th European Rolling Conference (ROLLING 2016)*. Graz, Austria, June 2016.
- [Boc93] Bochmann, E.: *Reibung als kritisches Phänomen in der Blechumformung*. Fortschritt-Berichte VDI.: Fertigungstechnik. Düsseldorf: VDI-Verlag, 1993.
- [Bow39] Bowden, F.P.; Tabor, D.: “The area of contact between stationary and moving surfaces”. In: *Proc. Roy. Soc.* 169.A (1939), p. 391.

- [Bow42] Bowden, F.P.; Tabor, D.: “Mechanism of metallic friction”. In: *Nature* 50/3798 (1942), pp. 197–199.
- [Bow43] Bowden, F.P.; Tabor, D.: “The Lubrication by Thin Metallic Films and the Action of Bearing Metals”. In: *Journal of Applied Physics* 14.3 (1943), pp. 141–151.
- [Bow45] Bowden, F.P.; Moore, A.J.W.: “Adhesion of lubricated metals”. In: *Nature* 155 (1945), pp. 451–452.
- [Bow50] Bowden, F.P.; Tabor, D.: *The friction and lubrication of solids, Part-I*. Oxford, UK, 1950.
- [Boz99] Bozzi, A.C.; De Mello, J.D.B.: “Wear Resistance And Wear Mechanisms Of Wc-12%Co Thermal Sprayed Coatings In Three-Body Abrasion”. In: *Wear* 233–235 (1999), pp. 575–587.
- [Bre00] Breedveld, P.E.: “An Alternative Model For Static And Dynamic Friction In Dynamic System Simulation”. In: *1st IFAC-conference on Mechatronic systems*. Vol. 2. Darmstadt, Sept. 2000, pp. 717–722.
- [Bri03] In: *Surface Analysis by Auger and X-Ray Photoelectron Spectroscopy*. Ed. by Briggs, D.; Grant, J.T.: IMPublications, Chichester, UK and SurfaceSpectra Ltd., Manchester, UK, 2003.
- [Bro17] Broitman, E.: “Indentation Hardness Measurements at Macro-, Micro-, and Nanoscale: A Critical Overview”. In: *Tribol. Lett.* 65:23 (2017).
- [Buc71] Buckley, D.H.: “Adhesion of Various Metals to a Clean Iron Surface studied with LEED and Auger Emission Spectroscopy”. In: *Wear* 20.1 (May 1971), pp. 89–103.
- [Buy04] Buyanovski, I.A.; Ignatieva, Z.I.; Zaslavsky, R.N.: “Tribochemistry of Boundary Lubrication Processes”. In: *Mechanical Tribology: Materials, Characterization and Application*. Ed. by Totten, G. E.; Liang, H.: New York: Marcel Dekker, Inc., 2004. Chap. 11.
- [Can95] Canudas de Wit, C.; Olsson, H.; Aström, K.J.; Lischinsky, P.: “A new model for control of systems with friction”. In: *IEEE Trans Autom Control* 40.3 (1995), 419–425.
- [Cha79] Challen, J.M.; Oxley, P.L.B.: “An explanation of the different regimes of friction and wear using asperity deformation models”. In: *Wear* 53 (1979), 229–243.
- [Cha84] Challen, J.M.; Oxley, P.L.B.: “Slip-line fields for explaining the mechanics of polishing and related processes”. In: *International Journal of Mechanical Sciences* 26 (1984), 403–418.
- [Cia00] Ciavarella, M.; Demelio, G.; Barber, J.R.; Jang, Y.H.: “Linear elastic contact of the Weierstrass profile”. In: *Proc. R. Soc. Lond. A* 456 (2000), pp. 387–405.
- [Coh15] Cohen, T.; Durban, D.: “Steady shock waves in porous plastic solids”. In: *International Journal of Solids and Structures* 71 (2015), pp. 70–78.
- [Cor13] Coronado, J.J.; Rodríguez, S.A.; Sinatora, A.: “Effect of particle hardness on mild-severe wear transition of hard second phase materials”. In: *Wear* 301 (2013), pp. 82–88.

- [Cos17] Costa, H.L.; Oliveira Junior, M.M.; de Mello, J.D.B.: “Effect of debris size on the reciprocating sliding wear of aluminium”. In: *Wear* 376–377 (2017), pp. 1399–1410.
- [Cun71] Cundall, P.A.: “A computer model for simulating progressive large scale movements of blocky rock systems”. In: *Proceedings of the symposium of the international society of rock mechanics 1* (1971), pp. 132–150.
- [Czi00] Czichos, H.: *Tribology: A systems approach to the science and technology of friction, lubrication and wear*. Amsterdam: Elsevier Science(chap.4.5), 2000.
- [Czi15] Czichos, H.; Habig, K-H.: *Tribologie-Handbuch: Tribometrie, Tribomaterialien, Tribotechnik*. Wiesbaden: Springer Fachmedien, 2015.
- [Dah68] Dahl, P.R.: “A solid friction model”. In: *The Aerospace Corporation, El Segundo, California 90245, TOR 158* (1968 (called up on 17.04.2018)), pp. 3107–18. URL: <https://apps.dtic.mil/dtic/tr/fulltext/u2/a041920.pdf>.
- [Dan09] Dante, R.; Vannucci, F.; Durando, P.; Galetto, E.; Kajdas, C.: “Relationship between wear of friction materials and dissipated power density”. In: *Tribology International* 42 (2009), pp. 958–963.
- [De 00] De Chiffre, L.; Lonardo, P.; Trumpold, H.; Lucca, D.A.; Goch, G.; Brown, C.A.; Raja, J.; Hansen, H.N.: “Quantitative Characterization of Surface Texture”. In: *CIRP Annals* 49.2 (2000), pp. 635–652.
- [Der52] Deriagin, B.V.: “What is the friction”. In: *Publishing house of academy of sciences of USSR* (1952).
- [Des02] Descartes, S; Berthier, Y.: “Rheology and flows of solid third bodies: background and application to an MoS1.6 coating”. In: *Wear* 252 (2002), 546—556.
- [Det02] Deters, L.; Fischer, A.; Santner, E.; Stolz, U.: *Arbeitsblatt 07 - Tribologie*. Gesellschaft fur Tribologie, 2002.
- [Deu95] Deutscher, O.: “Verschiedene Verfahren zur Einstellung einer gezielten Rauheit von Kaltband”. In: *Stahl u. Eisen* (July 1995), pp. 39–45.
- [Die15] Dienwiebel, M.; Scherge, M.: “Nanotribology in Automotive Industry”. In: *Fundamentals of Friction and Wear on the Nanoscale*. Ed. by E.: Gnecco E.; Meyer. Switzerland: Springer International Publishing, 2015, pp. 657–668.
- [Doe10] Doege, E.; Behrens, B-A: *Handbuch Umformtechnik: Grundlagen, Technologien, Maschinen (German)*. 2., bearbeitete Auflage. Berlin Heidelberg: Springer-Verlag, 2010.
- [Doe76] Doege, E.: “Wichtige Einflussgrossen beim Tiefziehen”. In: *wt—Zeitschrift fur industrielle Fertigung* 66 (1976), pp. 615–616.
- [Dor85] Dorinson, A.; Ludema, K.C (ed.) *Mechanics and chemistry in lubrication*. tribology series 9. Amsterdam: Elsevier, 1985.
- [Ebn05] Ebnesajjad, S.; Khaladkar, P.R.: “Properties of Neat (Unfilled) and Filled Fluoropolymers”. In: *Fluoropolymers Applications in the Chemical Processing Industries*. Ed. by Ebnesajjad, S.; Khaladkar, P.R. Norwich, NY: William Andrew Publishing, 2005, pp. 15 –115. ISBN: 978-0-8155-1502-9. DOI: <https://doi.org/10.1016/B978-081551502-9.50006-5>. URL: <http://www.sciencedirect.com/science/article/pii/B9780815515029500065>.

- [Ema17] Emami, A.; Khaleghian, S.; Su, C.; Taheri, S.: “Comparison of Multiscale Analytical Model of Friction and Wear of Viscoelastic Materials With Experiments”. In: *ASME International Mechanical Engineering Congress and Exposition*. Vol. 9: Mechanics of Solids, Structures and Fluids. Tampa, Florida, USA, Nov. 2017.
- [Eul50] Euler, L.: *Sur le frottement des corps solides*. Histoire de l’Académie Royale à Berlin, iv (1748), 1750, p. 313.
- [Fay92] Fayeulle, S.; Vannes, A.B.; Vincent, L.: “First Body Behavior Before Debris Formation”. In: ed. by Dowson, D.; Dalmaz, G.; Childs, T.H.C.; Taylor, C.M.; Godet, M.: Ohio, USA: Elsevier, 1992. Chap. 6, pp. 229–235.
- [Fen10] Feng, Z.-Q.; He, Q.-C.; Zeng, Q.; Joli, P.: “Theory of Nanoindentation”. In: *Handbook of Nanophysics*. Ed. by Sattler, K.: Boca Raton, USA: CRC Press, 2010. Chap. 26, pp. 26–1–15.
- [Fis11] Fischer-Cripps, A.C.: *Nanoindentation, Mechanical Engineering*. 1. New York, USA: Springer Science+Business Media, LLC, 2011, p. 313.
- [Fog67] Fogg, B.: “Preliminary study of the influence of stress and deformation in the substrate on junction growth and friction”. In: *Proceedings of the Institution of Mechanical Engineers* 182 (1967–1968), pp. 152–161.
- [Fou14] Fouvry, S.; Paulin, S.: “An effective friction energy density approach to predict solid lubricant friction endurance: Application to fretting wear”. In: *Wear* 319 (2014), pp. 211–226.
- [Fri08] Fritz, A.H.; Schulze, G.: ed. *Fertigungstechnik (German)*. Berlin Heidelberg: Springer-Verlag, 2008.
- [Fro14] Fronhoffs, C.; Kopplin, K.-H.; Lewe, T.; Macharev, F.; Steinebrunner, J.; Steinebrunner, F.: “Steel for highest paint appearance quality in automotive application”. In: *4th International Conference on Steels in Cars and Trucks*. Braunschweig, 2014, pp. 102–114.
- [Gaa09] Gaard, A.; Krakhmalev, P.; Bergström, J.: “Influence of tool steel microstructure on origin of galling initiation and wear mechanisms under dry sliding against a carbon steel sheet”. In: *Wear* 267 (2009), pp. 387–393.
- [Gao06] Gao, Y-F.; Bower, A.F.: “Elastic-plastic contact of a rough surface with Weierstrass profile”. In: *Proc. R. Soc. A* 462 (2006), pp. 319–348.
- [Gao10] Gao, R.X.; Sah, S.; Mahayotsanun, N.: “On-line measurement of contact pressure distribution at tool–workpiece interfaces in manufacturing operations”. In: *Manufacturing Technology* 59 (2010), pp. 399–402.
- [Gar95] Garnham, J.E.: “The Wear of Bainitic and Pearlitic Steels”. PhD thesis. University of Leicester, Mar. 1995.
- [Giu09] Giuseppe, C.: “A slightly corrected Greenwood and Williamson model predicts asymptotic linearity between area and load”. In: *Journal of the Mechanics and Physics of Solids* 57 (2009), 1093–1102.
- [God84] Godet, M.: “The third body approach: a mechanical view of wear”. In: *Wear* 100 (1984), pp. 437–452.

- [God98] Godet, M.; Play, D.; Berthe, D.: “An attempt to provide a unified treatment of tribology through load carrying capacity, transport and continuum mechanics”. In: *J. of Lubrication Tech.* 102.2 (198), pp. 236–246.
- [Gre54] Green, A.P.: “The plastic yielding of metal junctions due to combined shear and pressure”. In: *Journal of the Mechanics and Physics of Solids* 2 (1954), pp. 197–211.
- [Gre66] Greenwood, J.A.; Williamson, J.B.P.: “Contact of nominally flat surfaces”. In: *Proceedings of the Royal Society A: Mathematical Physical and Engineering Sciences* 295 (1966), pp. 300–316.
- [HSM11] HSM Stahl- und Metallhandel GmbH: *Werkstoffdatenblatt 1.2379 / X153CrMoV12 Werkzeugstahl, Kaltarbeitsstahl.* (called up on 21.02.2019). URL: [https://www.hsm-stahl.de/fileadmin/user\\_upload/datenblatt/HSM\\_Datenblatt\\_1.2379.pdf](https://www.hsm-stahl.de/fileadmin/user_upload/datenblatt/HSM_Datenblatt_1.2379.pdf).
- [Hac09] Hackl, A.; Zunko, H.; Antrekowitsch, H.; Brisbeger, R.: “Entwicklung von Zn-Al-Mg-Legierung zum Verzinken von Warmband mittels CVGL-Technologie”. In: *Berg- und hüttenmännische Monatshefte : BHM* 154 (2009), p. 398.
- [Hak07] Hakamada, M.; Nakamoto, Y.; Matsumoto, H.; Iwasaki, H.; Chena, Y.; Kusuda, H.; Mabuchi, M.: “Relationship between hardness and grain size in electrodeposited copper films”. In: *Materials Science and Engineering A* 457 (2007), 120–126.
- [Ham04] Hamrock, J.B.; Schmid, R.S.; Jacobson, O.B.: *Fundamentals of Fluid Film Lubrication.* New York, USA: Marcel Dekker, 2nd Ed., 2004.
- [Har22] Hardy, B.W.; Doubleday, I.: “Boundary lubrication – The Paraffin Series”. In: *Proceedings of the Royal Society A: Mathematical Physical and Engineering Sciences* 100.707 (Mar. 1922).
- [Hay68] Hayes, T.L.; Pease, R.F.W.: “The Scanning Electron Microscope: Principles and Applications in Biology and Medicine”. In: *Advances in Biological and Medical Physics* 12 (1968), pp. 85–137.
- [Hella] Helmut Fischer GmbH: *FISCHERSCOPE X-RAY Product Line X-Ray Fluorescence Measuring Instruments for the Measurement of Coating Thickness and Material Analysis.* (called up on 01.02.2019). URL: [http://www.fischer-technology.com/fileadmin/documents/broc/EN/BROC\\_X-RAY\\_Product\\_Line\\_952-008\\_en.pdf](http://www.fischer-technology.com/fileadmin/documents/broc/EN/BROC_X-RAY_Product_Line_952-008_en.pdf).
- [Hella] Helmut Fischer GmbH: (called up on 25.02.2019). URL: <http://www.helmut-fischer.de/en/germany/>.
- [Her14] Hersey, M.: “The laws of lubrication of horizontal journal bearings”. In: *Journal of the Washington Academy of Sciences* (1914), p. 4.
- [Hes90] Hess, D.P.; Soom, A.: “Friction at a lubricated line contact operating at oscillating sliding velocities”. In: *Trans. of the ASME, J. of Trib.* 112.2 (1990), pp. 147–152.
- [Hil50] Hill, R.: *The Mathematical Theory of Plasticity.* Oxford Univ. Press, 1950.
- [Hof13] Hofmann, S.: *Auger- and X-Ray Photoelectron Spectroscopy in Material Science — A User-Oriented Guide.* Berlin Heidelberg: Springer, 2013.

- [Hol13] Hol, J.: “Multi-scale friction modeling for sheet metal forming”. PhD thesis. University of Twente, 2013.
- [Hol99] Holm, R.: *Electric contact: Theory and application*. Berlin Heidelberg: Springer, 1999.
- [Hsu01] Hsu, S.M.; Gates, R.S.: “Boundary Lubrication and Boundary Lubricating Film”. In: *Modern Tribology Handbook - Principle of Tribology*. Ed. by B.: Bhushan. Vol. 1. Boca Raton, USA: CRC Press, 2001.
- [Jenll] Jenoptik: (called up on 07.06.2018). URL: <https://www.jenoptik.com>.
- [Jim11] Jiménez, A.-E.; Bermúdez, M.-D.: “Friction and Wear”. In: *Tribology for Engineers - A practical guide*. Ed. by Davim, J.P.: Cambridge, UK: Woodhead Publishing, 2011. Chap. 2.
- [Joh70] Johnson, W.; Sowerby, R.; Haddow, J.B.: *Plane-strain Slip-line Fields*. London, UK: Edward Arnold, 1970.
- [Jun13] Jung, B.; Lee, H., Park, H.: in: *International Journal of Solids and Structures* 50 (2013), 2719—2724.
- [Kaj04] Kajdas, C.K.: “Tribochemistry”. In: *Mechanical Tribology: Materials, Characterization and Application*. Ed. by Totten, G. E.; Liang, H.: New York, USA: Marcel Dekker, Inc., 2004. Chap. 6.
- [Kap00] Kapoor, A.; Franklin, F.J.: “Tribological layers and the wear of ductile materials”. In: *Wear* 245 (2000), pp. 204–215.
- [Kar12] Kardes, N.: “Deep Drawing of Round and Rectangular Cups”. In: *Sheet Metal Forming - Fundamentals*. Ed. by Altan, T; Tekkaya, A.E.: ASM International, 2012. Chap. 8, pp. 107–127.
- [Kar13] Karupannasamy, D.K.: “Friction modeling on multiple scales for deep drawing processes”. PhD thesis. University of Twente, Nov. 2013.
- [Kar16] Karthik, A.V.: “Vegetable Oil as a Forming Lubricant for Deep Drawing of AA6061”. In: *International Journal of Engineering Science and Computing* 6.7 (2016), pp. 1580–1582.
- [Kar85] Karnopp, D.: “Computer simulation of stick-slip friction in mechanical dynamic systems”. In: *Journal of Dynamic Systems, Measurement and Control, Transactions of the ASME* 107.1 (1985), 100—103.
- [Kat03] Kato, H.: “Severe–mild wear transition by supply of oxide particles on sliding surface”. In: *Wear* 255 (2003), 426—429.
- [Kat97] Kato, K.: “Abrasive wear of metals”. In: *Tribology International* 30 (1997), pp. 333–338.
- [Kha16] Khan, M. H.; Gali, O.A.; Edrisy, A.; Riahi, A.R.: “Effect of oxidation and surface roughness on the shear strength of single-lap-joint adhesively bonded metal specimens by tension loading”. In: *Applied Adhesion Science* 4 (2016), p. 21.
- [Kij07] Kijima, H.; Bay, N.: “Contact Conditions in Skin-pass Rolling”. In: *Annals of the CIRP* 56 (2007), pp. 301–306.

- [Kij08a] Kijima, H.; Bay, N.: “Skin-pass rolling II—Studies on roughness transfer and elongation under pure normal loading”. In: *International Journal of Machine Tools & Manufacture* 48 (2008), pp. 1308–1312.
- [Kij08b] Kijima, H.; Bay, N.: “Skin-pass rolling I—Studies on roughness transfer and elongation under pure normal loading”. In: *International Journal of Machine Tools & Manufacture* 48 (2008), pp. 1313–1317.
- [Kim07] Kim, H.; Hyun Sung, J.; Sivakumar, R.; Altan, T.: “Evaluation of stamping lubricants using the deep drawing test”. In: *International Journal of Machine Tools and Manufacture* 47 (2007), pp. 2020–2032.
- [Kim08] Kim, H.; Han, J.; Yan, Q.; Altan, T.: “Evaluation of Tool Materials, Coatings and lubricants in Forming Galvanized Advanced High Strength Steels (AHSS)”. In: *CIRP Annals-Manufacturing Technology* 57.1 (2008), pp. 299–304.
- [Kir13] Kirkhorn, L.; Bushlya, V.; Andersson, M.; Stahl, J.-E.: “The influence of tool steel microstructure on friction in sheet metal forming”. In: *Wear* 302 (2013), pp. 1268–1278.
- [Kli94] Klimczak, T.; Jonasson, M.: “Analysis of real contact area and change of surface texture on deep drawn steel sheets”. In: *Wear* 179.1–2 (1994), pp. 129–135.
- [Klo06] Klocke, F.; König, W.: *Fertigungsverfahren, Umformen (German)*. Berlin Heidelberg: Springer, 2006.
- [Kra14] Kralik, V.; Nemecek, J.: “Comparison of nanoindentation techniques for local mechanical quantification of aluminium alloy”. In: *Materials Science & Engineering* A618 (2014), pp. 118–128.
- [Kra61] Kramer, I.R.; Demer, L.J.: “The effect of surface removal on the plastic behavior of aluminium single crystals”. In: *Trans. AIME* 221 (1961), pp. 780–6.
- [Kra77] Kragelski, I.V.; Dobichin, M.N.; Kombalov, V.S.: *Osnovi rasshiotov na trenie i iznos (Russian)*. Moscow: Mashinostroenie, 1977.
- [Laf06] Lafaye, S.; Gauthier, C.; Schirrer, R.: “The ploughing friction: analytical model with elastic recovery for a conical tip with a blunted spherical extremity”. In: *Tribology Letters* 21.2 (2006), pp. 95–99.
- [Lam17] Lammers, K.R.; van de Langkruis, J.; van Eenennaam, J.: “FIB/TEM analysis of hot dip galvanised AlMgZn coatings for automotive steel applications”. In: *Tata Steel tech. papers* (2017 (called up on 08.12.18)). URL: [https://www.tatasteeleurope.com/static\\_files/Downloads/Automotive/Tech%20papers/MagiZinc\\_FIB-TEM%20analysis%20of%20hot%20dip%20galvanized%20AlMgZn%20coatings%20for%20automotive%20steel%20applications.pdf](https://www.tatasteeleurope.com/static_files/Downloads/Automotive/Tech%20papers/MagiZinc_FIB-TEM%20analysis%20of%20hot%20dip%20galvanized%20AlMgZn%20coatings%20for%20automotive%20steel%20applications.pdf).
- [Lan94] Lange, K.: *Handbook of Metal Forming*. Series in Energy. Michigan, USA: Society of Manufacturing Engineers; New Ed edition, Sept. 1994.
- [Lar07] Larsen, T.; Andersen, T.L.; Thorning, B.; Horsewell, A.; Vigild, M.E.: “Comparison of friction and wear for an epoxy resin reinforced by a glass or a carbon/aramid hybrid weave”. In: *Wear* 262 (2007), pp. 1013–1020.

- [Law11] Lawanwong, K.; Pornputsiri, N.; Luangsopapun, G.: “An Investigation of Adhesion Wear Behavior of Tool Steel on Blanking Die”. In: *International Conference on Advanced Materials Engineering IPCSIT*. Vol. 15. Singapore, 2011, pp. 25–30.
- [Lec05] Lecornu, L.: “(b) Sur le frottement de glissement”. In: *Comptes Rendu des Séances de l’Academie des Sciences* 140.6 (1905), pp. 635–637.
- [Lia15] Liao, J.; Xin, X.: “Investigation of Experimental investigation of deep drawing of C-rail benchmark using various lubricants”. In: *MATEC Web of Conferences: EDP Sciences*. Vol. 21. Les Ulis, France, 2015, p. 04011.
- [Lin16] Linsler, D.: “Einlaufverhalten einer untereutektischen AlSi-Legierung unter Berücksichtigung des Randzonengefüges”. PhD thesis. Karlsruher Institut für Technologie, Feb. 2016.
- [Liu15a] Liu, X.; Liu, Z.; Wei, Y.: “Ploughing friction and nanohardness dependent on the tip tilt in nano-scratch test for single crystal gold”. In: *Computational Materials Science* 110 (2015), pp. 54–61.
- [Liu15b] Liu, Y.F.; Li, J.; Zhang, Z.M.; Hu, X.H.; Zhang, W.J.: “Experimental comparison of five friction models on the same test-bed of the micro stick-slip motion system”. In: *Mech. Sci.* 6 (2015), pp. 15–28.
- [Lu,15] Lu, X.; Khonsari, M.M.; Gelinck, E.R.M.: “The Stribeck Curve: Experimental Results and Theoretical Prediction”. In: *ASME J. Tribol.* 128.4 (2015), 789–794.
- [Maj91] Majumdar, A.; Bhushan, B.: “Sheet Metal Forming Simulation in Industry”. In: *Journal of Tribology* 113.1 (1991), pp. 1–11.
- [Mar00] Marder, A.R.: “The metallurgy of zinc-coated steel”. In: *Progress in Materials Science* 45.3 (2000), pp. 191–271.
- [Mar15] Marquéz, M.B.S.; Boussaada, I.; Mounier, H.; Niculescu, S.I.: *Analysis and control of oilwell drilling vibrations: a time-delay systems approach*. Switzerland: Springer International Publishing, 2015.
- [Mar88] Martens, A.: “Schmieröluntersuchungen [oil studies]”. In: *Mitteilungen aus den Königlichen Technischen Versuchsanstalten zu Berlin, Ergänzungsheft III [releases from the Royal Technical Testing Institutes of Berlin, complementary volume III]* (1888), pp. 1–37.
- [Mas04] Masen, M.A.: “Abrasive tool wear in metal forming processes”. PhD thesis. University of Twente, 2004.
- [Mat08] Mate, C.M.: *Tribology on the small scale: A bottom up approach to friction, lubrication and wear*. Oxford university press, 2008.
- [Mat15] Materion, Performance Alloys: “Introduction to Friction”. In: *TECHNICAL TIDBITS* 73 (Jan. 2015 (called up on 20.05.2018)). URL: <https://materion.de.com/-/media/files/alloy/newsletters/technical-tidbits/issue-no-73---introduction-to-friction.pdf>.
- [McB25] McBain, J.W.; Hopkins, D.G.: “On Adhesives and Adhesive Action”. In: *J. Phys. Chem.* 29(2) (1825), pp. 188–204.
- [Mei05] Meiler, M.; Jaschke, H.: “Lubrication of Aluminium Sheet Metal within the Automotive Industry”. In: *Advanced Materials Research* 6-8 (2005), pp. 551–558.

- [Mel12] Melih, E.: “Multiscale physics-based modeling of friction”. PhD thesis. University of Illinois at Urbana-Champaign, 2012.
- [Men11] Menezes, P.L.; Kishore, K.; Kailas, S.V.; Lovell, R.M.: “Role of Surface Texture, Roughness, and Hardness on Friction During Unidirectional Sliding”. In: *Tribology Letters* 41 (2011), pp. 1–15.
- [Men13] Menezes, P.L.; Nosonovsky, M.; Kailas, S.; Lovell, M.: “Friction and Wear”. In: *Tribology for Scientists and Engineers*. Ed. by Menezes, P.L.; Nosonovsky, M.; Ingole, S.P.; Kailas, S.; Lovell, M.: New York, USA: Springer, 2013, pp. 43–91.
- [Min88] Minsky, M.: “Memoir on inventing the confocal scanning microscope”. In: *Scanning* 10 (1988), 128–138.
- [Mis12] Mishra, M.; Egberts, P.; Bennewitz, R.; Szlufarska, I.: “Friction model for single-asperity elastic-plastic contacts”. In: *Phys. Rev. B* 86.4 (July 2012), p. 045452. DOI: 10.1103/PhysRevB.86.045452. URL: <https://link.aps.org/doi/10.1103/PhysRevB.86.045452>.
- [Mul62] Mulhearn, T.O.; Samuels, L.E.: “The Abrasion Of Metals: A Model Of The Process”. In: *Wear* 5 (1962), pp. 478–498.
- [Nak18] Nakamura, M.: “X-Ray Photoelectron Spectroscopy”. In: *Compendium of Surface and Interface Analysis – The Surface Science Society of Japan Editor*. Springer Singapore, 2018. Chap. 132.
- [Nie11] Nielsen, P.S.; Paldan, N.A.; Calaon, M.; Bay, N.: “Scale effects in metal-forming friction and lubrication. Proceedings of the Institution of Mechanical Engineers”. In: *Journal of Engineering Tribology* 225.9 (2011), pp. 924–931.
- [Nie17] Nielsen, C.V.; Bay, N.: “Overview of friction modelling in metal forming processes”. In: *Procedia Engineering* 207 (2017), pp. 2257–2262.
- [Nin17] Nine, H.D.: “The applicability of Coulomb’s friction law to drawbeads in sheet metal forming”. In: *Journal of Applied Metalworking* 2.3 (2017), pp. 200–210.
- [Oka18] Okano, Y.: “Scanning Electron Microscopy”. In: *Compendium of Surface and Interface Analysis – The Surface Science Society of Japan Editor*. Springer Singapore, 2018. Chap. 91.
- [Oli86] Oliver, W.C.; Hutchings, R.; Pethica, J.B.: “Measurement of Hardness at Indentation Depths as Low as 20 Nanometres”. In: *Microindentation Techniques in Materials Science and Engineering*. Philadelphia, USA: ASTM STP 889, 1986, pp. 90–108.
- [Oli92] Oliver, W.C.; Pharr, G.: “An improved technique for determining hardness and elastic modulus using load and displacement sensing indentation experiments”. In: *J. Mater. Res.* 7(6) (1992), pp. 1564–1583.
- [Oni73] Onions, R.A.; Archard, J.F.: “The contact of surfaces having a random structure”. In: *J. Phys. D: Appl. Phys.* 6 (1973).
- [Pac18] Packham, D.E.: “Theories of Fundamental Adhesion”. In: *Handbook of Adhesion Technology*. Ed. by da Silva, L.F.M.; Öchsner, A.; Adams, R.D.: Springer, 2018.
- [Pac92] Packham, D.E.: “The Mechanical Theory of Adhesion- Changing Perceptions 1925-1991”. In: *J. Adhesion* 39 (1992), pp. 137–144.

- [Par04] Parlitz, U.; Hornstein, A.; Engster, D.; Al-Bender, F.; Lampaert, V.; Tjahjowidodo, T.; Fassois, S.D.; Rizos, D.; Wong, C.X.; Worden, K.; Manson, G.: “Identification of pre-sliding friction dynamics”. In: *Chaos* 14.2 (2004), pp. 420–430.
- [Per06] Persson, B.N.J.: “Contact mechanics for randomly rough surfaces”. In: *Surface Science Report* 61 (2006), p. 201.
- [Per08] Pereira, M.P.; Duncan, J.L.; Yan, W.; Rolfe, B.: “Contact pressure evolution and its relation to wear in sheet metal forming”. In: *Wear* 265 (2008), pp. 1687–1699.
- [Per09] Pereira, M.P.; Duncan, J.L.; Yan, W.; Rolfe, B.: “Contact pressure evolution at the die radius in sheet metal stamping”. In: *journal of materials processing technology* 209.3 (2009), pp. 3532–3541.
- [Per98] Persson, B.N.J.: *Sliding Friction: Chap. 9 - Boundary Lubrication*. Berlin Heidelberg: Springer, 1998, pp. 269–288.
- [Phyll] Physical Electronics. *XPS / ESCA*. (called up on 06.06.2018). URL: <https://www.phl.com/surface-analysis-techniques/xps-esca.html>.
- [Pin05] Pintaude, G.; Albertin, E.; Sinatora, A.: “A review of abrasive wear mechanisms of metallic materials”. In: *Conference: ABRASION WEAR RESISTANT ALLOYED WHITE CAST IRON FOR ROLLING AND PULVERIZING MILLS*. Vol. 1. Sao Paulo, Brazil, 2005, 201–217.
- [Pod12] Podgornik, B.; Vilhena, L.M.; Sedlaček, M.; Rek, Z.; Žun, I.: “Effectiveness and design of surface texturing for different lubrication regimes”. In: *Meccanica* 47 (2012), 1613–1622.
- [Ptull] PtU – Darmstadt. *Tribologische Wirkmechanismen, Prozessoptimierung und Oberflächengestaltung*. (called up on 17.10.2017). URL: [https://www.ptu.tu-darmstadt.de/mu\\_forschung/mu\\_tribologieundoberflaechentechnik\\_1/index.de.jsp](https://www.ptu.tu-darmstadt.de/mu_forschung/mu_tribologieundoberflaechentechnik_1/index.de.jsp).
- [Puj12] Pujante, J.; Pelcastre, L.; Vilaseca, M.; Casellas, D.; Prakash, B.: “Investigations into wear and galling mechanism of aluminium alloy-tool steel tribopair at different temperatures”. In: *Wear* 308 (2012), 193–198.
- [Rab65a] Rabinowicz, E.: *Friction and Wear of Materials*. New York, USA: John Wiley & Sons, Inc., 1965.
- [Rab65b] Rabinowicz, E.; Mutis, A.: “Effect of abrasive particle size on wear”. In: *Wear* 65 (1965), pp. 381–390.
- [Ran26] Rankin, D.: *Elastic range of friction*. *Phys. Mag.*, VIII, 1926, p. 806.
- [Ren11] Renouf, M.; Cao, H.-P.; Nhu, V.-H.: “Multiphysical modeling of third-body rheology”. In: *Tribology International* 44.3 (2011), pp. 417–425.
- [Rie11] Riener, C.K.; Preis, K.; Achammer, E.; Angeli, G.; Arndt, M.; Duchoslav, J.; Itani, H.; Stifter, D.; Hingerl, K.: “Nano-characterisation of the surface of HDG Zn–Al–Mg–coated steel sheets”. In: *Proceedings - 8th International Conference on Zinc and Zinc Alloy Coated Steel Sheet, Galvatech 2011*. Genoa, Italy, 2011, pp. 91–102.
- [Rig88] Rigney, D.A.: “Sliding wear of metals”. In: *Ann. Rev. Mater. Sci.* 18 (1988), pp. 141–163.

- [Rol08] Roll, K.: “Simulation of Sheet Metal Forming- Necessary developments in the future”. In: *LS-DYNA Anwenderforum*. Bamberg, 2008.
- [Rud13] Ruderman, M.; Bertram, T.: “Two-state dynamic friction model with elasto-plasticity”. In: *Mechanical Systems and Signal Processing* 39 (2013), pp. 316–332.
- [SMS11] SMS-SIEMAG: *SKIN-PASS MILLS for a perfect finish*. (call up on 21.02.2018). URL: [http://www.sms-siemag.com/download/W6\\_7\\_304E\\_Skin-Pass\\_Mills\\_References.pdf](http://www.sms-siemag.com/download/W6_7_304E_Skin-Pass_Mills_References.pdf).
- [Sac44] Sackmann, B.W.; Burwell, J.T.; Irvine, J.W.: “Measurements of the Adhesion Component in Friction by Means of Radioactive Indicators”. In: *Journal of Applied Physics* 459.15 (1944).
- [Sah05] Sahoo, P.: *Engineering tribology*. New Delhi, India: Prentice Hall of India Private Ltd, 2005.
- [Sak18] Sakamoto, T.: “Focused Ion Beam Scanning Electron Microscope”. In: *Compendium of Surface and Interface Analysis – The Surface Science Society of Japan Editor*. Springer Singapore, 2018. Chap. 31.
- [Sas81] Sasada, T.; Norose, S.; Mishina, H.: “The Behaviour of Adhered Fragments Interposed Between Sliding Surfaces and the Formation Process of Wear Particles”. In: *J. of Lubrication Tech.* 103.2 (Apr. 1981), pp. 72–80.
- [Sch03a] Scherge, M.; Pöhlmann, K.; Gervé, A.: “Wear measurement using radionuclide-technique (RNT)”. In: *Wear* 254(9) (2003), pp. 801–817.
- [Sch03b] Scherge, M.; Shakhvorostov, D.; Pöhlmann, K.: “Fundamental wear mechanism of metals”. In: *Wear* 255 (2003), pp. 395–400.
- [Sch14a] Schlarb, T.: “Einlaufverhalten einer untereutektischen Aluminium-Silicium-Legierung unter Berücksichtigung des Ausgangsgefüges”. Diplomarbeit. Karlsruher Institut für Technologie, Institut für Angewandte Materialien IAM, 2014.
- [Sch14b] Schuler GmbH: *Handbuch der Umformtechnik*. Heidelberg: Schuler, 2014.
- [Sch42] Schnurmann, R.: “Amontons’ law, Traces of Frictional Contact, and Experiments on Adhesion”. In: *Journal of Applied Physics* 235.13 (1942), p. 235.
- [Sch93] Schedin, E.; Lehtinen, B.: “Galling mechanisms in lubricated systems: a study of sheet metal forming”. In: *Wear* 170 (1993), pp. 119–130.
- [Sch94] Schedin, E.: “Galling mechanisms in sheet forming operations”. In: *Wear* 179 (1994), 123–128.
- [Sem06] Semiatin, S.L. (Ed): *Volume 14B Metalworking: Sheet Forming*. Ohio, USA: ASM International, 2006.
- [Sha04] Shakhvorostov, D.; Pöhlmann, M.; Scherge, M.: “An energetic approach to friction, wear and temperature”. In: *Wear* 257.1-2 (2004), pp. 124–130.
- [Sha14] Shaffer, S.: *Generating a Stribeck Curve in a Reciprocating Test*. 2014 (called up on 09.05.2018). URL: [https://www.bruker.com/fileadmin/user\\_upload/8-PDF-Docs/SurfaceAnalysis/TMT/ApplicationNotes/AN1004\\_RevA2\\_Generating\\_a\\_Stribeck\\_Curve\\_in\\_a\\_Reciprocating\\_Test-AppNote.pdf](https://www.bruker.com/fileadmin/user_upload/8-PDF-Docs/SurfaceAnalysis/TMT/ApplicationNotes/AN1004_RevA2_Generating_a_Stribeck_Curve_in_a_Reciprocating_Test-AppNote.pdf).

- [Shi12] Shizhu, W.; Ping, H.: *Principles of tribology*. Singapore: John Wiley & Sons, 2012.
- [Shr16] Shram, V.G.; Lysyannikov, A.V.; Kovaleva, M.A.: “The Mechanism of Lubricants Protective Layers Formation in Friction Sliding”. In: *Procedia Engineering* 150 (2016), pp. 458–463.
- [Sie56] Siebel, E; Panknin, W.: *Die Gesetzmäßigkeiten beim Tiefziehen*. Industrie-Anzeiger 78, 1956.
- [Sig15] Sigvant, M.; Hol, J.; Chezan, T.; van den Boogaard, A.H.: “Friction modeling in sheet metal forming simulations: Application and validation on an U-bend product”. In: *Proc. of FTF*. Zürich, Switzerland, 2015.
- [Sig16] Sigvant, M.; Pilthammar, J.; Hol, J.; Wiebenga, J.H.; Chezan, T.; Carleer, B.; van den Boogaard, A.H.: “Friction and lubrication modeling in sheet metal forming simulations of a Volvo XC90 inner door”. In: *IOP Conference Series: Materials Science and Engineering*. Vol. 159. 1. Linz, Austria, 2016.
- [So,04] So, H.: “Metallic Tribo-oxides: Formation and Wear Behavior”. In: *Mechanical Tribology: Materials, Characterization and Application*. Ed. by Totten, G. E.; Liang, H.: New York, USA: Marcel Dekker, Inc., 2004. Chap. 3.
- [Som14] Sommer, K.; Heinz, R.; Schöffler, J.: *Verschleiß metallischer Werkstoffe: Erscheinungsformen sicher beurteilen*. Wiesbaden: Springer, 2014. Chap. 2.
- [Son92] Song, J.F.; Vorburger, T.V.: “Surface Texture”. In: *Friction, Wear and Lubrication*. Ed. by G.E.: Totten. Vol. 18. Ohio, USA: ASM International, 1992, pp. 334–345.
- [Sta00] Stachowiak, G.B.: “Particle angularity and its relationship to abrasive and erosive wear”. In: *Wear* 241 (2000), 214 – 219.
- [Sta04] Stachowiak, G.B.; Stachowiak, G.W.: “Wear mechanisms in ball-cratering tests with large abrasive particles”. In: *Wear* 256 (2004), pp. 600–607.
- [Sta93] Stachowiak, G.W.; Batchelor, A.W. (Ed.) *Engineering tribology, Tribology Series*. Vol. 24. Amsterdam, the Netherlands: Elsevier, 1993, pp. 613–635.
- [Str02] Stribeck, R.: “Die wesentlichen Eigenschaften der Gleit- und Rollenlager [the main characteristics of the sliding and roller bearings]”. In: *Zeitschrift des Vereins Deutscher Ingenieure [Journal of the Association of German Engineers]* 36 (Band 46) (1902), pp. 1341–48, 1463–70.
- [Sun87] Sundararajan, G.: “A new model for two-body abrasive wear based on the localization of plastic deformation”. In: *Wear* 117.1 (1987), pp. 1–35.
- [Swe00] Swevers, J.; Al-Bender, F.; Ganseman, C.G.; Projogo, T.: “An integrated friction model structure with improved presliding behavior for accurate friction compensation, Automatic Control”. In: *IEEE Transactions* 45.4 (2000), 675–686.
- [Tab59] Tabor, D.: “Junction growth in metallic friction: the role of combined stresses and surface contamination”. In: *Proceedings of the Royal Society of London. Series A, Mathematical and Physical Sciences* 251 (1959), pp. 378–393.

- [Tab92] Tabor, D.: “Friction as a dissipative process”. In: *Fundamentals of Friction: Macroscopic and Microscopic Processes. NATO ASI Series (Series E: Applied Sciences)*. Ed. by Singer, I. L.; Pollock, H.M.: vol. 220. Dordrecht: Springer, 1992, pp. 3–24.
- [Tee78] Teer, D.G.; Arnell, R.D.: “Friction Theories”. In: *Principles of Tribology*. Ed. by J.: Halling. London: THE MACMILLAN PRESS LTD, 1978.
- [Tholl] Thomson Industries, Inc.: *The Pressure Velocity (PV) Relationship for Lead Screws*. (called up on 28.10.2018). URL: [https://www.thomsonlinear.com/downloads/articles/The\\_Pressure\\_Velocity\\_Relationship\\_for\\_Lead\\_Screws\\_tae.pdf](https://www.thomsonlinear.com/downloads/articles/The_Pressure_Velocity_Relationship_for_Lead_Screws_tae.pdf).
- [Thu79] Thurston, R.H.: *Determination of the Laws and Coefficient of Friction by New Methods and with New Apparatus*. London: Trübner and Co., 1879.
- [Thw82] Thwaite, E.G.: “Surface Topography Measurement and Analysis”. In: *Aust. J. Phys.* 35 (1982), pp. 777–84.
- [Thylla] Thyssenkrupp Steel Europe AG: *Dualphasen-Stahl – maßgeschneidertes Portfolio für modernen Leichtbau*. (called up on 15.06.2018). URL: <https://www.thyssenkrupp-steel.com/de/produkte/feinblech-oberflaechenveredelte-produkte/mehrphasenstahl/dualphasenstahl/>.
- [Thyllb] Thyssenkrupp Steel Europe AG: *Weicher Stahl (Tiefziehstahl und Emaillierstahl)*. (called up on 15.06.2018). URL: <https://www.thyssenkrupp-steel.com/de/produkte/feinblech-oberflaechenveredelte-produkte/weicher-stahl/weicher-stahl.html>.
- [Vil17] Vilhena, L.M.; Ramalho, A.; Cavaleiro, A.: “Grooved surface texturing by electrical discharge machining (EDM) under different lubrication regimes”. In: *Lubrication Science*. 29 (2017), 493–501.
- [Viz04] Vizintin, J.: “Oil Surface: Additive Reaction Mechanisms”. In: *Mechanical Tribology: Materials, Characterization and Application*. Ed. by Totten, G. E.; Liang, H.: New York: Marcel Dekker, Inc., 2004. Chap. 9.
- [Vol02] Vollersten, F.; Plancak, M.: “On possibilities for the determination of the coefficient of friction in hydroforming of tubes”. In: *J. Mater. Process. Technol.* 125–126 (2002), pp. 412–420.
- [Wag97] Wagner, S.: *Tribologische Untersuchungen in der Blechumformung*. Berlin-Heidelberg: Springer-Verlag, 1997.
- [Wan12] Wang, Y.A.; Li, J.X.; Yan, Y.; Qiao, L.J.: “Effect of pv factor on sliding friction and wear of copper-impregnated metallized carbon”. In: *Wear* 289 (2012), pp. 119–123.
- [Wan15] Wang, W.; Wang, K.; Zhao, Y.; Hua, M.; Wei, X.: “A study of galling initiation in friction coupling stretch bending with advanced high strength hot-dip galvanized sheet”. In: *Wear* 328–329 (2015), 286–294.
- [Wan73] Wanheim, T.: “Friction at high normal pressure”. In: *Wear* 25 (1973), pp. 225–244.
- [Wan74] Wanheim, T.; Bay, N.; Petersen, A.S.: “A theoretically determined model for friction in metal working processes”. In: *Wear* 28 (1974), pp. 251–258.

- [War95] Warren, T.L.; Krajcinovic, D.: “Fractal Models of Elastic–Perfectly Plastic Contact of Rough Surfaces Based on the Cantor Set”. In: *International Journal of Solids and Structures* 32.19 (1995), pp. 2907–2922.
- [Wen11] Wen, S.; Huang, P.: “Properties of lubricants”. In: *Principles of Tribology*. Ed. by Singer, I.L.; Pollock, H.M.: Singapore: John Wiley & Sons (Asia) Pte, 2011, pp. 1–22.
- [Wes01] Westeneng, J.D.: “Modelling of contact and friction in deep drawing processes”. PhD thesis. University of Twente, 2001.
- [Whe84] Wheeler, D.R.: “Tribological Applications of Surface Analysis”. In: *NASA Report TM-83707* (1984).
- [Whi03] Whitehouse, D.J.: *Handbook of Surface and Nanometrology*. Boca Raton, USA: Taylor & Francis Group, LLC, 2003.
- [Whi70] Whitehouse, D.J.; Archard, J.F.: “The Properties of Random Surfaces of Significance in their Contact”. In: *Proc. R. Soc. Lond. A* 316 (1970), pp. 97–121.
- [Wic02] Wicklung, O.: “Modelling and Control of Temper Rolling and Skin Pass Rolling”. In: *Metal Forming Science and Practice*. Ed. by Lenard, J.G.: Oxford, UK: Elsevier Science Ltd, 2002. Chap. 15.
- [Wil04] Willner, K.: “Elasto-Plastic Normal Contact of Three-Dimensional Fractal Surfaces Using Halfspace Theory”. In: *Journal of Tribology* 126 (2004), pp. 28–33.
- [Wil78] Wilson, W.R.D.: “Friction and Lubrication in Sheet Metal Forming”. In: *Mechanics of Sheet Metal Forming: Material Behavior and Deformation Analysis*. Ed. by Koistinen, D.P.; Wang, N-M.: New York, USA: plenum Press, 1978, pp. 157–177.
- [Wil92] Williams, J.A.; Hyncica, A.M.: “Abrasive wear in lubricated contacts”. In: *J. Phys. D: Appl. Phys.* 25 (1992), pp. 81–90.
- [Wil95] Wilson, W.R.D.; Hsu, T.C.; Huang, X.B.: “A Realistic Friction Model for Computer Simulation of Sheet Metal Forming Processes”. In: *ASME J. Eng. Ind.* 117.2 (1995), 202–209.
- [Woy10] Woydt, M.; Wäsche, R.: “The history of the Stribeck curve and ball bearing steels: The role of Adolf Martens”. In: *Wear* 268 (2010), pp. 1542–1546.
- [Yan98] Yan, W.; Komvopoulos, K.: “Contact Analysis of Elastic–Plastic Fractal Surfaces”. In: *Journal of Applied Physics* 84.7 (1998), pp. 3617–3624.
- [Zum98] Zum Gahr, K.H.: “Wear by hard particles”. In: *Tribol. Int.* 31 (1998), pp. 587–596.
- [ter96] ter Haar, R.: “Friction in sheet metal forming, the influence of (local) contact conditions and deformation”. PhD thesis. University of Twente, May 1996.
- [van06a] van der Heide, E.; Huis in t Veld, A.J.; Schipper, D.J.: “The effect of lubricant selection on galling in a model wear test”. In: *Wear* 251 (2006), pp. 973–979.
- [van06b] van der Heide, E.; Schipper, D.J.: “Friction and Wear in Lubricated Sheet Metal Forming Processes”. In: *Handbook of Lubrication and Tribology, Vol. II Application and Maintenance*. Ed. by Totten, G. E.: Boca Raton, USA: Taylor & Francis, 2006. Chap. 28.